2014

INCREASING THE SELECTIVITY AND SENSITIVITY OF GAS SENSORS FOR THE DETECTION OF EXPLOSIVES

Daniel Mallin
University of Rhode Island, daniel.p.mallin@gmail.com

INCREASING THE SELECTIVITY AND SENSITIVITY OF GAS SENSORS FOR THE DETECTION OF EXPLOSIVES

BY

DANIEL MALLIN

A THESIS SUBMITTED IN PARTIAL FULFILLMENT OF THE REQUIREMENTS FOR THE DEGREE OF

MASTER OF SCIENCE

IN

CHEMICAL ENGINEERING

UNIVERSITY OF RHODE ISLAND

2014

MASTER OF SCIENCE THESIS

OF

DANIEL MALLIN

APPROVED:

Thesis Committee:

Major Professor Otto Gregory

Everett Crisman

Tao Wei

Nasser H. Zawia

DEAN OF THE GRADUATE SCHOOL

UNIVERSITY OF RHODE ISLAND
2014

ABSTRACT

Over the past decade, the use of improvised explosive devices (IEDs) has increased, domestically and internationally, highlighting a growing need for a method to quickly and reliably detect explosive devices in both military and civilian environments before the explosive can cause damage. Conventional techniques have been successful in explosive detection, however they typically suffer from enormous costs in capital equipment and maintenance, costs in energy consumption, sampling, operational related expenses, and lack of continuous and real-time monitoring. The goal was thus to produce an inexpensive, portable sensor that continuously monitors the environment, quickly detects the presence of explosive compounds and alerts the user.

In 2012, here at URI, a sensor design was proposed for the detection of triacetone triperoxide (TATP). The design entailed a thermodynamic gas sensor that measures the heat of decomposition between trace TATP vapor and a metal oxide catalyst film. The sensor was able to detect TATP vapor at the part per million level (ppm) and showed great promise for eventual commercial use, however, the sensor lacked selectivity. Thus, the specific objective of this work was to take the original sensor design proposed in 2012 and to make several key improvements to advance the sensor towards commercialization.

It was demonstrated that a sensor can be engineered to detect TATP and ignore the effects of interferent H_2O_2 molecules by doping SnO_2 films with varying amounts of Pd. Compared with a pure SnO_2 catalyst, a SnO_2, film doped with 8 wt. % Pd had the highest selectivity between TATP and H_2O_2. Also, at 12 wt. % Pd, the response to

TATP and H_2O_2 was enhanced, indicating that sensitivity, not only selectivity, can be increased by modifying the composition of the catalyst.

An orthogonal detection system was demonstrated. The platform consists of two independent sensing mechanisms, one thermodynamic and one conductometric, which take measurements from the same catalyst simultaneously and provide a redundancy in response for positive explosive identification. TATP, 2,6-DNT and ammonium nitrate were reliably detected. Each analyte displayed a unique conductometric signature and the results indicated a detection limit at the ppb level.

A preconcentrator was designed to enhance the sensitivity of the sensor and was successfully demonstrated. The magnitude of the sensor response increased from by 50% and the preconcentrator could be operated semi-continuously, maintaining one of the most attractive features of this sensor platform: the capability to operate in real time. A method to filter out extraneous heat signals from sensor response using a dynamic control was also successfully demonstrated and will likely be a fixture in all sensor experimentation and design moving forward.

Finally, two MEMS based sensor platforms were designed and fabricated. It was theoretically demonstrated that the newest iteration of the MEMS sensor consumes considerably less power due to thinner membranes, a smaller active surface area and an overall smaller thermal mass, allowing for the possibility of creating networks of sensor arrays, even in a portable device.

ACKNOWLEDGMENTS

I would like to first acknowledge my adviser, Dr. Otto J. Gregory, for his guidance, his experience and his patience. Being your student these past few years has truly been a privilege and I would like to extend my thanks, for everything you've done for me.

I would also like to acknowledge a few fellow students, without whom this research would not have been possible. Thank you to Ben Jacques, Mitch Champlin, Liz Shokunbi, Zach Caron, Matin Amani, and especially Yun Chu who was an instrumental partner and mentor. A special thanks to Mr. Mike J. Platek for his guidance as well. Our labs would most definitely not function without you.

I would like to express gratitude to my committee members: Dr. Crisman, Dr. Davis and Dr. Wei, for their advice and guidance. All the faculty members and staff of the Department of Chemical Engineering are also greatly appreciated. Thank you to Dr. Oxley and her students in the Chemistry Department for their cooperation and assistance.

Finally, to my family: the biggest thank you for your constant love and support. And to Heather: I love you and appreciate everything you've done for me. I couldn't have made it this far without you.

TABLE OF CONTENTS

LIST OF TABLES

LIST OF FIGURES

CHAPTER 1

INTRODUCTION

Over the past decade, the use of improvised explosive devices (IEDs) has increased, domestically and internationally [1-3]. Explosives are frequently used by terrorists to induce fear, and if not stopped, to inflict massive damage and injury. Major events in recent history involving IEDs include the 1993 truck bomb that killed six people at the World Trade Center, the Oklahoma City bombing in 1995, the 2001 shoe bombing, the London subway bombing of 2005, and most recently the Boston Marathon bombing in 2013, among many others [1-4]. The lives threatened by IEDs are also not all civilian. As of 2013, more than 60% of all combat casualties from conflict in Iraq and Afghanistan were the result of IEDs [1]. That amounts to over 3,200 killed and 33,000 wounded. Elsewhere in the world, an average of 700 explosions per month are the result of an improvised explosive attack [2]. This highlights a growing need for a method to quickly and reliably detect explosive devices in both military and civilian environments before the explosive can cause damage.

Yet, there are currently few methods available that can be used to successfully detect explosive compounds in this way. Conventional spectroscopy techniques, while being very sensitive and selective for the identification of unknown substances, are often expensive and require the resources of a full laboratory, impractical in a portable device [5]. The current industry standard for explosive detection involves

taking a sample of some sort, using a cotton swab. This type of testing is impractical if it is necessary to screen many people in a short time. It is also rather invasive, as the swab must contact the person's hands, clothing or luggage, and it requires the time for collection. Canine units have also been used throughout history to locate bombs with a great degree of accuracy [5]. However, the animals can be expensive and time consuming to maintain and many studies have shown that, although dogs have incredible olfactory senses, they are not infallible. Sensors have therefore been employed as "electronic noses" to replace the real ones [6-7].

The goal is thus to produce an inexpensive, portable sensor that continuously monitors the environment, quickly detects the presence of explosive compounds and alerts the user. In 2012, here at URI, a sensor design was proposed for the detection of triacetone triperoxide (TATP), a particularly dangerous explosive frequently used in IEDs because of its relatively simple synthesis from commonly found ingredients [8]. TATP readily sublimes at room temperature and is in relatively high concentration in the vapor phase [9], but is difficult to detect using conventional explosive detection techniques because peroxide based explosives are notoriously difficult to detect, making it of particular interest [7].

The design entailed a thermodynamic gas sensor that measures the heat of decomposition between trace TATP vapor and a metal oxide catalyst film [8]. The sensor was able to detect TATP vapor at the part per million level (ppm) and due to the robust nature of the sensor, it showed great promise for eventual commercial use, however, there were a few critical limitations. An ideal sensor must meet two important criteria: (1) the sensor must respond to one environmental stimulus is

insensitive to any other stimuli likely to be encountered during its operation and (2) the limit of detection (LOD) of the sensor must be below the threshold which the stimuli occurs [10]. The proposed thermodynamic sensor, while it was very successful detecting TATP at trace levels, would also detect the chemical intermediates acetone and hydrogen peroxide (H_2O_2), resulting in a false positive. TATP was also the only explosive analyte under investigation and whether it would be able to detect other energetic materials with far lower vapor pressures was uncertain. These issues needed to be addressed.

Thus, the specific objective of this work was to take the original sensor design proposed in 2012 and to make several key improvements to advance the sensor towards commercialization. This was done by increasing the selectivity for TATP of the metal oxide catalyst film using combinatorial chemistry techniques. Also, by combining a second independent sensing mechanism with the original thermodynamic sensor onto one orthogonal sensor platform, a redundancy system is in place to mitigate the detection of false positives. To increase the sensitivity of the sensor, a preconcentrator device was paired with the sensor to lower the limit of detection. Finally, in order to make the sensor more portable and efficient, a MEMS version of the sensor was designed and fabricated.

References

[1] Wilson, Clay. "Improvised Explosive Devices (IEDs) in Iraq and Afghanistan: Effects and Countermeasures." (2007): 1-3. Federation of American Scientists, 21 Nov. 2007. Web. 3 Sept. 2014.

[2] Barbero, Michael D. "Improvised Explosive Devices Are Here to Stay." *The Washington Post*. N.p., 18 May 2013. Web. 6 Sept. 2014.

[3] Saukko, Pekka, and Jay A. Siegel. "Improvised Explosive Devices." *Encyclopedia of Forensic Sciences*. Amsterdam: Elsevier, Academic, 2013. 59-63. Print.

[4] Intelligence Reform and Terrorism Prevention Act of 2004, Public Law, December 2004, 108-458.

[5] Caygill J. S., Davis F. and Higson S. P., "Current trends in explosive detection techniques," *Talanta*, vol. 88, pp. 14-29, 2012.

[6] Arshak K., Moore E., Lyons G. M., Harris J. and Clifford S., "A review of gas sensors employed in electronic nose applications," *Sensor Review*, vol. 24, pp. 181-198, 2004.

[7] Singh S., "Sensors-An effective approach for the detection of explosives," *Journal of Harzardous Materials*, vol. 144, pp. 15-28, 2007.

[8] Amani M., Chu Y., Waterman K. L., Hurley C. M., Platek J. M., Gregory O.J., "Detection of Triacetone Triperoxide (TATP) using a thermodynamic based gas sensor", *Sensors and Actuators B*, 162 (2012) 7-13.

[9] Oxley J. C., Smith J. L., Shinde K. and Moran J., "Determination of the vapor density of triacetone triperoxide (TATP) using a gas chromatography

headspace technique," *Propellants, Explosives, Pyrotechnics*, vol. 30, pp. 127-130, 2005.

[10] Barsan N., Koziej D. and Weimar U., "Metal oxide-based gas sensor research: How to," *Sensors and Actuators B*, vol. 121, pp. 18-35, 2007.

CHAPTER 2

LITERATURE REVIEW

2.1 Introduction to Explosives

An explosive is any substance that undergoes a rapid chemical reaction involving a large release of heat and gas byproducts that exert a high pressure on the environment [1]. This reaction can be initiated by a variety of factors, including friction, impact, shock, spark, flame or heating. Explosives can be categorized several different ways, but adhere to this general definition.

2.1.1 Classification of Explosive Compounds

Generally, most organic explosives have similar chemical structures. Covalently bonded chemical groups (nitro, nitramine, nitrate ester, etc.) are common since they facilitate internal redox reactions where covalent bonds like N-N and N-O break to form gaseous products like N_2 and CO_2 [1]. Because chemical structure is an indicator of how an explosive will behave, energetic compounds can be classified this way [2].

Beyond chemical structure explosives are also categorized based on their performance [3], as illustrated in Figure 2.1. An explosive is either a low or high energy explosive. Low energy explosives are propellants, smokeless powder, black powder or pyrotechnics. Low energy explosives deflagrate meaning rapid oxidation reactions propagate radially outward through the available explosive material away from the point of ignition coupled with a rapid release of gasses and heat. A low

energy explosive thus will burn and not explode unless confined in a vessel. When a low energy explosive is deflagrated in a closed shell, the pressure will increase until it reaches the critical pressure required to break the walls of the shell generating a shock wave due to the pressure difference between the inside and the outside of the vessel. In this way, a low explosive can be made to explode even though that may not be its intended purpose. For example, a pipe bomb, a very common IED, confines a deflagrating energetic material, like black powder, and relies on the gas release to rupture the pipe and propel the shrapnel through the atmosphere [4].

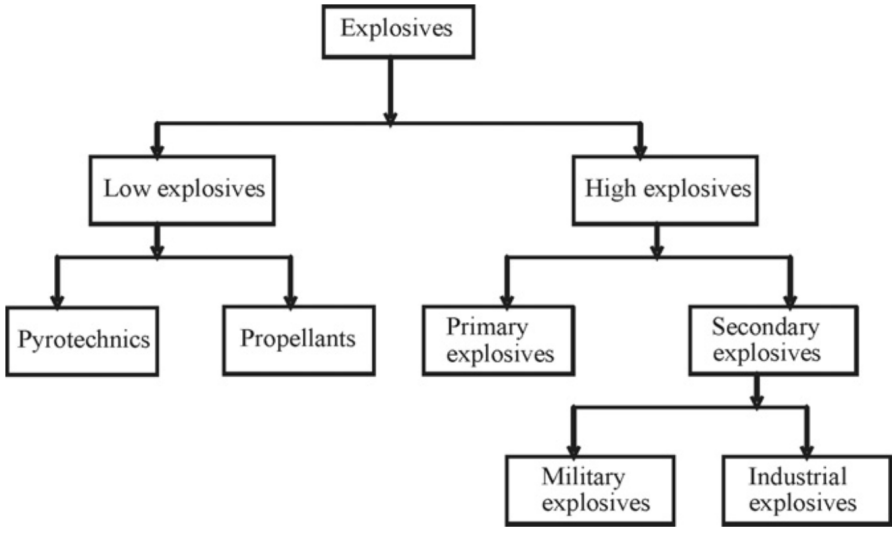

Figure 2.1 Hierarchy of explosives based on structure and performance.

High energy explosives do not require a shell or vessel in order to explode. Rather than deflagrate, high explosives detonate, meaning the rapid oxidation reactions happen at supersonic speeds, generating a shock wave on its own. High energy explosives are divided into two sub-categories based on how easily they are ignited. Primary explosives, often chemically unstable, require minimal energy to ignite. Secondary explosives are more stable and require either more energy or very

specific conditions to ignite, but often provide a much stronger explosion [4]. Often an easily-ignitable primary explosive will be paired with a secondary explosive to provide the necessary ignition energy to cause detonation.

2.1.2 Common Commercial Explosives

2,4,6-trinitrotoluene (TNT) is one of the most common commercially available explosives for military and commercial applications. It is valued because it is insensitive to shock and friction, which reduces the risk of accidental detonation. TNT melts at 80 °C, below its spontaneous detonation temperature, allowing it to be poured as well as safely combined with other explosives. TNT neither absorbs nor dissolves in water, which allows it to be used effectively in wet environments. Additionally, it is stable compared to other high explosives. Because of its widespread use, TNT is the standard by weight against which all explosives are typically compared [4-5].

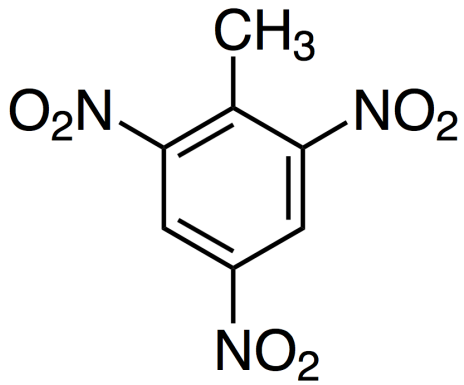

Figure 2.2 Molecular structure of trinitrotoluene (TNT).

RDX is another commonly found high explosive, particularly in weaponized devices. It considered to be one of the most powerful high explosives, with a detonation power 1.5 times greater by mass than TNT. It is also one of the most stable at room temperature, and will only deflagrate with the application of heat, requiring a

significant ignition charge for detonation to occur. It can be used by itself, but it is commonly found in a explosive mixtures [1,6].

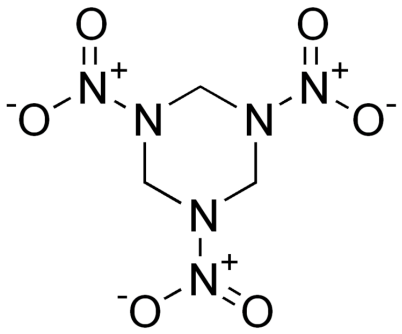

Figure 2.3 Molecular structure of RDX.

Nitroglycerine is an important energetic material historically. It is a powerful high explosive but in its pure form shows a high sensitivity to impact and mechanical stimuli. Thus it was impractical as a commercial explosive until 1867 when Alfred Nobel demonstrated how liquid nitroglycerine could be made into a stable gel by pairing it with an adsorbent, creating a material that later became known as dynamite. Nitroglycerine can be mixed with a range of adsorbents and additives to yield gelatinous explosives like dynamite, gelignite, blasting gelatin and propellants like cordite and ballistite [4-6].

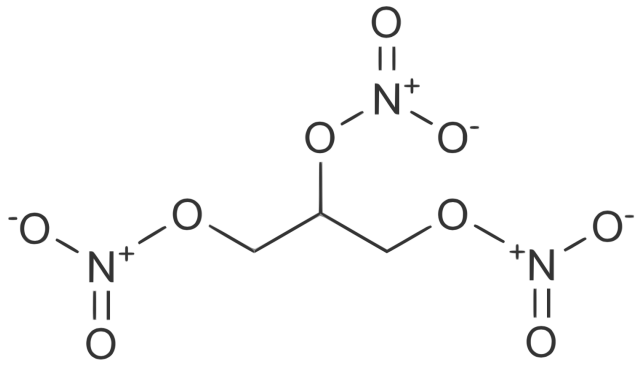

Figure 2.4 Molecular structure of nitroglycerin.

Pentaerythritol tetra nitrate (PETN) is a nitrate ester energetic explosive like nitroglycerine and is similarly sensitive to impact and mechanical stimuli in its pure form, however it is slightly more stable, thus it is used in many different explosive mixtures. PETN, mixed with TNT, is largely used as a secondary explosive in military applications. Associated with triacetone triperoxide (TATP) as an initiator, PETN is also used in terrorism attacks [6,7].

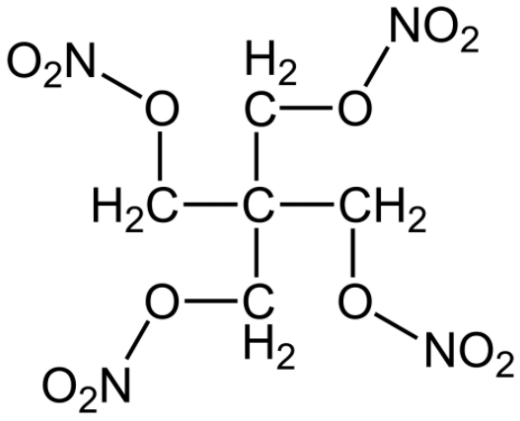

Figure 2.5 Molecular structure of pentaerythritol tetra nitrate (PETN)

Ammonium nitrate (NH4NO3) is commonly used in agriculture as a nitrogen fertilizer, but also as an oxidant agent in explosives. For use in explosives sensitized by high explosive ingredients, ammonium nitrate should be of a dense and non-

absorbent character, while for uses in conjunction with fuel oil, an absorbent form of ammonium nitrate is required. Ammonium nitrate is the main component of ammonium nitrate fuel oil (ANFO), a widely used bulk industrial explosive mixture which accounts for 80% of the explosives used annually in North America [5-6]. ANFO is used in coal mining, quarrying, metal mining and civil construction in undemanding applications. The popularity of ANFO is largely attributable to its low cost and high stability.

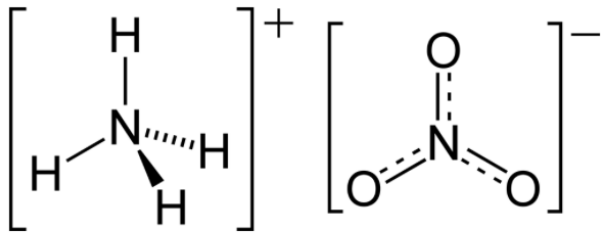

Figure 2.6 Molecular structure of ammonium nitrate.

2.1.3 Common Explosives Used in IEDs

Triacetone triperoxide (TATP) is one of the most commonly employed explosive compounds in IEDs because it can by synthesized from commonly found, inexpensive ingredients [7]. An organic peroxide explosive, TATP is extremely sensitive to heat, shock and friction. It is produced from hydrogen peroxide (H_2O_2)and acetone (C_3H_6O) in presence of strong acid (sulfuric acid) [8]. TATP has a relatively high vapor pressure which allows it sublime under room temperature [9]. Also, it is a very powerful explosive which produces approximately 80% of outward force that TNT produces with the same amount of explosive [4].

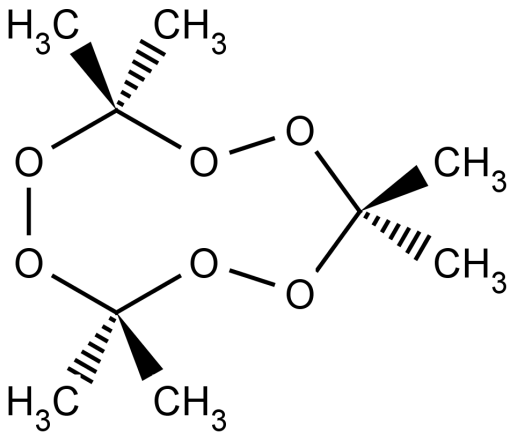

Figure 2.7 Molecular structure of triacetate triperoxide (TATP).

HMTD (hexamethylene triperoxide diamine) is another common homemade explosive, also from the peroxide family, used by terrorists in suicide bombings and other attacks [7]. HMTD is extremely sensitive to shock, heat and friction, making it dangerous to manufacture but ideal as a detonator. HMTD has been used in a large number of suicide bombing and other terrorist attacks all over the world [7].

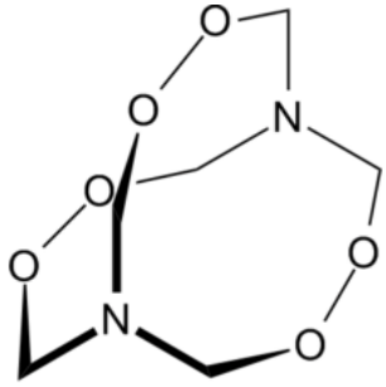

Figure 2.8 Molecular structure of HMTD

Ammonium nitrate fuel oil (ANFO) described above as a common commercial explosive is also frequently used by terrorists due to its low price, ease of use and availability [7]. Similar to ammonium nitrate, urea nitrate ($(NH_2)_2COH\text{-}NO_3$) is

another fertilizer- based high explosive that has been used in IEDs in many terrorist attacks, including the car bombs in Israel, Iraq and Afghanistan, and various other attacks elsewhere in the world [10-11]. Urea nitrate can be produced by simply mixing urea and nitric acid under controlled temperature.

This overview of explosives is important when considering the threat of IEDs. "Improvised" is the key word, for while weapons-grade explosives would better suit their purpose, militant groups and terrorists with limited resources will often have to get creative. For instance, peroxide based energetic compounds, like TATP, account for no more than 7-8% of all commercial and U. S. military explosive usage combined because TATP itself is unstable and dangerous, and their are often safer alternatives readily available [6]. But TATP and HMTD are used in IEDs all over the globe because of convenience [7].

Also, a secondary goal in constructing an IED is avoiding detection. Commercially made explosives contain a chemical tag, an inert compound that is easily detected and identified. The tag is usually a volatile organic compound easily picked up by a sensor or a bomb-sniffing dog [7]. It also has a forensic purpose, allowing authorities to trace the materials used in a bomb back to where it was made. Recent statistics on IEDS, however, indicate that only approximately 1 in 5 devices used in an explosive attack were constructed using commercially purchased or stolen explosives [1], meaning most IEDs are constructed with home-made explosives, which won't contain any chemical tag. To complicate matters, recent trends have shown that IEDs are often constructed using explosive chemicals that are deliberately

difficult to detect, primarily members of the peroxide explosive family, like TATP, making it priority for detection research [3].

2.2 Spectroscopic Techniques

Spectroscopic methods have been widely employed in the detection and identification of unknown substances. Generally speaking, samples are drawn from the air into a mass spectrometer where they are ionized. The resultant ions are separated via electrical and magnetic fields according to their mass charge ratio and are subsequently detected and quantified. These methods are typically highly selective and sensitive, but suffer from high turnover rates, large equipment and operating costs and low portability. Current research into the use of such devices focuses on reducing costs and minimization without sacrificing resolution [3].

2.2.1 Infra-red spectroscopy

Infra-red (IR) spectroscopy uses the infrared region of the electromagnetic spectrum to identify characteristic bonds and functional groups. Specifically a molecule's resonance frequency is measured—the frequency of the absorbed radiation that matches the transition energy of the bond or group that vibrates. The challenge with this technique is that chemical species with similar functional groups are difficult to distinguish between. Primera-Pedroso et al. reported an IR technique for the detection of high explosive residues that involve collecting the molecules on a metallic surface and obtaining an IR signature using fiber optic coupled Reflection/Absorption IR spectroscopy (RAIRS) [12].

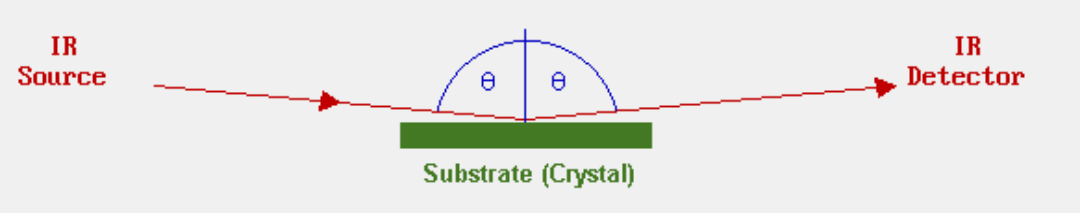

Figure 2.9 Schematic depicting the specular reflectance technique employs in Reflection/Absorption IR spectroscopy (RAIRS).

The technique relies on specular reflectance, meaning the incident IR beam is directed at the sample at an angle, passes through the sample, reflects off the metallic surface, passes through the sample again and is finally picked up by an IR detector. This method produced reportedly low detection limits for TNT, PETN, DNT and HMX but suffered from low selectivity. TNT, DNT and their analog dinotrobenzene (DNB) were nearly indistinguishable [13].

2.2.2 Ion mobility spectroscopy

Ion mobility spectroscopy (IMS) is one of the most widely used detection techniques due to its ability to characterize the sample both qualitatively and quantitatively as well as the low detection limits often attainable [14]. IMS works by characterizing a sample through the mobility of ions through the gas phase of the instrument while an electric field is applied. The sample vapors are ionized at atmospheric pressure before introduction into the drift tube. The drift times are related to the mass of the ions and by determining the mass to charge ratio, it is possible to identify components within the sample through comparison with known standards. The most commonly used ionization sources are the radioactive isotopes ^{63}Ni and ^{241}Am, which evoke a safety and environmental concern, especially when considering the production of a portable or handheld device. Investigation into enabling the

miniaturization and portability of an IMS apparatus for field deployment has increased. For instance, one particular group attempted to employ a corona discharge for ionization to minimize the risk associated with radioactive substances. However, while many groups are focusing on the scaling down of IMS, the size requirements of the detection mechanism presents a significant challenge. Decreasing the length of the drift tube, thereby decreasing the distance the ions have to travel to the detector, would cause a significant decline in sensitivity.

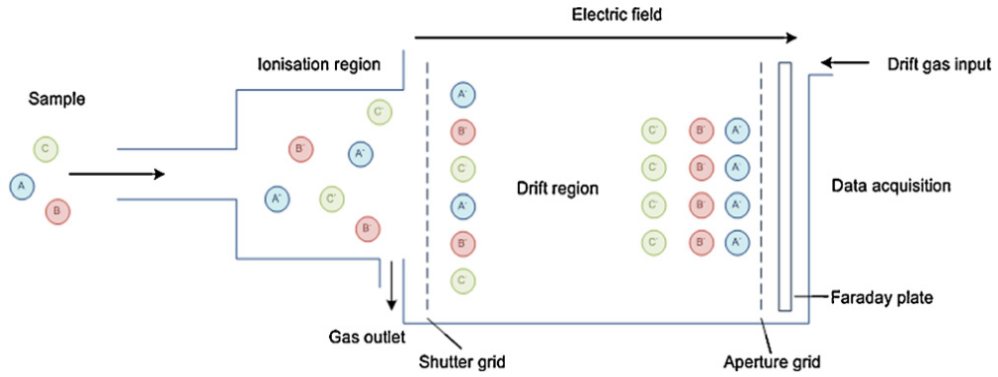

Figure 2.10 Simplified schematic of ion mobility spectrometer for detection of solids.

Concerning specifically the detection of explosives, IMS is the most successful and widely used technology for the detection of trace level nitro-organic explosives on handbags and carry on-luggage in airports throughout the US [14]. TNT, 2,4-DNT and 2,6-DNT, RDX, PETN and TATP have been widely studied with IMS technology [14-23], but TNT showed the most favorable response over any other explosives. This is likely because the gas phase chemistry of TNT is relatively simple and product ions have good thermal and chemical stability.

2.2.3 Mass spectroscopy

Mass spectrometry (MS) is a widely used technique in explosives detection because of its specificity in identifying substances and the speed at which results are obtained. MS separates and analyzes the chemical composition of an ionic species according to its mass/charge ratio. A sample enters an ionization chamber, then are accelerated towards an electromagnet that deflects the ions at an angle directly dependent on their mass charge ratio. They are subsequently collected and characterized by how far they've been deflected. Coupled technology has been used to enhance the mass resolving capability of mass spectrometry, one common combination being gas chromatography-mass spectrometry (GC/MS). Different particles are pre-separated with a gas chromatograph prior being introduced into ion source of mass spectrometer. Bench scale analysis of trace level explosives including ethylene glycol dinitrate (EGDN), DNT, TNT, PETN, RDX and Tetryl have been reported with great success and sensitivity[24-26]. The greatest barrier preventing MS from more widespread use is the substantial costs and space requirements to operate the device, coupled with a relatively lengthy sample preparation.

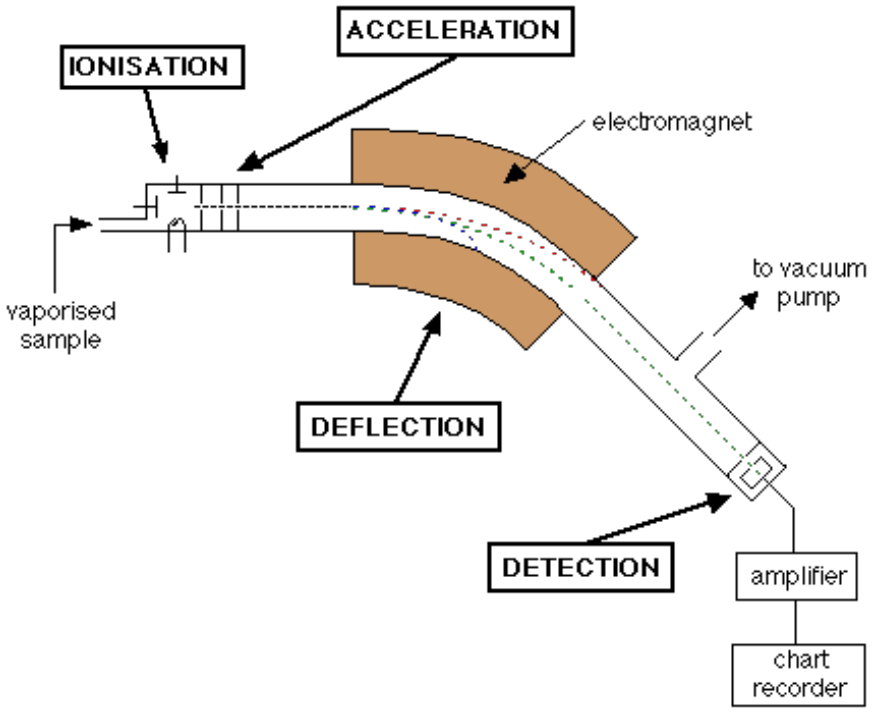

Figure 2.11 Simplified schematic of mass spectroscopy.

2.2.4 Raman spectroscopy

Raman spectroscopy measures the vibrational transitions in a sample through the collection and analysis of scattered photons once the sample has undergone laser excitation. An energy difference between the incident and the scattered photons can be observed when the molecule is excited by photon from ground state to excited state, or the other way around. The resulting spectra can be used as a fingerprint that can identify individual components of the sample. Due to the near instantaneous results and the ability to analyze samples at a substantial distance from the instrumentation, Raman spectroscopy has shown potential as an explosives detection system [7] and there has been considerable work in the area, especially in the creation of a miniature device [27-33].

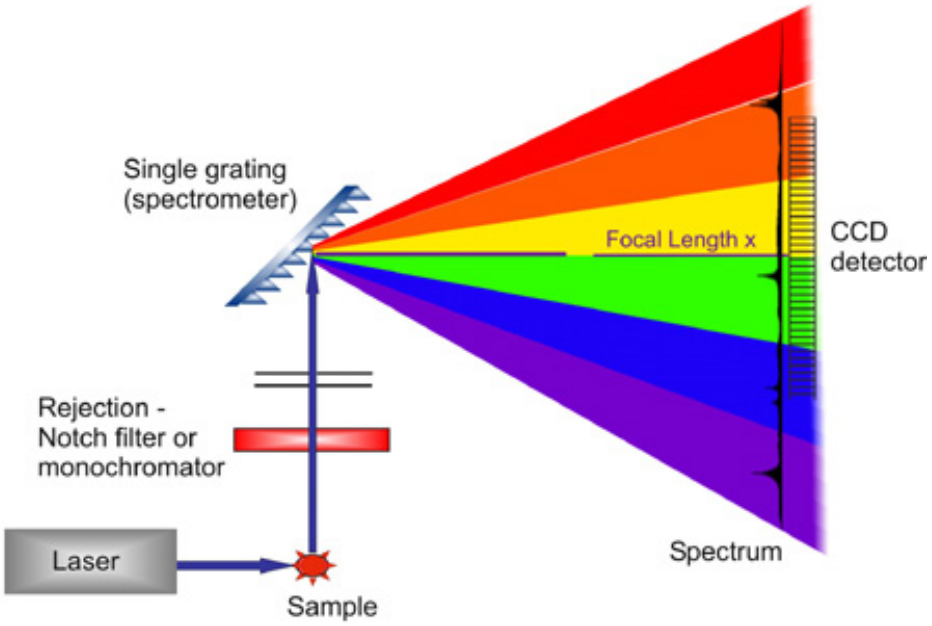

Figure 2.12 Simplified schematic of Raman spectroscopy.

One group was able to show the specific detection of TNT, DNT, RDX, and TATP was possible at distances up to 7 meters [33]. Detection limits for Raman spectroscopy, however, are not as low as other techniques; the detection limits for TNT and RDX were an order of magnitude lower than when using IMS. Also, due to ambient light interference, the device must be operated in an indoor, controlled environment and in the dark, limiting its current applications in field tests.

2.2.5 Terahertz spectroscopy

Terahertz technology has demonstrated the capabilities to both detect and identify trace and bulk explosives. Terahertz region usually refers to the frequency range of electromagnetic radiation between 0.1 and 10 THz. The most commonly used methods for terahertz spectroscopy are Fourier transform infrared (FTIR) spectroscopy and terahertz time-domain (THz-TDS) spectroscopy. Compared with FTIR, THz-TDS

spectroscopy has the advantage of more frequency coverage and higher signal-to-noise ratio (SNR). With advances in laser technology, small time-domain systems are available for handheld or remote detection [34-35]. Other techniques for generation of THz radiation include photo-mixing and electronic spectroscopy.

Detection of DNT, TNT, RDX, PETN and ammonium nitrate using terahertz spectroscopy in both gas phase and solid phase have been widely reported [36-44]. However, this technology suffers from several drawbacks that include: the frame rate speed, a loss of attenuation as distance from sample increases, and power requirements for the system [44].

2.3 Sensors

The alternative to spectrometry that can potentially address many of its issues is the use of low-cost, portable sensors [2]. Sensors contain an immobilized active material which can selectively recognize the target explosive via a number of physical phenomena. Transduction then occurs (via optics, electrochemistry or some other means) to convert the physical response to a measurable property. Sensors in general are very specific to their target analyte, however sensitivity is an issue. Most advances in sensors specifically for the detection of explosive compounds focuses on increasing sensitivity and lowering the detection limit. Yet, compared with spectroscopic instruments, gas sensors have the capability of performing continuous, real-time environmental monitoring and require fewer resources to manufacture, operate and maintain. Multiple sensors can also be networked and operated simultaneously to scan for several analytes at a time, while keeping the possibility of a portable device due to

their size. There are many types of sensors that operate on a variety of chemical properties. The most common types employed in the detection of explosives are outlined here.

2.3.1 Conductometric Sensors

Conductive sensors are a sensing system that measures the change in conductivity due to the interaction between a conducting material and the target analyte molecule. Conducting polymer composites and metal oxides (mostly semiconductors) are the most commonly utilized materials in conductivity sensors [45].

Polymer composites contain conducting particles suspended in an insulating polymer matrix. Gas molecules diffuse into the polymer, causing the polymer film to expand. The resulting expansion causes a reduction of the conducting pathways for charge carriers and an increase in the electrical resistance of the composite [46]. The drawbacks of polymers are their constrained detection range with certain gases and limited lifetime, though they do not require a heating element to operate.

Metal oxide gas sensors are based on measuring the conductivity change of the semiconducting material. Known more popularly as conductometric sensors, they are one of the most investigated groups of gas sensors due to the low cost of production, the flexibility of their use and their wide range of possible applications [47-48]. The conductivity change in the metal oxide is caused by the addition or removal of charge carriers by the physical adsorption to the oxide surface by the analyte molecule or the molecule's catalytic decomposition products. The sensitivity of conductometric sensor depends on many parameters, including film quality (thickness, density, grain

size, crystal structure and defects, etc.), type and loading of dopants, temperature at which the sensor is operated and species of target molecules [49-50]. Film quality varies from selected deposition approaches, including but not limited to chemical vapor deposition (CVD), RF sputtering or spin-coating, and post-deposition heat treatment protocols [51-53].

The detection of explosives, including DNT, TNT, RDX, and PETN using conductometric sensors has been widely reported [54-56], with detection limits as low as part per billion. However, conductometric sensors lack selectivity to molecules with similar functional groups, thus limiting their application in explosive recognition.

2.3.2 Optical Sensors

Owing to the number and reliability of optical methods, a vast number of optical transduction techniques can be used for sensor development [2]. These may employ linear optical phenomena, including absorption, fluorescence, phosphorescence, polarization, rotation, interference, etc., or non-linear phenomena, such as second harmonic generation. The choice of a particular optical method depends on the nature of the application and desired sensitivities.

One common type of optical sensor employed to detect explosive compounds are fiber optic sensors. They rely on the changes in the frequency or intensity of electromagnetic radiation (e.g. visible, infrared) to detect and identify the presence of chemicals. The system employs an array of sensory materials attached to the distal tips of an optical fiber bundle. Each sensor within the array responds differentially to vapor exposure so the array's fluorescence response patterns are unique for each analyte. Fiber optics are usually coupled with other optical techniques composing a

integrated sensor that uses optical fiber to detect chemicals by monitoring the changes in the frequency or intensity of electromagnetic radiation. Trace amount of DNT, TNT, PETN and RDX were reported being detected employing fiber optic sensors [57-59].

Fluorescence sensors have been widely used in detecting heavy metals, ions, combustible and toxic gases, etc. Fluorescence occurs when an orbital electron in a molecule is excited to a higher quantum state by some type of energy, then relaxes to its ground state by emitting a photon [60]. Semiconducting polymers are excellent candidates for fluorescent materials due to their electron rich behavior. Nitro-aromatic explosives (which are typically electron deficient) bind to these electron rich semiconducting polymers and quench their fluorescence by an electron transfer mechanism, generating a measurable electronic signal. Due to its high sensitivity and ease of operation, fluorescence sensors have been used in identification of nitro-aromatic explosives in recent years, including TNT, DNT, PETN, etc. [60-63]. Miniaturization has also been studied and Caron et al. were able to detect trace amount of TNT on a piece of cotton using a portable fluorescent device [62]. A major disadvantage, however, of fluorescence sensors (and optical sensors in general) is their lack of selectivity and several interfering factors (temperature, pressure, humidity, etc.) can alter sensor response.

2.3.3 Mass Sensors

Mass sensors typically adsorb the chemicals of interest onto the surface and the device detects change in mass. The detection can be accomplished through changes in surface acoustic waves (SAW) or by actual bending or a change in the shape of the

device as mass is accumulated (micro-cantilever devices) [64]. Mass sensors can be very sensitive to trace levels of the target analyte, but suffer from short lifetimes due to the irreversible nature of some analyte-sensor interactions.

SAW sensors are composed of a piezoelectric substrate with an input and output interdigitated transducer deposited on top of the substrate. The sensitive membrane, which can be a polymer or liquid crystal, is placed between the transducers which measure the disturbance in sound waves caused by the chemical interference of the analyte. If a vapor is present on the surface, it will interact and alter the properties of the wave (frequency, amplitude, or phase). SAW devices have been used for detecting explosives such including DNT and TNT [64].

Quartz crystal microbalance (QCM) based sensors rely on a typical micro-cantilever that measures the surface force induced by the interaction with the substance [2]. The resulting differential stress leads to the bending of the cantilever. This QCM sensor has the advantage of superior mass sensitivity, smaller size and low cost. Explosives including TNT, RDX, TATP and PETN have been reported of successful detection using QCM sensors [65-67].

2.3.4 Calorimetric Sensors

All chemical reactions and physical changes have an associated generation or consumption of energy, mostly in the form of heat. Thus, quantitatively measuring this thermal energy change can provide a simple and universal method for characterizing chemical or physical processes [68]. This type of thermal analysis, also known as calorimetry, is a widely used technique for obtaining both qualitative and quantitative information about thermal transitions associated with a particular material or process.

Explosives and energetic materials are designed to provide enormous amount of energy during chemical reaction leading to explosion, making calorimetry an ideal technique for their detection [69]. One major disadvantage is the requirement of such a device to be in a constrained and isolated space for accurate measurements, and thus would be challenging to implement in a portable device and difficult to obtain continuous measurements. Differential scanning calorimetry (DSC) can be employed to meet all the challenges. It measures the differential heating power between a sample and a reference material as their temperature is varied in a range of interest, directly determining the thermodynamic properties of the sample [70]. Several researches are reported using a DSC technique for explosive detection [71-73]. Still, DSC suffers from a lack of stability and is inability to conduct analysis quantitatively.

2.4 Detection of TATP Using a Thermodynamic Gas Sensor

In the fall of 2012, our research group at URI was presented with a unique problem: the specific detection of the triacetone triperoxide (TATP), a dangerous explosive compound [71]. Unlike most other explosives, TATP contains no nitro or metal groups, instead unstable peroxide bonds facilitate its explosive nature. As a result, it does not fluoresce and has no significant absorption in the ultraviolet region of the spectrum, making it difficult to detect with most conventional spectroscopy techniques. Several endeavors were successful in detecting TATP, but many suffered from the aforementioned limitations of bench-top techniques, including slow response times, low sensitivity, portability issues and barriers preventing continuous

monitoring. TATP however is a volatile compound and readily sublimes at room temperature, making it the ideal candidate for vapor phase detection. A sensor was thus developed to continuously detect vapor phase TATP in real-time.

In designing the sensor, a thin-film sensor employing a metal oxide catalyst was chosen. The sensor works by measuring the heat generated or consumed by the catalyst in the presence of TATP vapor, principles used in calorimetry. A digital control system enables a thin-film microheater, coated with the metal oxide catalyst, to be scanned over a specific temperature range. The power difference caused by the catalytic reaction to TATP can be recorded at different temperatures, generating a signature curve unique to TATP and the specific metal oxide, which can then be used to identify an unknown vapor as TATP.

This approach and sensor design has several key advantages. It was hypothesized that TATP and the metal oxides would interact differently at different temperatures. Metal oxide films are robust enough withstand the necessary temperatures in a full thermal scan [48]. Other material candidates, like several varieties polymers, would not be able to withstand the temperature. The sensors designed in this way can also be produced at a low cost and in bulk, also allowing for a great amount of control over the species of metal oxide used [50]. Their dimensions allow use in portable devices and for the potential to network multiple sensors at once, each employing a different metal oxide.

Results from sensor testing confirmed these advantages. Figure 2.13 shows the sensor's resoponse to 8 ppm TATP using a number of different catalysts including WO_3-TiO_2, V_5O_5, SnO_{2-x}, ZnO and Nb_2O_3. Each of the five oxide catalysts show a

unique response as a function of temperature ranging from no significant peak response for Nb_2O_3 to well defined peaks for both SnO_{2-x} and ZnO. Figure 2.14 compares the sensor's response as a function of temperature to TATP with that of hydrogen peroxide (H_2O_2), one of the suspected decomposition products of TATP. Two different metal oxide catalysts were used and in each plot, the responses to TATP and H_2O_2 were similar in shape and magnitude. This suggested that the sensors were detecting H_2O_2 when TATP vapors were delivered to the sensor, evidence that H_2O_2 was the product of catalytic decomposition. Under normal conditions, in the absence of a catalyst, it is widely reported that the major decomposition product of high purity TATP in air is acetone [8-9,74-75]. Therefore, the expected result would have been that TATP tracked the response of acetone, and not H_2O_2. The fact that the opposite had occurred reinforces the idea that catalytic decomposition at elevated temperatures is the detection mechanism.

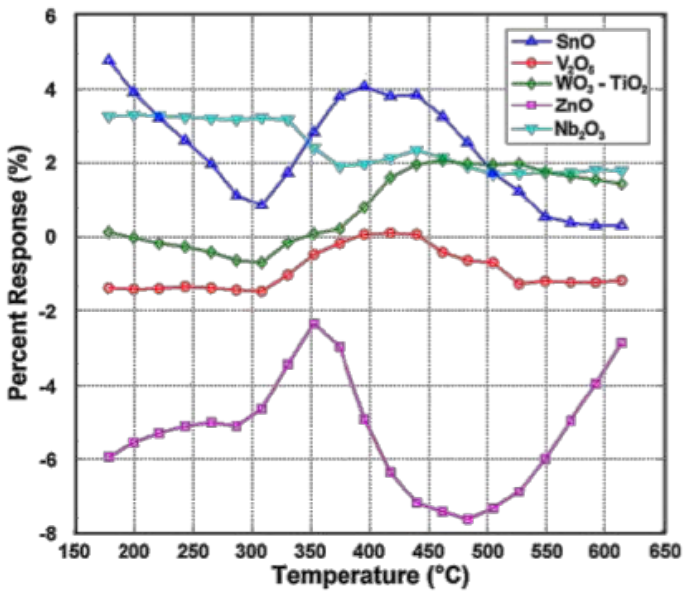

Figure 2.13 Response as a function of temperature using several catalysts to detect TATP (8 ppm) including WO_3–TiO_2, V_2O_5, SnO_{2-x} and ZnO, measured using the static testing approach.

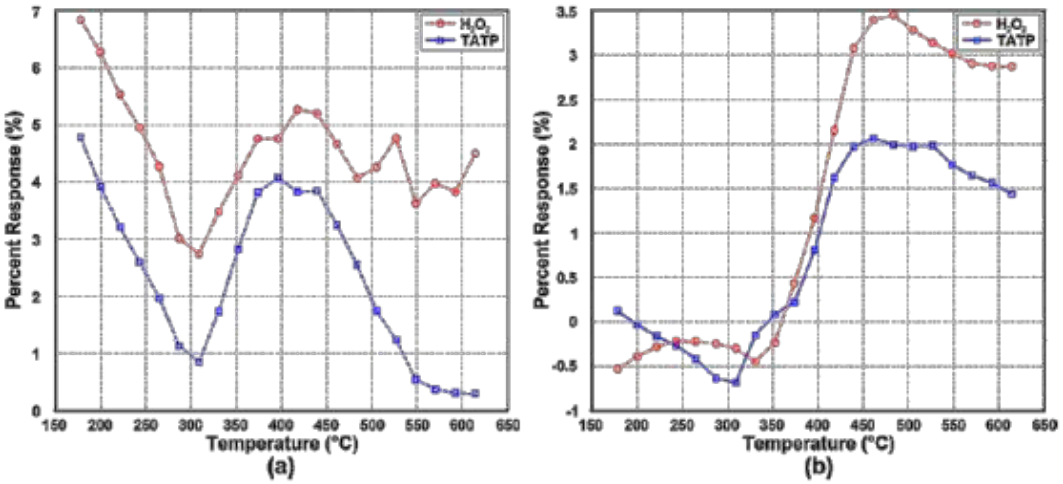

Figure 2.14 Percent response in 8 ppm TATP and 9 ppm H_2O_2 as a function of temperature for (a) tin oxide and (b) tungsten oxide catalysts, measured using the static testing approach.

In order to investigate this further, the responses to acetone and peroxide using both stoichiometric and non-stoichiometric copper oxide to acetone and peroxide were obtained, as seen in Figure 2.15. Using both films, the response to acetone is much greater in magnitude than that of H_2O_2 and again the responses of TATP track peroxide. These plots also show that non-stoichiometric copper oxide (CuO-Cu_2O) reacts to H_2O_2, but by changing the catalyst to stoichiometric copper oxide (Cu_2O), the signal was dampened. This suggested that results can be improved by specifically engineering the catalyst film to select for or against a chemical species, opening up several possibilities for catalyst enhancement.

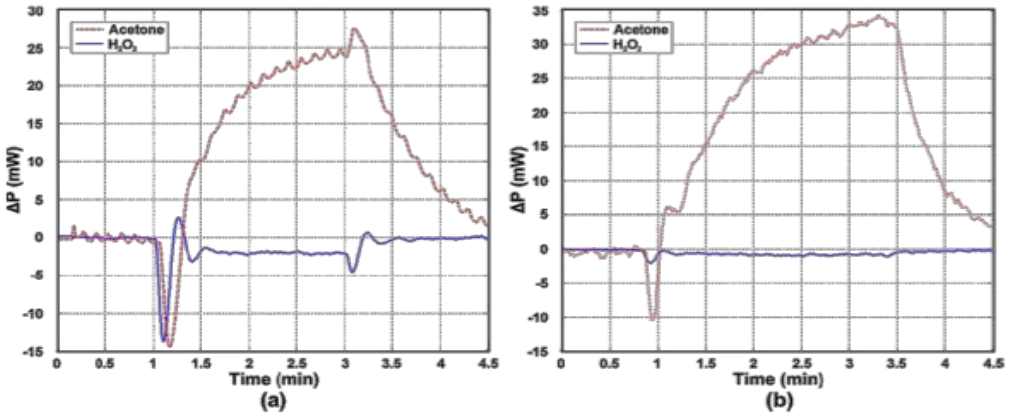

Figure 2.15 Response of (a) CuO–Cu_2O and (b) Cu_2O in acetone and H_2O_2 at 330℃.

2.4 Enhancing Detection

The original thermodynamic sensor was able to successfully detect TATP vapor at the part per million level (ppm) and due to the robust nature of the sensor, it showed great promise for eventual commercial use. However, there were a few critical limitations. An ideal sensor must meet two important criteria: (1) the sensor must respond to one environmental stimulus and be insensitive to any other stimuli likely to be encountered during its operation and (2) the limit of detection (LOD) of the sensor must be below the threshold which the stimuli occurs [2]. The proposed thermodynamic sensor, while it was very successful detecting TATP at trace levels, would also detect the chemical intermediates acetone and hydrogen peroxide (H_2O_2), resulting in a false positive. The responses to TATP and H_2O_2 were very similar, opening the possibility for false positives. TATP was also the only explosive analyte under investigation and whether it would be able to detect other energetic materials with far lower vapor pressures was uncertain. These issues needed to be addressed. In order to address the shortcomings, a variety of methods were employed to increase

sensitivity and selectivity in order to progress the sensor towards eventual field testing and commercialization.

2.4.1 Nanocomposite Catalysts

A number of investigators have employed metal oxide catalysts in a variety of gas sensor platforms. Metal oxide semiconductors, for example, have been successfully used to detect trace levels of toxic gases such as CO, HS_2, H_2 and NO_X [76-78]. A majority of these conductometric sensors employed metal oxide catalysts, and as such exhibited responses that depend on changes in the electrical properties of the catalyst when exposed to the target gas. These include changes in electrical conductivity [76-78], changes in dielectric constant of the metal oxide [79], and change in work function [80-81]. Other responses reflect changes in optical properties of the metal oxide catalyst [82-83]. However, one disadvantage in using metal oxides, as well as all other types of solid-state gas sensors, is their poor selectivity due to their inability to distinguish between complex target molecules [76]. In a previous study, a gas sensor was demonstrated, which was capable of detecting TATP at trace levels using a SnO_2 catalyst based on the catalytic decomposition of TATP to form hydrogen peroxide [71]. However, those sensors exhibited little or no selectivity between TATP and hydrogen peroxide, making them susceptible to false positives in the presence of other peroxides and related precursors.

Researchers [83-84] have reported that the sensitivity of metal oxide based sensors can be enhanced by the direct exchange of electrons between the oxide semiconductor and noble metals such as Pd, Au, and Pt. The addition of such metals increased the rate of specific reactions on the surface of oxide crystals due to spill-

over effects, which actually changed the reaction mechanism in some cases through modification of surface energy states [83-84]. In our case, additions of palladium to SnO_2 catalysts may not only lower the detection limit by increasing the decomposition rate of TATP, but may also provide a different reaction path to avoid forming intermediates, such as H_2O_2 and thus, provide a sensor response to TATP that is significantly different from H_2O_2. Consequently, a gas sensor employing metal oxide catalysts with improved sensitivity and selectivity over H_2O_2 was the motivation for this study.

In the present investigation, we utilized combinatorial chemistry techniques to screen the Pd:SnO_2 nanocomposite catalysts with various palladium loadings for the purpose of optimizing sensor sensitivity and selectivity. Our thermodynamic sensor platform measures the heat effect associated with the interaction of a target gas molecule with the nanocomposite metal oxide catalyst deposited over the surface of a microheater. The heat effect associated with the catalytic decomposition of TATP was monitored by thermally scanning the microheater from room temperature to 450℃. The characteristic heat affects were measured as the target molecules of interest such as TATP, H_2O_2 and acetone were passed over the catalyst coated microheater. In this way, the controlled addition of palladium to a SnO_2 matrix was used to systematically investigate sensor response and selectivity of TATP over that of H_2O_2.

2.4.2 Orthogonal Gas Sensors

Sensors that rely on measuring the electrical conductivity changes in a semiconducting metal oxide, also known as conductometric sensors, have been widely exploited due to their excellent sensitivity under atmospheric conditions. Metal oxides

such as SnO, SnO_2, In_2O_3, WO_3, TiO_2 and ZrO_2 have been used to detect simple gas molecules at trace levels and even complex explosive compounds. The change in resistivity of the metal oxide when exposed to target molecules is due to adsorption or reaction processes when target gases interact with the surface of metal oxide. Here, the free charge carriers are transferred from the semiconductor to the target gas or vice versa. Gases of the same type, either acceptor gases (which tend to accept free electrons) or donor gases (which tend to lose free electrons), will cause similar changes in resistivity, which makes it difficult to determine the nature of the interactions at the gas/solid interface. All of this translates into poor selectivity, which is a major drawback that impedes the application of conductometric sensors [46-53].

The original thermodynamic based gas sensor is capable of detecting explosives at the part per million level. It measures the heat effect due to the catalytic decomposition of target molecules. The sensor has relatively high selectivity down to the part per million level among peroxide based compounds [85]. To further improve its sensitivity without sacrificing selectivity to threat chemical compounds, this thermodynamic sensing platform was combined with a conductometric platform, in such a way that the same catalyst was simultaneously interrogated by two techniques. Combining these two complimentary sensing techniques provides a certain redundancy in sensor response that mitigates the detection of false positives and negatives. One major challenge was that most catalysts with stoichiometric amount of oxygen exhibited maximum sensitivity in terms of the thermodynamic signal (response from thermodynamic platform) while the conductometric signal (response from the conductometric platform) requires a catalyst with non-stoichiometric amount

of oxygen. Thus, a hybrid catalyst with multiple oxidation states was developed as part of the study to fulfill this requirement. Two different metal oxide catalysts were employed to detect explosives using this new platform and to confirm that this approach is a viable one.

2.4.3 Preconcentration

Modifying the sensor design to intrinsically decrease the limit of detection can only go so far. Air has complex characteristics and there are far more variables to consider when moving from a carefully controlled bench-top experiment using purified air to an actual realistic air sample from an airplane jetway or other public location. Air is a heterogeneous system composed of gases, liquids and solid particles and can easily change due to weather effects. The particular analyte that is under investigation may also be so dilute in the atmosphere that it falls below the already low detection limit of the sensor [86].

Further methods can be implemented to increase the surface are of the catalyst to ensure more explosive particles come in contact with the film and react, thereby increasing the sensor signal. Eventually, however, the detection limit will reach a plateau due to the physical limitations of the detection mechanism [48]. Therefore, extrinsic methods must be used to ensure more of the analyte is delivered to the sensor, and one common method of accomplishing this is pre concentration. Generally speaking, the term “preconcentrator” refers to a device used on a gas sample before it is delivered to the sensor that collects the analyte under investigation, thus the sensor will have more analyte to respond to. In analytical chemistry, preconcentration is often used before GC, MS etc. if an analyte is particularly dilute [89].

There are two primary methods of preconcentration: active and passive. Active preconcentration involves a controlled volume of a gas sample through or over an absorbent medium that will trap the analyte molecules. This method enables an efficient turnover and the adsorbent material can be varied to suit a particular analyte, or multiple adsorbents can be used to attract multiple analytes. However, a pump or flow control system is required to control the flow of sampled gas to the adsorbent surface [86]. Passive preconcentration relies more on the diffusion of the analyte particles through a specific medium to the adsorbent. It relies on the creation of a concentration gradient between the gas sample and the strong adsorbent through the medium. Passive prconcentrators are often simple in design and do not require a volume control mechanism. They do, however, operate on a slower-time scale because the rate of preconcentration is wholly dependent on the rate of diffusion though the chosen medium. Additionally, a different device must be made per each adsorbent material used. Passive preconcentration are thus only suited for batch processes and for longer collection periods [86].

Equally important to the preconcentrator's ability to absorb a particular analyte is its ability to desorb the analyte when required. Commercially, this is accomplished by use of a solvent or by thermal desorption. Passive preconcentrators used for batch processes will use a solvent, dichloromethane or carbon disulfide being the most common, but this method is undesirable because whatever detector or sensor is then used for the analyte must be able to discriminate between the trace components and the bulk solvent. Thermal desorption is thus used more often and can be implemented in an active or passive preconcentrating system. It involves heating the absorbent

material to force desorption. It works particularly well with volatile organic compounds [86-87].

Material selection is thus an important factor in preconcentration design [86,97]. The material must be a good adsorbent at cold or room temperatures and must be capable of desorption at elevated temperatures. It must also not react with the analyte or change the analyte in any way prior to detection. Typical adsorbents include rubbery polymers, granular polymers and granular carbon nanotube structures. Providers of such adsorbents typically provide extensive absorption and desorption data for different volatile organic molecules in order to allow the specific selection of a material for a specific purpose. There is very little data for the same absorbents concerning most of the common energetic or explosive materials, so adsorption selection can be difficult [91].

Polymers are a frequently used sorbent material, likely because different polymer films can be made with a variety of monomers with an assortment of functional groups fairly easily [94]. As a result, polymer films are often rather specific adsorbents, only attracting certain chemicals or chemical groups. Polystyrene is a common sorbent that has had much success in attracting volatile oxygenated compounds and (important for our purpose) nitro-amines like TNT. Polystyrene is often used because the as deposited surface area of a film is porous and has relatively high (around 350 m^2/g) giving polystyrene films a high retention volume. Another common polymer sorbent is poly(2,6-diphenyl-p-phenylene oxide), better known by its commercial moniker Tenax. Unlike polystyrene and other highly specific polymer sorbents, Tenax is a non-discriminating sorbent that will trap most organic compounds

with few exceptions, but by comparison the as deposited surface area is much lower at $30m^2/g$ thus it has a far lower retention volume. A serious drawback for polymer sorbents in general is their limited temperature stability. Many organic polymers begin to decompose at temperatures exceeding 200℃, restricting the use of thermal desorption [86,94].

Graphitized carbon blacks are also used as a non-specific, non-porous sorbents. The graphitization process eliminates specific adsorption sites and hinders the formation of hydrogen bonds, resulting in the poor adsorption of small polar molecules. This in an attractive material choice for high moisture environments, because graphitized carbon blacks have a low affinity for moisture [86].

Carbon molecular sieves (CMSs), which are microporous materials with a narrow pore-size distribution, intended to adsorb light hydrocarbons, which has been accomplished successfully for several applications. Often CMSs must be paired with a second type of sorbent to attract larger compounds because once adsorbed into the pores of a CMS, larger molecules desorb with great difficulty at much higher temperatures. They also have a strong affinity for water molecules, an undesirable characteristic for ambient air sampling where humidity is a constantly changing variable [86].

Carbon nanotubes have recently attracted attention due to their properties. They are essentially a sheet of graphite rolled into a tube as either single or multi-walled structures. The result is a very porous structure capable of adsorbing a variety of organic compounds. Nanotubes have shown highly favorable adsorption and

desorption with a relatively large retention volume, all while remaining unaffected by humidity, but lack the analyte specificity of other sorbents [86].

The most common sorbent used in air sampling is activated charcoal. It is useful in several preconcentration applications because it has a high specific surface area (800-1500 m^2/g), a broad pore-size distribution and excellent thermal stability. The drawbacks of charcoal, unfortunately, are many, including poor specificity, high water retention, the irreversible adsorption of compounds with certain functional groups, and a slight tendency to catalytically decompose certain analytes [86-91].

Challenges arise, however, when attempting to adapt preconcentration to a continuous monitoring system. Most conventional techniques are intended for batch use. For a preconcentrator to be used for the thermodynamic sensor design, it will have to be operated continuously, or at least semi-continuously. The most common method of real-time preconcentration is cryotrapping, which involves cooling the absorbent material to temperatures well below the boiling point of the volatile compounds being targeted [86]. The analyte would condense on the sorbent surface and then be siphoned off for analysis. This method enhances the trapping ability of the sorbent material, but with a few drawbacks. Compounds can condense onto the absorbent indiscriminately if the temperature is not tightly controlled. Cyotrapping can also be a troublesome method to use in a high moisture environment, since the primary condensate would be water. The analyte in question would still be diluted, defeating the preconcentrator's purpose. Another common method of continuous preconcentration is the use of sophisticated membrane systems to selectively filter incoming air samples of impurities for detection [93]. This method, however, is

mostly applied to particulates, as the engineering of membranes to filter vapors is a far more specific and daunting task.

Thus, in the realm of explosive detection, a preconcentrator designed for the specific purpose of real-time, continuous collection of vapor phase explosive molecules is desirable. This particular application requires efficiency in the adsorption and desorption of the analyte, as well as the efficiency switching from adsorption to desorption mode. Above all, it must also be cost effective, easily maintained and robust. This particular work investigates the design of a simple and inexpensive preconcentrator for the detection of explosive compounds, such as TATP, DNT and AN, which relies on spin-coated polymer films as the adsorbent. Experiments were designed to evaluate the efficiency of polystyrene as an adsorbent and to evaluate its effectiveness during continuous operation.

2.4.4 MEMS

A limitation of the thermodynamic sensor is its size. The time it takes to heat the sensor to a predetermined set-point and the time it takes for the sensor to thermodynamically respond to explosive molecules is dependent on the thermal mass of the sensor. In terms of portability, it is desirable to minimize the power requirements of the sensor. Its physical size also limits the amount of sensors that can be organized into sensor arrays. The next logical step to improve the performance of the sensor is to minimize the design, thus a microelectromechanical system (MEMS) based sensor has been proposed to address the shortcomings of the solid state sensor.

Microelectromechanical systems are microscopic devices that utilize the mechanical properties of silicon to form flexible membranes capable of moving in

response to changes in pressure, rather than on the electrical properties of silicon like an integrated circuit. By detecting this motion and converting it to an electrically measurable signal, pressure can be accurately sensed. Examples of MEMS based sensors include acceleration sensors used for automobile air bag deployment control, pressure sensors mounted on the tip of catheters for use in intracardiac monitoring of blood pressure, and chemical sensors that quantitatively detect gaseous compounds. MEMS based sensors yield many advantages which make it an ideal platform for repeatability and mass production. Due to the relatively small scale, integrated circuit fabrication techniques allow hundreds or thousands of identical devices to be built simultaneously on a single silicon wafer. Compared to building up a device from individual components, the simplicity of fabrication greatly reduces the cost and improves the reliability. Meanwhile, MEMS can be packaged into arrays and integrated with electronics that require much less power, which often find applications where weight, power and space are critical [95-98].

For sensor application, one of the most important advantages of MEMS is that they improve sensitivity and reduce the response time.. With smaller scale, much less heat consumption is required for MEMS devices, which would greatly benefit sensors where most of the energy is spent to heat the ceramic substrate. Silicon which usually is employed as the substrate material of MEMS device, has relatively small heat capacity (19.79 J/mol·K) but larger thermal conductivity (149 W/m·K), and thus can reach designated temperature in a shorter period of time, compared with other materials, i.e. aluminum oxide. As a result, faster response time can be expected.

References

[1] Agrawal J. P. and Hodgson R. D., Organic Chemistry of Explosives, Chichester, UK: John Wiley & Sons, Ltd, 2007.

[2] Singh, S., "Sensors-An effective approach for the detection of explosives," Journal of Harzardous Materials, vol. 144, pp. 15-28, 2007.

[3] Caygill, F. Davis and S. P. Higson, "Current trends in explosive detection techniques," Talanta, vol. 88, pp. 14-29, 2012.

[4] Kubota, Naminosuke. Propellants and Explosives: Thermochemical Aspects of Combustion. Weinheim: Wiley-VCH, 2007. Print.

[5] T. Urbanski, Chemistry and Technology of Explosives, London: Pergamon Press, 1964.

[6] Meyers, Sydney, and Edward S. Shanley. "Industrial Explosives - a Brief History of Their Development and Use." *Journal of Hazardous Materials* 23.2 (1990): 183-201. Web.

[7] Saukko, Pekka, and Jay A. Siegel. "Improvised Explosive Devices." *Encyclopedia of Forensic Sciences*. Amsterdam: Elsevier, Academic, 2013. 59-63. Print.

[8] Oxley J. C., Smith J. L., Shinde K. and Moran J., "Determination of the vapor density of triacetone triperoxide (TATP) using a gas chromatography headspace technique," Propellants, Explosives, Pyrotechnics, vol. 30, pp. 127-130, 2005.

[9] Oxley J. C., Smith J. L., Shinde K. and Moran J., "Determination of the vapor density of triacetone triperoxide (TATP) using a gas chromatography

headspace technique," Propellants, Explosives, Pyrotechnics, vol. 30, pp. 127-130, 2005.

[10] Wilson, Clay. "Improvised Explosive Devices (IEDs) in Iraq and Afghanistan: Effects and Countermeasures." (2007): 1-3. Federation of American Scientists, 21 Nov. 2007. Web. 3 Sept. 2014.

[11] Barbero, Michael D. "Improvised Explosive Devices Are Here to Stay." *The Washington Post*. N.p., 18 May 2013. Web. 6 Sept. 2014.

[12] O. M. Primera-Pedrozo, Y. M. Soto-Feliciano and L. C. Pacheco-Londo, "Detection of high explosives using reflection absorption infrared spectroscopy with fiber coupled grazing angle probe/FTIR," Sensing and Imaging, vol. 10, pp. 1-13, 2009.

[13] J. Janni, B. D. Gilbert, R. W. Field and J. I. Steinfeld, "Infrared absorption of explosive molecule vapors," Spectrochimica Acta Part A: Molecular and Biomolecular Spectroscopy, vol. 53, pp. 1375-1381, 1997.

[14] S. D. Huang, L. Kolaitis and D. M. Lubman, "Detection of explosives using laser desorption in ion mobility spectrometry/mass spectrometry," Applied Spectroscopy, vol. 41, pp. 1371-1376, 1987.

[15] F. W. Karasek and D. W. Denney, "Detection of 2,4,6-trinitrotoluene vapours in air by plasma chromatography," Journal of Chromatography, vol. 93, pp. 141-147, 1974.

[16] G. E. Spangler and P. A. Lawless, "Ionization of nitrotoluene compounds in Negative ion plasma chromatography," Analytical Chemistry, vol. 50, pp. 884-892, 1978.

[17] S. D. Huang, L. Kolaitis and D. M. Lubman, "Detection of explosives using laser desorption in ion mobility spectrometry/mass spectrometry," Applied Spectroscopy, vol. 41, pp. 1371-1376, 1987.

[18] G. E. Spangler, J. P. Carrico and D. N. Campbel, "Recent advances in ion mobility spectrometry for explosives vapor detection," Journal of Testing and Evaluation, vol. 13, pp. 234-240, 1985.

[19] G. R. Asbury, J. Klasmeier and H. H. Hill, "Analysis of explosives using electrospray ionization/ion mobility spectrometry (ESI/IMS)," Talanta, vol. 50, pp. 1291-1298, 2000.

[20] G. A. Eiceman, D. Preston, G. Tiano, J. Rodriguez and J. E. Parmeter, "Quantitative calibration of vapor levels of TNT, RDX, and PETN using a diffusion generator with gravimetry and ion mobility spectrometry," Talata, vol. 45, pp. 57-74, 1997.

[21] T. Khayamian, M. Tabrizchi and M. T. Jafari, "Analysis of 2,4,6- trinitrotoluene, pentaerythritol tetranitrate and cyclo-1,3,5-trimethylene-2,4,6- trinitramine using negative corona discharge ion mobility spectrometry," Talanta, vol. 54, pp. 515-529, 2001.

[22] T. L. Buxton and P. B. Harrington, "Rapid multivariate curve resolution applied to identification of explosives by ion mobility spectrometry," Analytica Chimica Acta, vol. 434, pp. 269-282, 2001.

[23] G. A. Buttigieg, A. K. Knight, S. Denson, C. Pommier and M. B. Denton,"Characterization of the explosive triacetone triperoxide and detection

by ion mobility spectrometry," Forensic Science International, vol. 135, pp. 53-59, 2003.

[24] J. M. Perr, K. G. Furton and J. R. Almirall, "Gas chromatography positive chemical ionization and tandem mass spectrometry fot the analysis of organic high explosives," Talanta, vol. 67, pp. 430-436, 2005.

[25] J. A. Mathis and B. R. McCord, "The analysis of high explosives by liquid chromatography/electrospray ionization mass spectrometry: multiplexed detection of negative ion adducts," Rapid Communications in Mass Spectrometry, vol. 19, pp. 99-104, 2005.

[26] O. L. Collin, C. M. Zimmermann and G. P. Jackson, "Fast gas chromatography negative chemical ionization tandem mass spectrometry of explosive compounds using dynamic collision-induced dissociation," Mass Spectrometry, vol. 279, pp. 93-99, 2009.

[27] M. Wu, M. Ray, K. H. Fung, M. W. Ruckman, D. Harder and A. J. Sedlacek, "Stand-off Detection of Chemicals by UV Raman Spectroscopy," Applied Spectroscopy, vol. 54, pp. 196-220, 2000.

[28] M. D. Ray, A. J. Sedlacek and M. Wu, "Ultraviolet mini-Raman lidar for stand-off, in situ identification of chemical surface contaminants," Review of Scientific Instruments, vol. 71, pp. 3485-3489, 2000.

[29] N. Gupta and R. Dahmani, "AOTF Raman spectrometer for remote detection of explosives," Spectrochimica Acta A, vol. 56, pp. 1453-1456, 2000.

[30] J. C. Carter, S. M. Angel, M. Lawrence-Snyder, J. Scaffidi, R. E. Whipple and J. G. Reynolds, "Standoff Detection of High Explosive Materials at 50 Meters in

Ambient Light Conditions Using a Small Raman Instrument," Applied Spectroscopy, vol. 59, pp. 120-138, 2005.

[31] S. K. Sharma, A. K. Misra and B. Sharma, "Portable remote Raman system for monitoring hydrocarbon, gas hydrates and explosives in the environment," Spectrochimica Acta A, vol. 61, pp. 2404-2412, 2005.

[32] S. K. Sharma, A. K. Misra, P. G. Lucey, S. M. Angel and C. P. McKay, "Remote Pulsed Raman Spectroscopy of Inorganic and Organic Materials to a Radial Distance of 100 Meters," Applied Spectroscopy, vol. 60, pp. 871-876, 2006.

[33] C. Eliasson, N. A. Macleod and P. Matousek, "Noninvasive detection of concealed liquid explosives using Raman spectroscopy," Analytical Chemistry, vol. 79, pp. 8185-8189, 2007.

[34] J. Xu, H. Liu, T. Yuan, R. Kersting and X.-C. Zhang, "Advanced terahertz time-domain spectroscopy for remote detection and tracing," Proceedings of SPIE, vol. 5070, pp. 17-27, 2003.

[35] M. R. Leahy-Hoppa, M. J. Fitch and R. Osiander, "Terahertz spectroscopy techniques for explosives detection," Analytical and Bioanalytical Chemistry, vol. 395, pp. 247-257, 2009.

[36] Y. Hu, P. Huang, L. Guo, X. Wang and C. Zhang, "Terahertz spectroscopic investigations of explosives," Physics Letters A, vol. 359, pp. 728-732, 2006.

[37] T. Yuan, H. Liu, J. Xu, F. Al-Douseri, Y. Hu and X.-C. Zhang, "Terahertz time-domain spectroscopy of atmosphere with different humidity," Proceedings of SPIE, vol. 5070, pp. 28-37, 2003.

[38] R. J. Foltynowicz, R. E. Allman and E. Zuckerman, "Terahertz absorption measurement for gas-phase 2,4-dinitrotoluene from 0.05 THz to 2.7 THz," Chemical Physics Letters, vol. 431, pp. 34-38, 2006.

[39] W. R. Tribe, D. A. Newnham, P. F. Taday and M. C. Kemp, "Hidden object detection: security applications of terahertz technology," Proceedings of SPIE, vol. 5354, pp. 168-176, 2004.

[40] M. C. Kemp, P. F. Taday, B. E. Cole, J. A. Cluff, A. J. Fitzgerald and W. R. Tribe, "Security applications of terahertz technology," Proceedings of SPIE, vol. 5070, pp. 44-52, 2003.

[41] J. F. Federici, B. Schulkin, F. Huang, D. Gary, R. Barat, F. Oliveira and D. Zimdars, "THz imaging and sensing for security applications—explosives, weapons and drugs," Semiconductor Science and Technology, Vols. S266-S280, p. 20, 2005.

[42] D. J. Cook, B. K. Decker, G. Maislin and M. G. Allen, "Through container THz sensing: applications for explosives screening," Proceedings of SPIE, vol. 5354, pp. 55-62, 2004.

[43] Y. Chen, H. Liu, M. J. Fitch, R. Osiander, J. B. Spicer, M. Shur and X.-C. Zhang, "THz diffuse reflectance spectra of selected explosives and related compounds," Proceedings of SPIE, vol. 5790, pp. 19-24, 2005.

[44] H. Liu, Y. Chen, G. J. Bastiaans and X. Zhang, "Detection and identification of explosive RDX by THz diffuse reflection spectroscopy," Optics Express, vol. 14, pp. 415-423, 2006.

[45] K. Arshak, E. Moore, G. M. Lyons, J. Harris and S. Clifford, "A review of gas sensors employed in electronic nose applications," Sensor Review, vol. 24, pp. 181-198, 2004.

[46] B. C. Munoz, G. Steinthal and S. Sunshine, "Conductive polymer-carbon black composites-based sensor arrays for use in an electronic nose," Sensor Review, vol. 19, pp. 300-305, 1999.

[47] D. E. Williams, "Semiconducting oxides as gas-sensitive resistors," Sensors and Actuators B, vol. 57, pp. 1-16, 1999.

[48] N. Barsan, D. Koziej and U. Weimar, "Metal oxide-based gas sensor research: How to," Sensors and Acutators B, vol. 121, pp. 18-35, 2007.

[49] E. Schaller, J. O. Bosset and F. Escher, "Electronic noses and their application to food," LebensmittelWissenschaft und-Jechnologie, vol. 31, pp. 305-316, 1998.

[50] K. J. Albert, N. S. Lewis, C. L. Schauer, G. A. Sotzing, S. E. Stitzel, T. P. Vaid and D. R. Walt, "Cross reactive chemical sensor arrays," Chemical Reviews, vol. 100, pp. 2595-2626, 2000.

[51] J. Huang, D. Kuo and B. Shew, "The effects of heat treatment on the gas sensitivity of reactively sputtered SnO_2 films," Surface and Coatings Technology, vol. 79, pp. 263-267, 1996.

[52] Y. Hu, O. K. Tan, J. S. Pan, H. Huang and W. Cao, "The effects of annealing temperature on the sensing properties of low temperature nano-sized $SrTiO_3$ oxygen gas sensor," Sensors and Actuators B, vol. 108, p. 244–249, 2005.

[53] K. Kato, H. Omoto, T. Tomioka and A. Takamatsu, "Optimum packing density and crystal structure of tin-doped indium oxide thin films for high- temperature annealing processes," Applied Surface Science, vol. 257, p. 9207–9212, 2011.

[54] J. W. Gardner and P. N. Bartlett, Electronic Noses – Principles and Applications, Oxford, UK: Oxford University Press, 1999.

[55] J. Yinon, "Detection of explosives by electronic noses," Analytical Chemistry, vol. 75, pp. 99-105, 2003.

[56] K. Brudzewski, S. Osowski and W. Pawlowski, "Metal oxide sensor arrays for detection of explosives at sub-parts-per million concentration levels by the differential electronic nose," Sensors and Actuators B, vol. 161, pp. 528-533, 2012.

[57] X. Li, Q. Li, H. Zhou, H. Hao, T. Wang, S. Zhao, Y. Lu and G. Huang, "Rapid, on-site identification of explosives in nanoliter droplets using a UV reflected fiber optic sensor," Analytica Chimica Acta, vol. 751, pp. 112-118, 2012.

[58] K. J. Albert and D. R. Walt, "High speed fluorescence detection of explosive like," Analytical Chemistry, vol. 72, p. 1947–1955, 2000.

[59] L. C. Shriver-Lake, C. H. Patterson and S. K. Van Bergen, "New Horizons: explosive detection in soil extracts with a fiber-optic biosensor," Field Analytical Chemistry and Technology, vol. 4, pp. 239-245, 2000.

[60] A. P. Demchenko, Introduction to Fluorescence Sensing, Netherland: Springer Netherlands, 2009.

[61] J. Cho, A. Anandakathir, A. Kumar, J. Kumar and P. U. Kurup, "Sensitive and fast recognition of explosives using fluorescent polymer sensors and pattern recognition analysis," Sensors and Actuators B, vol. 160, p. 1237– 1243, 2011.

[62] T. Caron, M. Cuillemot, P. Montmeat, F. Veignal, F. Perraut, P. Prene and F. Serein-Spirau, "Ultra trace detection of explosives in air: Development of a portable fluorescent detector," Talanta, vol. 81, p. 543–548, 2010.

[63] M. P. Monterola, B. W. Smith, N. Omenetto and J. D. Winefordner, "Photofragmentation of nitro-based explosives with chemiluminescence detection," Analytical and Bioanalytical Chemistry, vol. 391, pp. 2617-2626, 2008.

[64] A. T. Nimal, U. Mittal, M. Singh, M. Khaneja, G. K. Kannan, J. C. Kapoor, V. Dubey, P. K. Gutch, G. Lal, K. D. Vyas and D. C. Gupta, "Development of handheld SAW vapor sensors for explosives and CW agents," Sensors and Actuators B, vol. 135, pp. 399-410, 2009.

[65] L. A. Pinnaduwage, V. Boiadjiev, J. E. Hawk and T. Thundat, "Sensitive detection of plastic explosives with self-assembled monolayer-coated microcantilevers," Applied Physics Letters, vol. 83, pp. 1471-1473, 2003.

[66] P. G. Datskos, N. V. Lavrik and M. J. Sepaniak, "Detection of explosive compounds with the use of microcantilevers with nanoporous coatings," Sensor Letters, vol. 1, pp. 25-32, 2003.

[67] D. Lubczyk, C. Siering, J. Lorgen, Z. B. Shifrina, K. Mullen and S. R. Waldvogel, "Simple and sensitive online detection of triacetone triperoxide explosive," Sensors and Actuators B, vol. 143, pp. 561-566, 2010.

[68] P. Bunyan, C. Baker and N. Rurner, "Application of heat conduction calorimetry to high explosives," Thermochimica Acta, vol. 401, pp. 9-16, 2003.

[69] Y. Liu, V. M. Ugaz, S. W. North, W. J. Rogers and S. Mannan, "Development of a miniature calorimeter for identification and detection of explosives and other energetic compounds," Journal of Hazardous Materials, vol. 142, pp. 662-668, 2007.

[70] B. Wang and Q. Lin, "Temperature-modulated differential scanning calorimetry in a MEMS device," Sensors and Actuators B, vol. 180, pp. 60- 65, 2013.

[71] M. Amani, Y. Chu, K. L. Waterman, C. M. Hurley, M. J. Platek and O. J. Gregory, "Detection of triacetone triperoxide (TATP) using a thermodynamic based gas sensor," Sensors and Actuators B, vol. 162, pp. 7-13, 2012.

[72] D. J. Whelan, R. J. Spear and R. W. Read, "The thermal decomposition of some primary explosives as studied by differential scanning calorimetry," Thermochimica Acta, vol. 80, p. 149–163, 1984.

[73] A. Burger and K. D. Wehrstedt, "Azodicarboxylates: Explosive properties and DSC measurements," Journal of Loss Prevention in the Process Industries, vol. 23, p. 734–739, 2010.

[74] R. S. Ladbeck and U. Karst, "Determination of triacetone triperoxide in ambient air," Analytical Chemistry, vol. 482, pp. 183-188, 2003.

[75] W. H. Zhang, W. D. Zhang and L. Y. Chen, "Highly sensitive detection of explosive triacetone triperoxide by an In2O3 sensor," Nanotechnology, vol. 21, p. 315502, 2010.

[76] N. Barsan, D. Koziej and U. Weimar, "Metal oxide-based gas sensor research: How to," Sensors and Actuators B, vol. 121, pp. 18-35, 2007.

[77] N. L. Hung, H. Kim, S. K. Hong and D. Kim, "Enhancement of CO gas sensing properties of ZnO thin films deposited on self-assembled Au nanodots," Sensors and Actuators B, vol. 151, pp. 127-132, 2010.

[78] G. Eranna, B. C. Joshi, D. P. Runthala and R. P. Gupta, "Oxide materials for development of integrated gas sensors: A comprehensive review," Critical Review of Solid State and Materials Sciences, vol. 29, pp. 111-188, 2004.

[79] W. H. Zhang, W. D. Zhang and L. Y. Chen, "Highly sensitive detection of explosive Triacetone triperoxide by an In_2O_3 sensor," Nanotechnoloy, vol. 21, p. 315502, 2010.

[80] I. Eisele, T. Doll and M. Burgmair, "Low Power gas detection with FET sensors," Sensors and Actuators B, vol. 78, pp. 19-25, 2001.

[81] K. Schierbaum, U. Weimar and W. Gopel, "Conductance, work function and catalytic activity of SnO_2-based gas sensors," Sensors and Actuators B, vol. 3, pp. 205-214, 1991.

[82] W. Y. Yang, W. G. Kim and S. W. Rhee, "Radio frequency sputter deposition of single phase cuprous oxide using Cu_2O as a target material and its resistive switching properties," Thin Solid Films, vol. 517, pp. 967-971, 2008.

[83] C. I. Pearce, R. A. Pattrick, D. J. Vaughan, C. M. Henderson and G. van der Laan, "Copper oxidation state in chalcopyrite: Mixed Cu d^9 and d^{10} characteristics," Geochimica, vol. 70, pp. 4635-4642, 2006.

[84] E. Vereshchaginam, R. A. Wolters and J. G. Gardeniers, "Measurement of reaction heats using a polysilicon based microcalorimetric sensor," Sensors and Actuators A, vol. 169, pp. 308-316, 2011.

[85] C. B. Lim and S. Oh, "Microstructure evolution and gas sensitivities of Pd- doped SnO_2-based sensor prepared by three different catalyst-addition process," Sensors and Actuators B, vol. 30, pp. 223-231, 1996.

[86] Ras, M. R., F. Borrull, and R. M. Marcé. "Sampling and Preconcentration Techniques for Determination of Volatile Organic Compounds in Air Samples." TrAC Trends in Analytical Chemistry, 28.3 (2009): 347-61.

[87] Wong, Ming-Yee, Wei-Rui Cheng, Mao-Huang Liu, Wei-Cheng Tian, and Chia-Jung Lu. "A Preconcentrator Chip Employing μ-SPME Array Coated with In-situ-synthesized Carbon Adsorbent Film for VOCs Analysis." Talanta 101 (2012): 307-13.

[88] Nakamoto, T., Y. Isaka, T. Ishige, and T. Moriizumi. "Odor-sensing System Using Preconcentrator with Variable Temperature." Sensors and Actuators B: Chemical 69.1-2 (2000): 58-62.

[89] Martin, Michael, Mark Crain, Kevin Walsh, R. Andrew Mcgill, Eric Houser, Jennifer Stepnowski, Stanley Stepnowski, Huey-Daw Wu, and Stuart Ross. "Microfabricated Vapor Preconcentrator for Portable Ion Mobility Spectroscopy." Sensors and Actuators B: Chemical 126.2 (2007): 447-54.

[90] Janssen, S., T. Tessmann, and W. Lang. "High Sensitive and Selective Ethylene Measurement by Using a Large-capacity-on-chip Preconcentrator Device." Sensors and Actuators B: Chemical (2014).

[91] Camara, E.h.m., P. Breuil, D. Briand, N.f. De Rooij, and C. Pijolat. "A Micro Gas Preconcentrator with Improved Performance for Pollution Monitoring and Explosives Detection." Analytica Chimica Acta 688.2 (2011): 175-82.

[92] Camara, E.h.m., P. Breuil, D. Briand, L. Guillot, C. Pijolat, and N.f. De Rooij. "Micro Gas Preconcentrator in Porous Silicon Filled with a Carbon Absorbent." Sensors and Actuators B: Chemical 148.2 (2010): 610-19.

[93] Camara, E.h.m., P. Breuil, and C. Pijolat. "Preconcentration Modeling for the Optimization of a Micro Gas Preconcentrator Applied to Environmental Monitoring." Procedia Chemistry 1.1 (2009): 662-65.

[94] Alfeeli, Bassam, Daniel Cho, Mehdi Ashraf-Khorassani, Larry T. Taylor, and Masoud Agah. "MEMS-based Multi-inlet/outlet Preconcentrator Coated by Inkjet Printing of Polymer Adsorbents." Sensors and Actuators B: Chemical 133.1 (2008): 24-32.

[95] Campbell, Stephen A. Fabrication Engineering at the Micro and Nanoscale. New York: Oxford UP, 2013. Print.

[96] Li, J.-B., K. Jiang, and G. J. Davies. "Novel Die-sinking Micro-electro Discharge Machining Process Using Microelectromechanical Systems Technology." Proceedings of the Institution of Mechanical Engineers, Part C: Journal of Mechanical Engineering Science 220.9 (2006): 1481-487.

[97] Yabuki, T., and O. Nakabeppu. "Heat Transfer Mechanisms in Isolated Bubble Boiling of Water Observed with MEMS Sensor." International Journal of Heat and Mass Transfer 76 (2014): 286-97.

[98] Rafiee, P., and G. Khatibi. "A Fast Reliability Assessment Method for Si MEMS Based Microcantilevers." Microelectronics Reliability, 54 (2014):2180-2184.

CHAPTER 3

METHODOLOGY

3.1 Sensor fabrication and characterization

Alumina substrates were pre-sputtered in an MRC 8667 sputtering system to deposit an alumina film to promote adhesion of Ni. Thin film nickel microheaters, having a nominal thickness of 4.5 μm, were deposited onto laser-perforated alumina substrates using an MRC Model 822 sputtering system. The Ni microheaters were annealed in flowing nitrogen at 900°C for 5 hours to improve the electrical stability and eliminate point defects as a result of the sputtering process. A 1μm thick alumina film was then deposited over the microheaters to prevent electrical shorts between the Ni and the oxide catalyst. The alumina film was also used to prevent the microheaters from interacting with oxygen and other gases present in the atmosphere. This microheater described here provides the foundation for all subsequent sensor designs.

3.1.1 SnO_2/Pd nanocomposite catalyst fabrication

SnO_2/Pd nanocomposite catalysts were co-sputtered from simultaneously energized SnO_2 and Pd targets in pure Ar onto an array of microheater sensors on alumina substrates in an MRC Model 8667 sputtering machine. A schematic of sensor placement relative to the sputtering targets is shown in Figure 3.1 and the sputtering parameters used for the deposition of the nanocomposite catalyst are given in Table 3.1. This approach generated a large number of essentially different catalysts with a continuously varying, spatially dependent chemistry.

	SnO_2	Pd
Diameter of targets (mm)	150	100
Vertical distance between specimen and target (mm)	75	75
Forward voltage (V)	480	480
Power density (W/cm^2)	1.70	3.8
Sputtering gas	Ar	Ar
Pressure (Torr)	$9*10^{-4}$	$9*10^{-4}$
Deposition rate (μm/hr)	0.49	0.28

Table 3.1 Parameters applied to SnO_2 and Pd targets during co-sputtering.

Palladium loadings ranged from 1 wt.% to 25 wt.% in the nanocomposite film. A cutaway view of the various layers comprising the sensor is shown in Figure 3.2. Following deposition, the films were annealed at 550°C in air to promote crystallization and further stabilize the oxide catalysts. The chemical composition and morphology of these catalysts were characterized using scanning electron microscopy (SEM) equipped with energy dispersive X-ray spectroscopy (EDS). The catalysts were also characterized using X-ray diffraction (XRD) and X-ray photoelectron spectroscopy (XPS). Pure tin oxide films were also prepared as catalysts for comparison purposes.

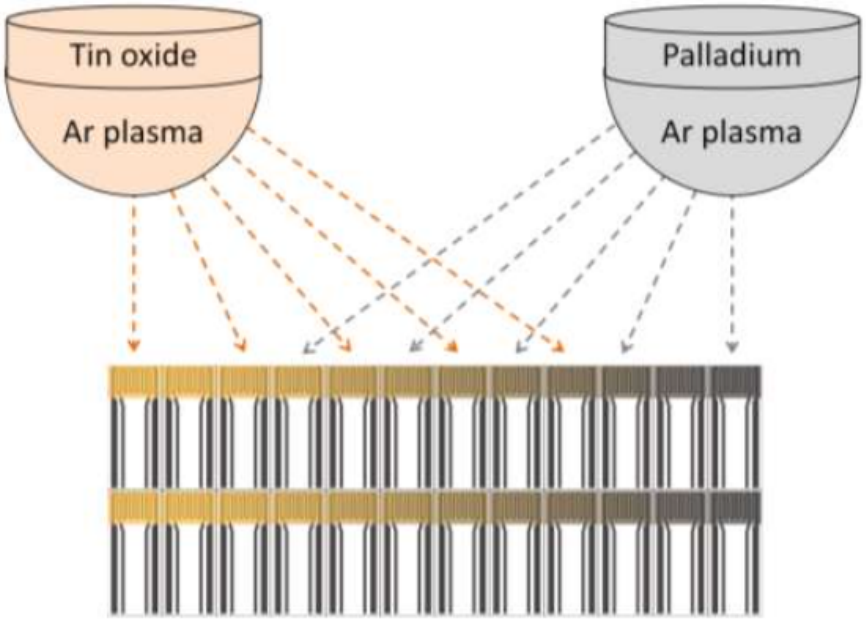

Figure 3.1 Overview of the Pd:SnO_2 co-sputtering process, in which an array of sensors were placed between two energized targets, resulting in that the sensors were coated with varying composition of catalysts.

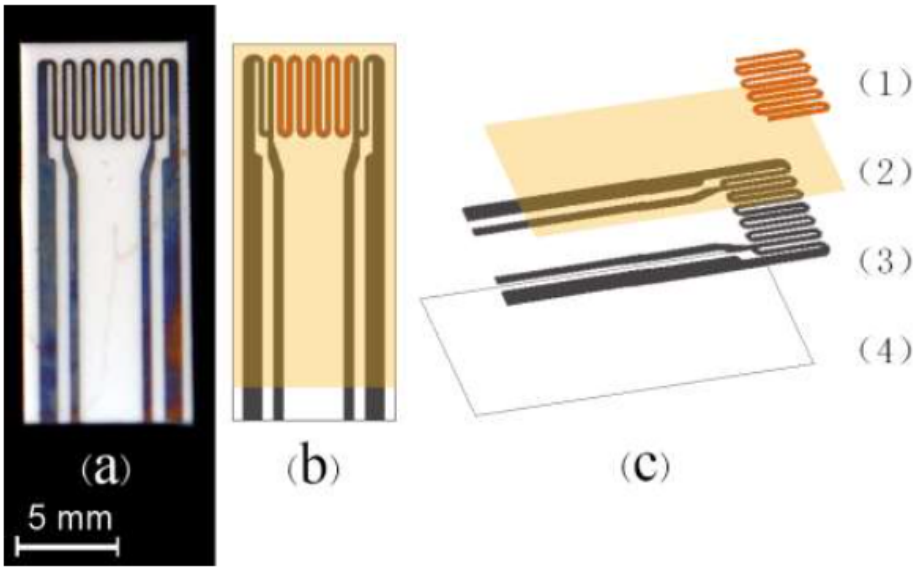

Figure 3.2 Actual picture and schematic demonstrating the size and structure of thermodynamic based sensor platform: (a) an actual picture, (b) top view and (c) expended view of schematic of the sensor showing catalyst film (1), alumina passivation layer (2), nickel microheater (3) and alumina substrate (4).

3.1.2 Orthogonal Sensor Fabrication

Over the serpentine area of a microheater, a 150 μm high purity alumina cement coating was applied. Both the sputtered alumina film and the thick alumina cement function as insulation layers to prevent the Ni microheaters from direct exposure to gas molecules and to prevent electrical shorts to the marginally conductive oxide catalyst. The cement is polished and the edges are beveled to accommodate the conductometric electrodes that are deposited next.

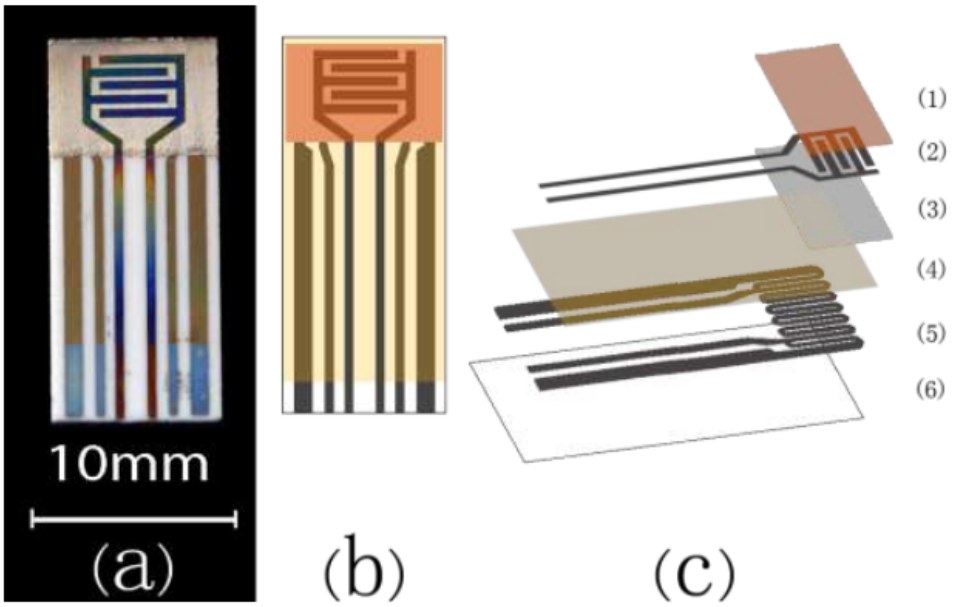

Figure 3.3 Schematic of orthogonal sensor showing an actual picture (a), the top view (b) and expanded views (c) of the metal oxide catalyst layer (1), nickel electrodes (2), alumina coatings (3-4), nickel microheater (5) and alumina substrate (6).

Ni electrodes were deposited over the alumina cement using an MRC 822 puttering system. Their purpose is to measure the change in electrical resistivity of the metal oxides when exposed to the target gas. SnO_2 and ZnO were subsequently deposited using a MRC 8667 sputtering system in pure argon, which produced a nonstoichiometric oxide. Both catalysts were then annealed at 450°C in nitrogen for 5 hours, densifying the film, eliminating point defects and releasing trapped argon

atoms. This was followed by a second heat treatment in a nitrogen/oxygen atmosphere (volume ratio of 95:5) for 5 minutes at the same annealing temperature. The second heat treatment ensured that the surface of catalyst film was stoichiometric, favorable for thermodynamic interactions between the catalyst and the analyte. Underneath the stoichiometric oxide was a much thicker nonstoichiometric oxide that was tailored for the conductivity measurement. The oxidation states of the metal oxide as a function of depth were characterized using X-ray photoelectron spectroscopy (XPS) to establish depth profiles and confirm the oxidation state in the oxide layer. A full schematic of the orthogonal sensor design is depicted in Figure 3.3.

3.1.3 Preconcentrator Design

The design of the preconcentrator is depicted in Figure 3.4. A K-type thermocouple was added to the sensor design to precisely monitor temperature. The sputtered alumina dielectric was deposited over both the microheater and the thermocouple. A polystyrene film was then deposited over the sensor surface using spin coating. Polystyrene beads were dissolved in dichloromethane, forming a viscous liquid. The microheater was masked to protect the electrical contacts and the viscous solution was decanted onto the surface and spun off at speeds in excess of 500 rpm. Factors that affect the thickness of the resulting film include the viscosity of the solution, controlled by the mass of polymer dissolved into a fixed volume of dischloromethane, and the rotational speed (higher speeds produce thinner films). Films were made of varying thickness to determine how film depths affects retention volume.

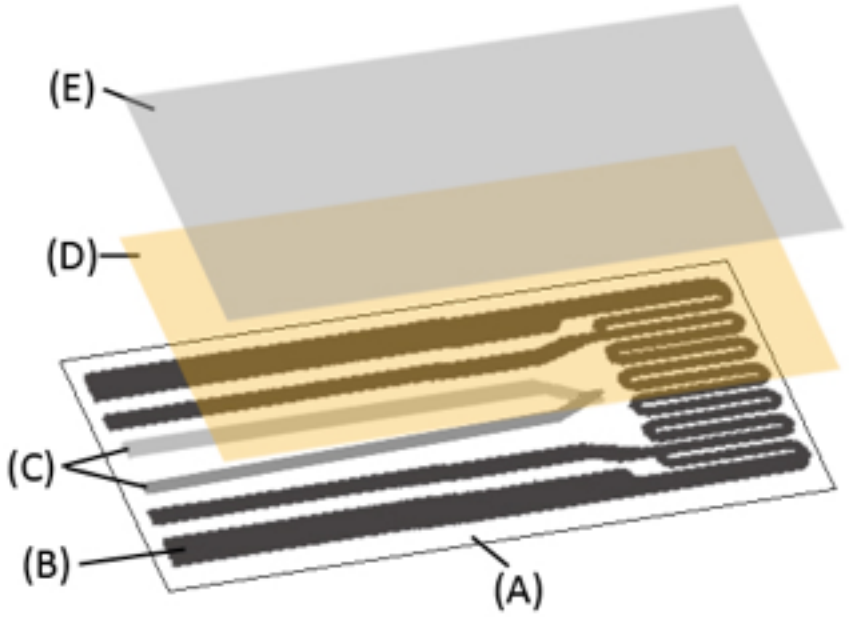

Figure 3.4 The pre-concentrator is comprised of (A) an alumina substrate, (B) a Ni microheater, (C) a K-type thin film thermocouple, (D) porous, sputtered alumina coating and (E) spin-coated polystyrene film.

3.2 Testing apparatus and protocol

The flow rate of inert gas (dry air) and target gas was precisely metered into the test chamber using two mass flow controllers and a digital flow meter, which produced a constant mass flow and allowed precise control over the target gas and inert gas mixtures delivered to the testbed. The desired vapor phase concentration of TATP was achieved by passing the carrier gas over a piece of filter paper impregnated with high purity TATP crystals in a flask maintained at constant temperature. When the target molecules were derived from liquid-based chemical solutions such as H_2O_2, or acetone in deionized water, air was bubbled through the flask containing dilute solutions to establish an equilibrium partial pressure in the vapor phase. A schematic of the test bed used to evaluate sensor performance is shown in Figure 3.5.

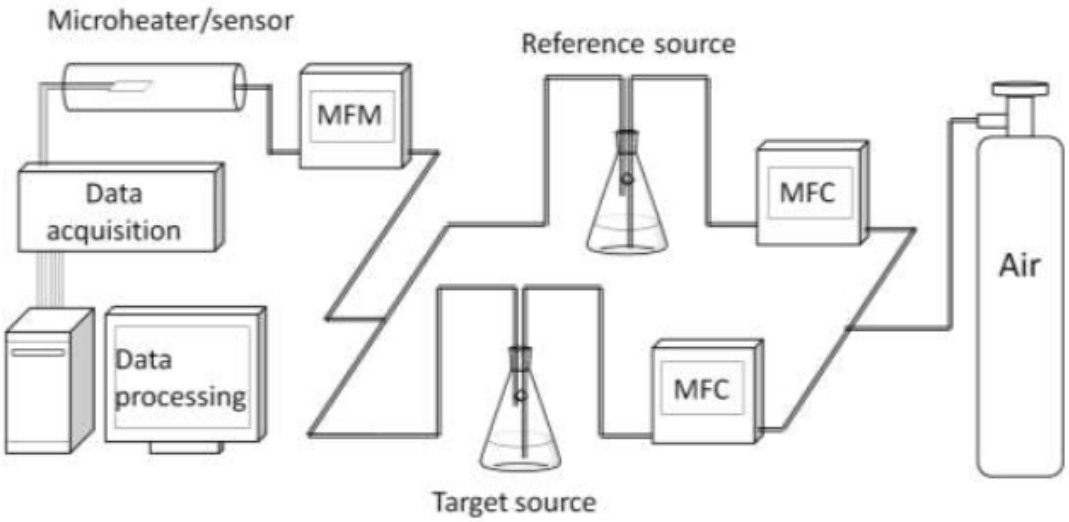

Figure 3.5 Apparatus used for the detection of TATP and H_2O_2 using a micro-calorimetric sensor.

The catalytic response was determined by measuring the heat affect associated with the interaction of the target molecules with a catalyst using a dynamic testing protocol. The catalyst-coated microheater was heated to a number of predetermined temperature set points by controlling the electrical resistance of the microheater, using a four-point probe method. The temperature coefficient of resistance (TCR) of the nickel microheater was independently calibrated and verified prior to each sensor test. The gas delivery system consisted of a series of mass flow controllers interfaced to a computer. In addition, a data acquisition system was also interfaced to a computer and controlled using LabView software. After reaching each temperature set point, the sensor was allowed to equilibrate for 360 seconds under constant inert gas flow. The target gas was then introduced into the test chamber for 180 seconds and then the reference gas was introduced for 180 seconds before the microheater was ramped to the next temperature set point. This testing sequence is referred to as an "off-on-off" protocol. The power required to maintain the sensor at a particular temperature was

recorded after the target gas was introduced and this temperature was maintained until the start of next step-increase in temperature. The heat effect at each temperature set point was measured by taking the difference in power required to maintain the temperature in the presence of the target gas and the power required to maintain the temperature in the presence of the inert gas. Prior to measuring the sensor response, the background power (sensor drift) was subtracted from the sensor response. Typically, all responses smaller than ±1.0 mW were considered background (noise), commonly due to small variations in the target and inert gas flow rates, drift in the baseline resistance of the nickel microheaters and other electrical instabilities. TATP, H_2O_2 and acetone were all tested using this protocol in combination with the co-sputtered SnO_2/Pd composite catalyst for the thermodynamic sensor.

3.2.1 Orthogonal Sensor Testing

For the orthogonal sensor, the flasks shown in the testing schematic, better suited for liquid based analyte testing, were replaced with stainless steel sample chambers as seen in Figure 3.6, to better test the TATP impregnated filter paper training aids as well as powder based explosives like 2,6-DNT and ammonium nitrate (AN). For the conductometric half of the orthogonal sensor, a voltage measurements across the semi-conductive SnO_2 or ZnO film was recorded by the data acquisition system. When target gas molecules contacted the metal oxide, the number of available charge carriers changed, resulting in a corresponding drop or rise in voltage. The same testing protocol described for the thermodynamic sensor is applied here, except the voltage across the conductometric electrodes and the power supplied to the microheater are measured and recorded simultaneously. Sensor responses to explosive

vapors as a function of target gas concentration were determined. The sensitivity, detection limit, response time and recovery time for AN, 2,6-DNT and TATP were evaluated for the conductometric platform and thermodynamic platform in the orthogonal sensor.

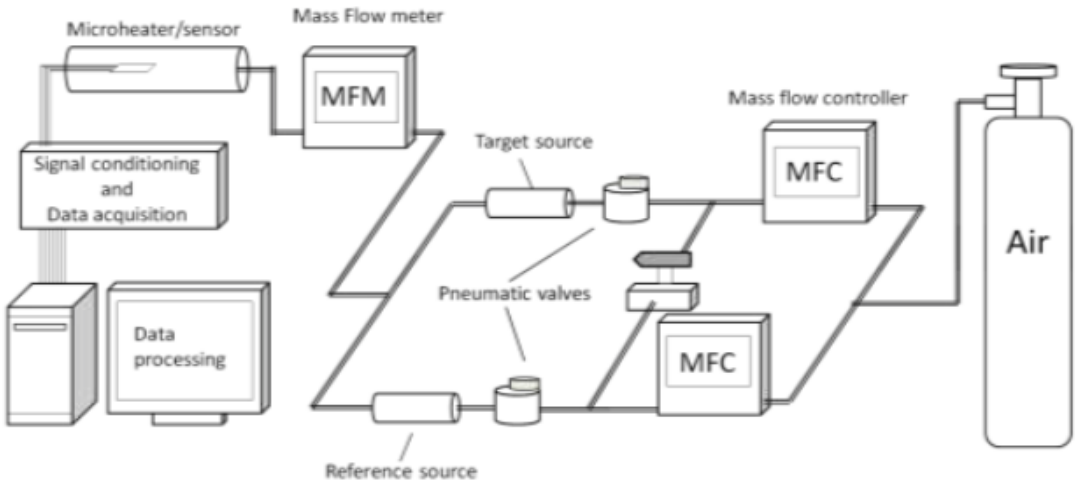

Figure 3.6 Apparatus used for TATP, 2,6-DNT and AN detection using orthogonal sensors.

These particular analytes (TATP, 2,6-DNT and AN) were chosen to evaluate the orthogonal sensor for a variety of reasons. All three explosives belong to different chemical groupings of energetic materials: TATP from the peroxides, 2,6-DNT from the aromatic nitro- group and AN from the acid salts [1]. TATP and AN were also chosen because they are commonly found in homemade explosives and are far more likely to be involved in a terrorist attack [2]. 2,6-DNT, while not as widely used as an explosive in industry as 2,4,6-trinitrotoluene (TNT), is a less dangerous alternative that has similar chemical structure and behavior [3]. Furthermore, DNT is a precursor to the synthesis of TNT, thus a homemade batch of TNT is likely to contain larger quantities of DNT over the commercially prepared explosive. 2,6-DNT was chosen

specifically over its isomer 2,4-DNT because 2,6-DNT has a higher ambient vapor pressure [4]. Finally, these three explosives represent a range of vapor pressures. TATP is a volatile compound and will thus have a high concentration in the vapor phase [5-6]. 2,6-DNT has a much lower vapor pressure but still within a detectable range [4,7]. AN has the lowest vapor pressure and represents a challenge for this vapor detection technique [4,7].

3.2.2 Dynamic Testing Protocol for Preconcentration Testing

Testing with the preconcentrator required modifications to the original testing apparatus. Immediately downstream from the explosive sample chamber a vessel was placed to contain the preconcentrator. The preconcentrator must be heated for the thermal desorption of the collected analyte to occur, so the microheater embedded underneath the polystyrene is connected to a constant current source and the voltage is measured across the thermocouple to precisely control and monitor the temperature. The added heat upstream from the sensor would result in a power change, independent of any catalyst-analyte interaction, thus a method needed to be devised to filter out any extraneous heat changes to isolate catalytic activity.

To accomplish this, downstream from the preconcentrator, the air was siphoned off into two different chambers, precisely monitored with mass flow controllers to ensure both chambers receive the same volume of air. In one chamber is a sensor coated with a passivating layer of alumina cement and a metal oxide catalyst, but in the other is a microheater coated with only with the cement dielectric. This sensor acts as a dynamic control. Both sensors were tested according to the thermodynamic testing protocol, all the while mirroring the other's temperature. The dynamic control

sensor responded to heat changes like the thermal desorption during preconcentrator operation, sensible heat effects, adsorption heat effects to the alumina dielectric and flow rate changes. The catalyst coated sensor picked up those same heat changes plus the heat change associated with any catalyst-analyte interactions, thus by subtracting the two signals, the extraneous heat effects can be filtered out, completely isolating the sensor response due to catalytic activity. A schematic of this modified testing apparatus is available in Figure 3.7. Because it is critical for the catalyst coated sensor and the dynamic control sensor to respond similarly to these extraneous heat effects, individual sensors were pre-screened for similar electrical and thermal properties and paired prior to testing.

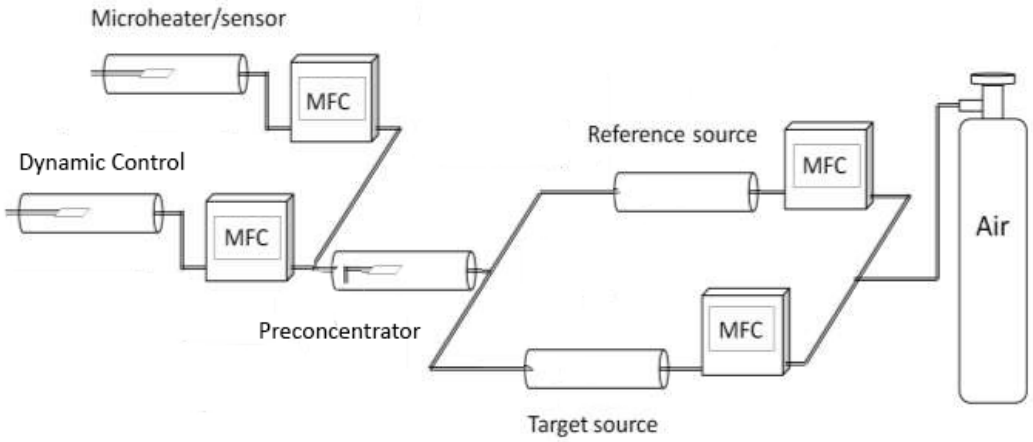

Figure 3.7 Apparatus used for preconcentrator testing, including using two sensors simultaneously: one coated with a catalyst and the other functioning as a dynamic control.

Several single-step tests were conducted in this apparatus. Air was passed over the preconcentrator and delivered to the sensor chambers for 60 seconds as a reference. Then target molecules were delivered to the preconcentrator and the sensor for 180 seconds. During this time, the preconcentrator was in a "collection phase"

meaning the polystyrene film was maintained at room temperature in order to allow any target explosive molecules to adsorb to the polymer surface. After the 180 seconds, current was applied to the microheater to rapidly heat the polymer film to 95ºC, allowing desorption to occur. This temperature is below the glass transition temperature of polystyrene, thus not warm enough to cause the polymer film to begin to flow. Analyte desorption continues for 120 more seconds, then the constant current source was turned off, allowing the preconcentrator to passively cool. Reference air is then passed through the system to observe the sensor's recovery time.

Tests such as this were completed while varying several different test parameters including polymer film thickness, analyte used, collection time and flow rate. Also, the effluent gas coming off the sensor and the preconcentrator was collected and analyzed using GC/MS to evaluate the effectiveness of the adsorbent as well as to determine whether the catalytic decomposition of TATP, DNT or AN takes place.

3.3 MEMS design

The main purpose of transferring the sensor platform to MEMS based platform was to produce a smaller footprint that consumes less heat. In addition to the thermodynamic sensor and conductometric sensor, a K-type thermocouple was incorporated into the MEMS system to monitor temperature activity. A schematic of the MEMS sensor is shown in Figure 3.8. The fabricated dimension of MEMS platform was 2.8 mm x 1.8 mm x 0.7 mm. One of the most important processes involved in the fabrication was etching processes, which in this study was used to

create a suspended plane (1 mm x 1 mm x 5 μm) which was supported by tiny bridges (0.1 mm x 0.1 mm x 5 μm) to reduce heat sink.

Etching in micromachining is a process in which layers are chemically removed from wafer during manufacturing. Etching pattern can be controlled by masking layers applied through photolithography processes. Isotropic etching refers to process in which etchant erode the substrate material equally in all directions, while anisotropic etching is controlled in limited directions to certain materials, which could avoid formation of cavities under masking layer. A (100) oriented silicon wafer was selected as the substrate material for this MEMS platform to favor anisotropic etching [8-9].

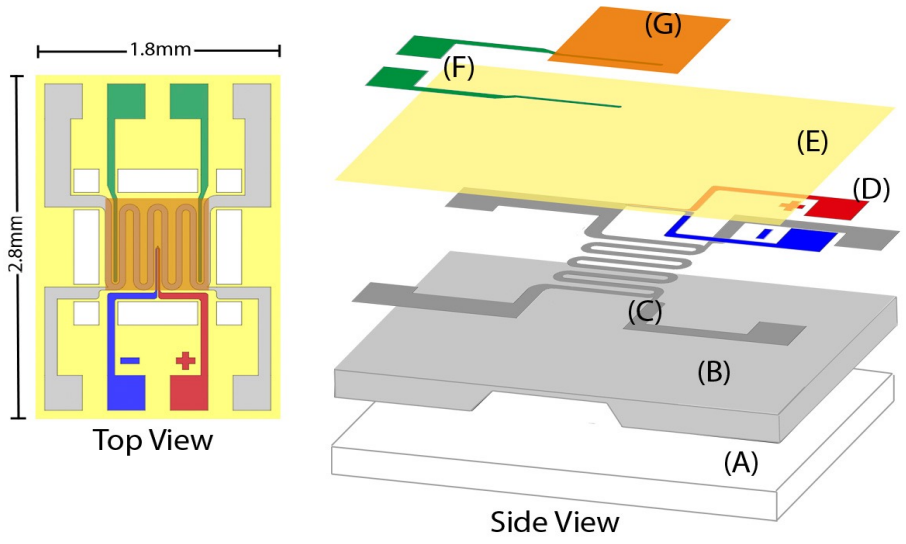

Figure 3.8 Schematics showing top view (left) and expanded view (right) of orthogonal sensor on a MEMS platform. Elements including (A) pyrex substrate, (B) silicon wafer, (C) nickel microheater, (D) type K thermocouple, (E) silicon oxide layer, (F) platinum electrodes and (G) metal oxide catalysts.

A 1.5 μm SiO_2 layer was thermally grown on both sides of the (100) oriented silicon wafer by heating at 1000°C for 48 hours. The wafer was then patterned using a positive photoresist and windows were etched into the SiO_2 using a hydrofluoric acid (HF) and ammonium fluoride (NH_4F) etchant. Since formation of extra hydrogen ions

is impeded by NH_4F this etching solution favored the etching of SiO_2 over Si. The photoresist was lifted off and a potassium hydroxide (KOH) etch was used to etch anisotropically into the Si at an elevated temperature resulting in the shape seen in Figure 3.9. The remaining thickness of Si was estimated to be less than 10 µm. A pyrex wafer was then anodically bonded to the Si wafer to fortify the substrate, forming a cavity in between the two wafers. Using photolithography and RF plasma sputtering, Ni microheaters and a type-K thermocouple were then deposited onto this reinforced wafer, followed by a SiO_2 insulation layer on top. Pt conductometric electrodes and a metal oxide catalyst layer were then sputtered over the SiO_2 insulation layer. Windows were etched to further reduce the thermal mass of the suspended plane using a third etchant, tetramethylammonium hydroxide (TMAH, $(CH_3)_4NOH$). Finally, the wafer was diced resulting in the finished MEMS sensor depicted in Figure 3.10.

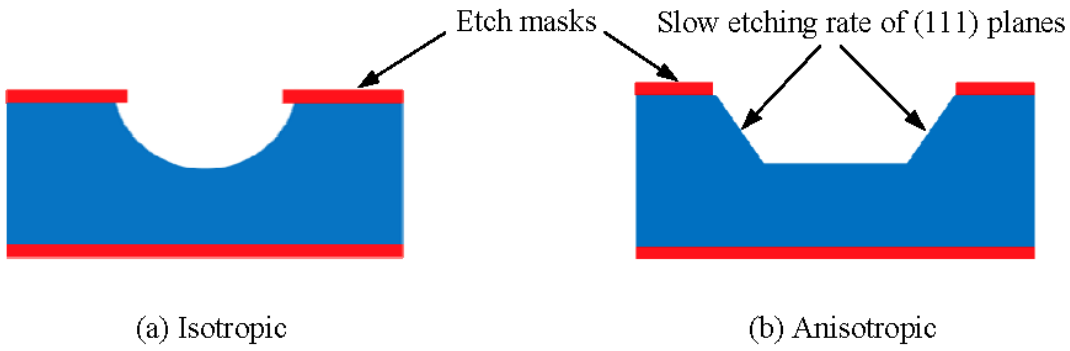

Figure 3.9 Etched shape using (a) an isotropic etch and (b) using an anisotropic etch.

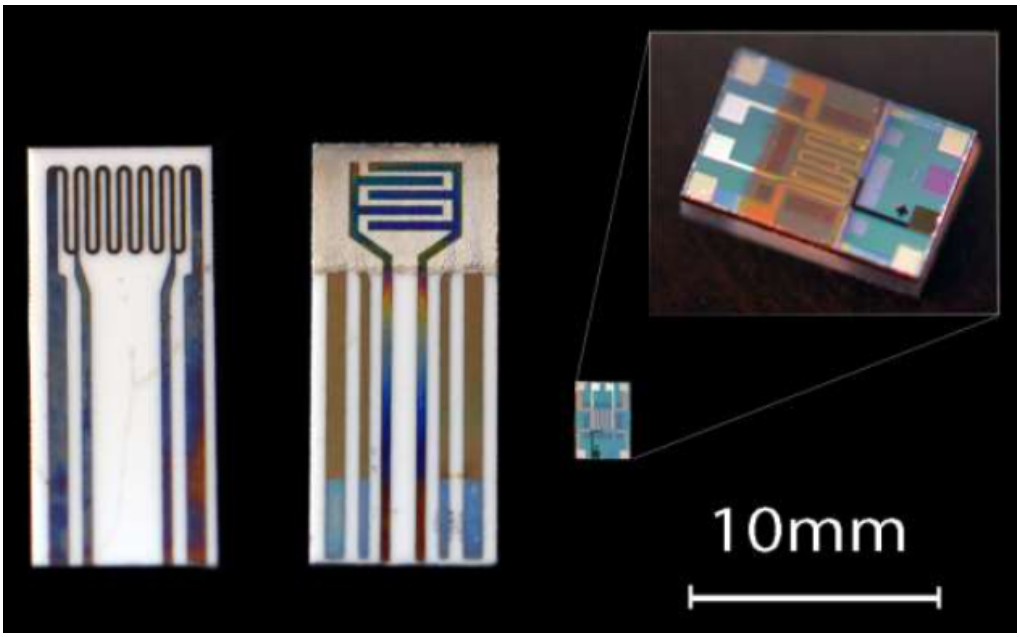

Figure 3.10 Photograph comparing the relative sizes of the solid state thermodynamic sensor (left), a solid state orthogonal sensor (center) and the MEMS design (right).

A second MEMS design was also produced with the assistance of the US Army Labs, depicted in Figure 3.11, and were manufactured using a similar procedure. This particular iteration incorporates four thermodynamic sensors with individual thermocouples onto one chip, allowing for the implementation of several different catalysts at once, or even a dynamic control. Each microheater is a Ti/Ni composite on top of Ti/Au bond pads and the active area is 0.25 mm x 0.25 mm, over 10 times smaller than the active area of the microheater in the single sensor MEMS design, providing an even smaller thermal mass. The membrane is also constructed using a stack of plasma-enhanced chemical vapor deposition (PECVD) films (150 nm SiO_2 / 100 nm Si_3N_4 / 100 nm SiO_2) and then back etched with xenon difluoride (XeF_2).

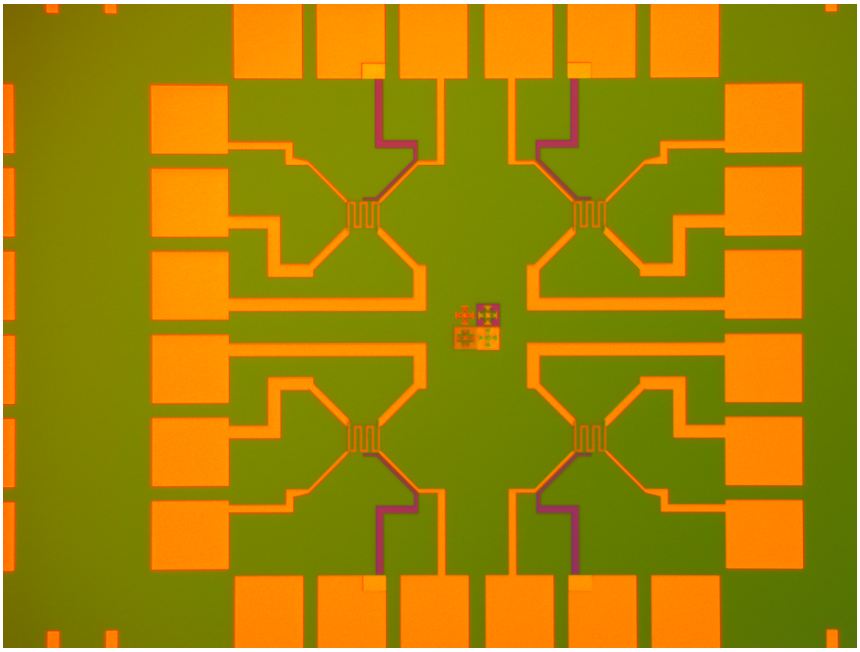

Figure 3.11 Latest MEMS design, incorporating four sensors to one 5 mm by 5 mm chip.

References

[1] Caygill, F. Davis and S. P. Higson, "Current trends in explosive detection techniques," Talanta, vol. 88, pp. 14-29, 2012.

[2] Wilson, Clay. "Improvised Explosive Devices (IEDs) in Iraq and Afghanistan: Effects and Countermeasures." (2007): 1-3. Federation of American Scientists, 21 Nov. 2007. Web. 3 Sept. 2014.

[3] Meyers, Sydney, and Edward S. Shanley. "Industrial Explosives - a Brief History of Their Development and Use." *Journal of Hazardous Materials* 23.2 (1990): 183-201. Web.

[4] Ewing, Robert G., Melanie J. Waltman, David A. Atkinson, Jay W. Grate, and Peter J. Hotchkiss. "The Vapor Pressures of Explosives." *TrAC Trends in Analytical Chemistry* 42 (2013): 35-48.

[5] Oxley J. C., Smith J. L., Shinde K. and Moran J., "Determination of the vapor density of triacetone triperoxide (TATP) using a gas chromatography headspace technique," Propellants, Explosives, Pyrotechnics, vol. 30, pp. 127-130, 2005.

[6] Oxley J. C., Smith J. L., Shinde K. and Moran J., "Determination of the vapor density of triacetone triperoxide (TATP) using a gas chromatography headspace technique," Propellants, Explosives, Pyrotechnics, vol. 30, pp. 127-130, 2005.

[7] G. A. Eiceman, D. Preston, G. Tiano, J. Rodriguez and J. E. Parmeter, "Quantitative calibration of vapor levels of TNT, RDX, and PETN using a

diffusion generator with gravimetry and ion mobility spectrometry," Talata, vol. 45, pp. 57-74, 1997.

[8] Zubel, Irena, Małgorzata Kramkowska, and Krzysztof Rola. "Silicon Anisotropic Etching in TMAH Solutions Containing Alcohol and Surfactant Additives." *Sensors and Actuators A: Physical* 178 (2012): 126-35.

[9] Iosub, Rodica, Carmen Moldovan, and M. Modreanu. "Silicon Membranes Fabrication by Wet Anisotropic Etching." *Sensors and Actuators A: Physical,* 99 (2002): 104-11.

CHAPTER 4

FINDINGS

4.1 Effect of Pd doped SnO2 on the selective detection of TATP

4.1.1 Chemical characterization and surface morphology

The morphology of the different nanocomposite catalysts were characterized by SEM and TEM, as shown in Figure 4.1. While most of the as-deposited catalysts are featureless, as might be expected given the non-equilibrium deposition processes used to form the composites, extensive micro-cracking was observed after annealing. This was attributed to the large volume change associated with crystallization of the amorphous phases in the nanocomposite [1]. In addition, as the palladium content in the nanocomposite was increased, the density of micro-cracks diminished and eventually disappeared from the microstructure when palladium loadings greater than 25 wt.%. EDS analysis was used in conjunction with TEM to confirm the chemistry of the dark, spherical particles observed in the SnO_2 matrix. These palladium particles had an average diameter of 20 nm, and EDS confirmed these were palladium particles in the SnO_2 matrix.

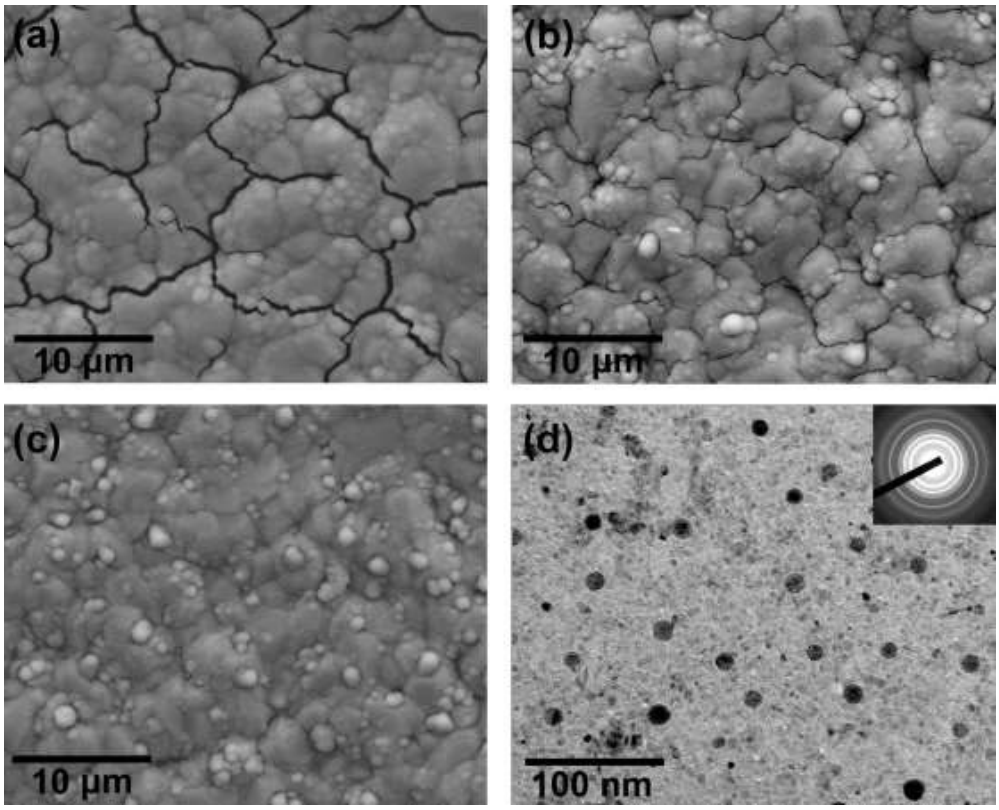

Figure 4.1 SEM image of as-annealed nanocomposite catalyst with palladium doping amount of (a) 2.2% wt.%, (b) 8 wt.% and (c) 12 wt.%, and (d) TEM micrographs of as-annealed nanocomposite catalyst with a 12 wt.% palladium loading.

The nano-composite catalysts, comprised of Pd nanoparticles in a SnO_2 matrix, were characterized by XRD, in the as-deposited and annealed condition (Figure 4.2). All nanocomposite catalysts, regardless of palladium loading, were amorphous in the as-deposited condition and became partially or fully crystalline after subsequent annealing steps. Peaks corresponding to the tetragonal form of SnO_2 were observed in the XRD patterns of the annealed catalysts with no preferred orientation or texture evident. A uniform 2θ shift of (0.01Å) was observed for the SnO_2 diffraction peaks relative to the literature values, which was likely caused by substitutional defects in the oxide. The PdO (101) peak was observed in all Pd "alloyed"

nanocomposites. However, the Pd (110) and Pd (220) peaks observed at higher palladium loadings all but disappear as the Pd loading decreases, as shown in Figure. 4.2, (3) through (5).

To further explore this phenomenon, the oxidation states of the as-annealed nanocomposite catalysts were characterized using XPS. As shown in Figure 4.3, the XPS spectra of pure SnO_2 and Pd: SnO_2 nanocomposites exhibited the same Sn $3d_{5/2}$ core level peak at 486.5 eV, suggesting that tin was present in +4 oxidation states in both specimens. Pure SnO_2 contains the +2 Sn state as indicated by the lower intensity and slight shifting of the main Sn peak. The Pd $3d_{5/2}$ peaks in the 2.2 wt.% nanocomposite were observed at 336.4 eV and 337.5 eV respectively, which is in good agreement with literature values corresponding to palladium in the +2 and +4 states [2-6]. The exact composition (at.%) was 0.17:0.83 (PdO_2:PdO), based on the peak area. As the palladium loading was increased to 12 wt.%, metallic palladium began to phase separate and the composition of PdO_2:PdO:Pd phases tended towards 0.084:0.723:0.193, respectively. When the palladium loading reached 32 wt.%, the metallic phase became dominant and the PdO_2 and PdO peaks disappeared. This was attributed to the differences in oxidation between palladium single crystals, which are more difficult to oxidize and the palladium particles in the SnO_2 [4]. This finding was in agreement with the disappearance of the palladium (110) and (220) peaks in the XRD patterns shown in Figure 4.2. It should be noted that XPS was also performed after the catalysts were exposed to peroxides, in which case the oxidation state of palladium remained the same.

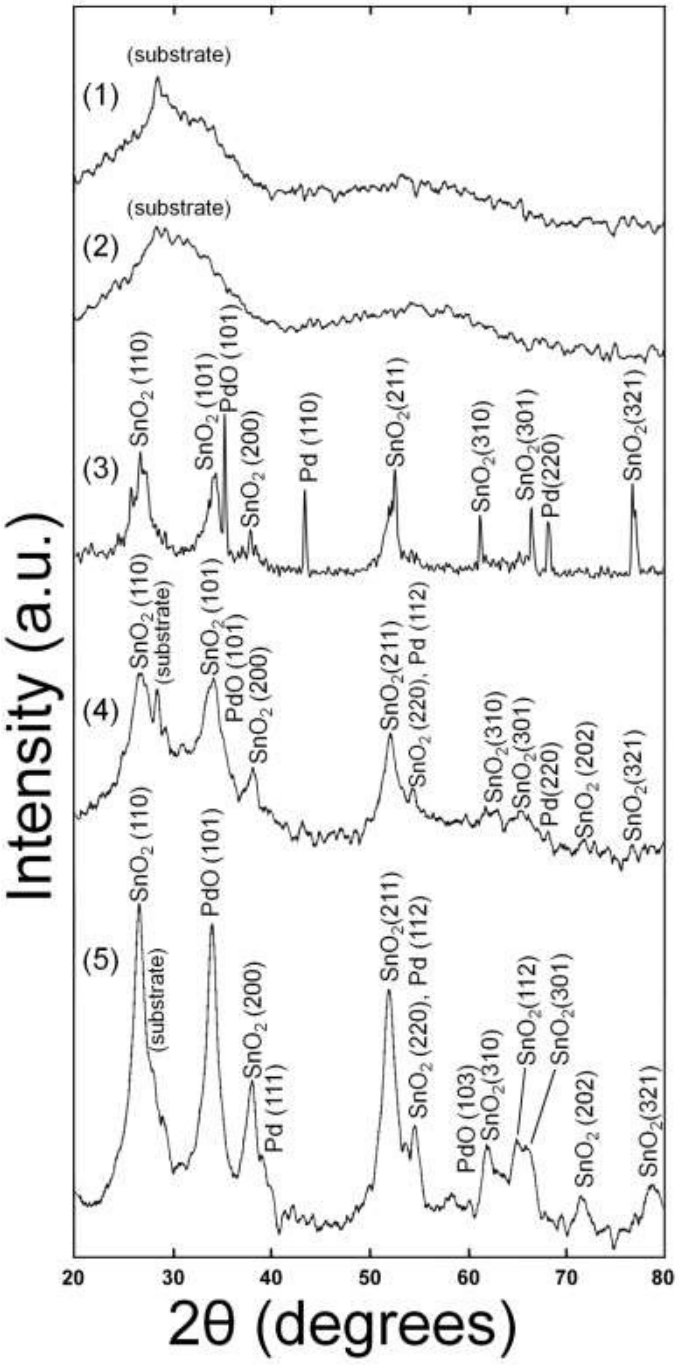

Figure 4.2 XRD patterns of as-deposited film with (1) 12 wt.% and (2) 2.2 wt.% loading palladium and annealed films with (3) 12 wt.% loading Pd, (4) 8 wt.% loading Pd, and (5) 2.2 wt.% loading Pd in the Pd: SnO_2 nanocomposite catalyst.

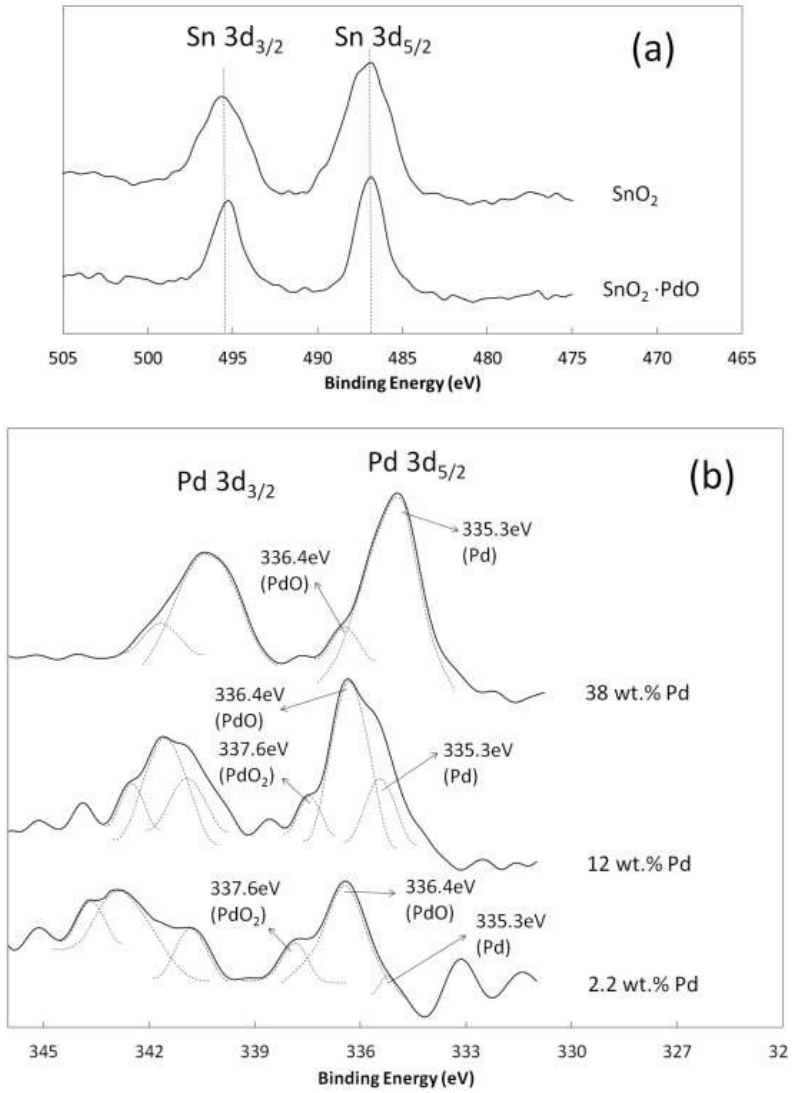

Figure 4.3 XPS spectra of (a) Sn $3d_{3/2}$ and $3d_{5/2}$ doublet for Pd doped and un-doped SnO_2, and (b) Pd $3d_{3/2}$ and $3d_{5/2}$ doublet corresponding to 2.2 wt.% loading Pd, 12 wt.% loading Pd and 38 wt.% loading Pd in the $PdSnO_2$ nanocomposite.

4.1.2 Sensor Measurements

Control experiments using un-doped SnO_2 catalysts at several temperature set points in the presence of 0.68 μg/ml TATP were conducted. Figure 4.4(a) illustrates the "off-on-off" testing protocol used for each run. Power difference was used to describe the sensor response, and was defined as power used to maintain temperature

in presence of target gas at each stage minus power used to maintain temperature in presence of an inert gas at the same stage. At temperatures below 240°C, a slightly exothermic reaction was observed at the surface of the SnO_2 catalyst, which was due to the decomposition reaction of TATP into diacetone diperoxide (DADP), acetone, H_2O and O_2/O_3 [7]. However, as the temperature was increased beyond 240°C, the reaction tended to become endothermic and peaked at 395℃. Accompanying this change in sign of the response was a change in the reaction kinetics, which was apparent from the reduced response time for the exothermic reaction compared to the endothermic sensor response. As the temperature was increased, TATP and its intermediate decomposition products continued to oxidize in the presence of air and a large amount of H_2O was generated. Heat absorbed by H_2O overwhelmed the heat released by the decomposition and oxidation reactions of TATP, which led to a power increase to maintain temperature. These sign changes are very telling with respect to the uniqueness of the sensor response (signature) and along with the magnitude of response can alleviate false positives. The details of reaction path remained unknown to researchers to date due to the complexity of the reaction.

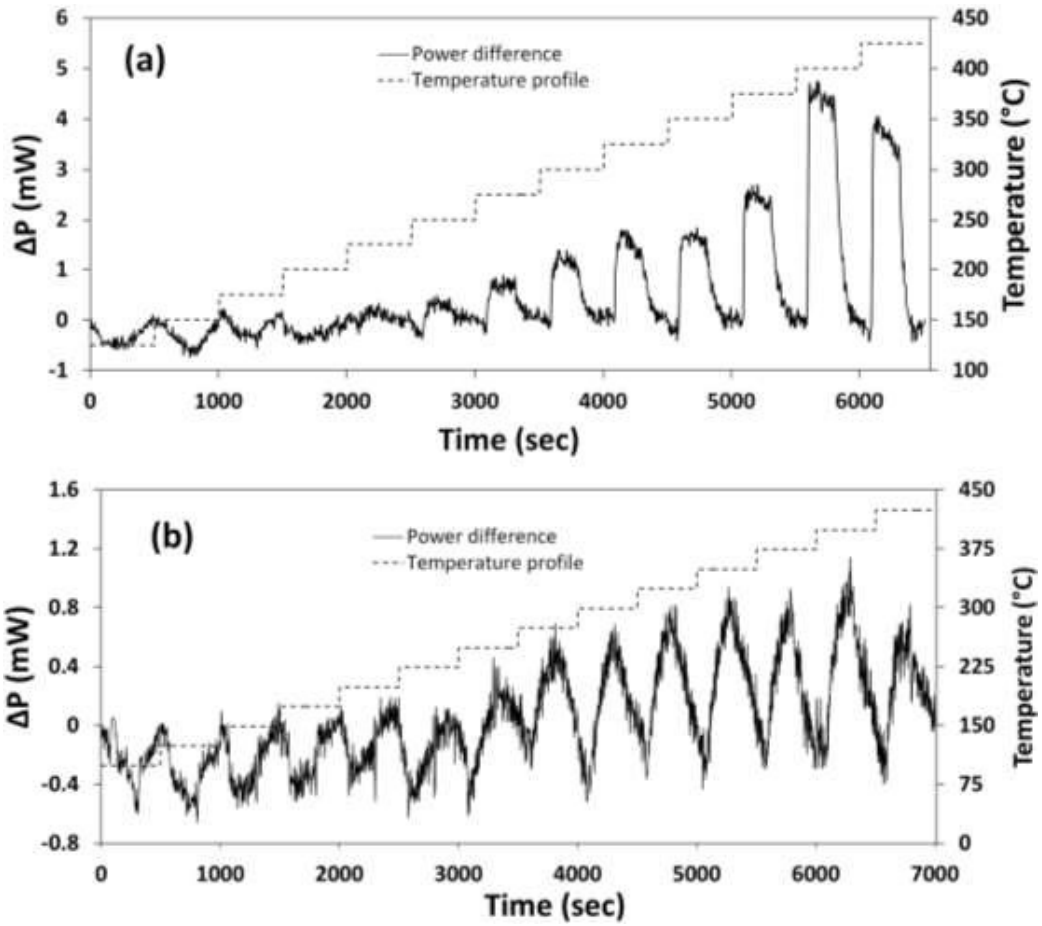

Figure 4.4 Response of thermodynamic sensor to 0.68μg/ml TATP using a SnO_2 catalyst, which was thermally scanned various temperature steps between 135°C – 435°C using (a) compressed dry air and (b) compressed nitrogen as carrier gas.

A comparative experiment was conducted to confirm this conclusion by using nitrogen as carrier gas to get the TATP molecules into the gas stream. As shown in Figure 4.4(b), the heat effect in the low temperature range (120°C – 240°C) exhibited the same sign and magnitude (response), and the same transition temperature; i.e. from a negative heat effect to a positive heat effect compared with results in Figure 4.4(a). This indicates that the same catalytic decomposition process was taking place. However, the magnitude of the response to TATP at high temperature range (280°C – 455°C) when using nitrogen as the carrier gas was much smaller which suggests that much less heat was consumed by H_2O to maintain temperature. This is because TATP

was not completely oxidized due to the absence of an oxidant and thus, much less H_2O was generated.

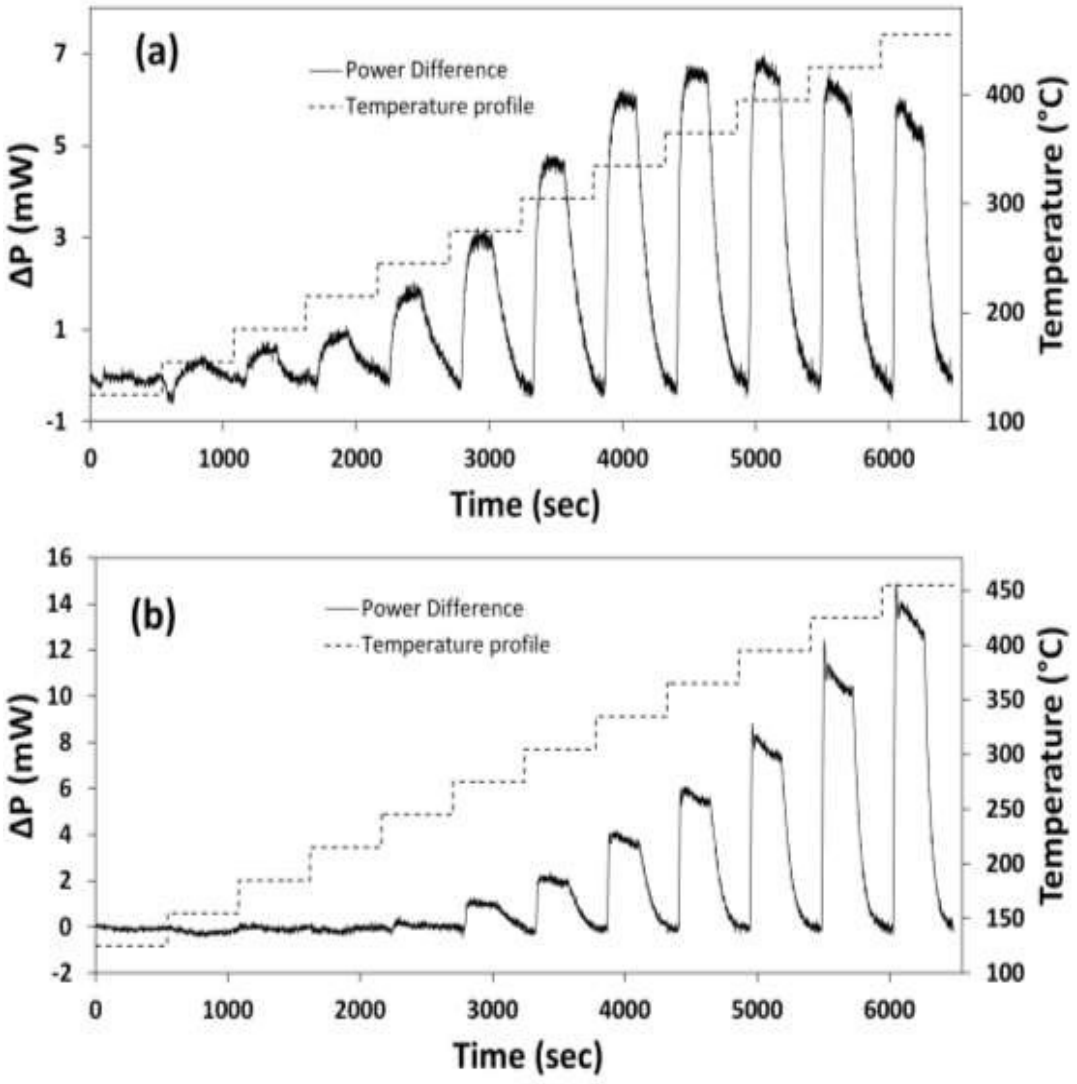

Figure 4.5Response of thermodynamic sensor using a 12 wt.% loading Pd nanocomposite catalyst to (a) 0. 68μg/ml TATP and (b) 0.225 μg/ml H_2O_2 at various temperature steps.

When compared to tests performed using pure SnO_2, the Pd: SnO_2 nanocomposite catalysts showed very different behavior (sensor response versus temperature) when exposed to TATP and H_2O_2 as shown in Figure 4.5(a). Unlike pure SnO_2, the nanocomposite catalyst clearly exhibited a positive response to TATP at low temperatures (120°C – 240°C) and reached a maximum with amplified response at

395°C without the obvious exothermic reaction. This suggested that a large amount of H_2O had already been generated at low temperature. This change in behavior from that of pure SnO_2clearly shows the role that palladium played in modification of reaction mechanism. However, as shown in Figure 4.5(b), the catalyst exhibited little or no response to H_2O_2 until a temperature of 275°C was reached, and then kept increasing as temperature was raised to 455°C.

The sensor responses as a function of vapor concentration were also performed in both H_2O_2 and TATP to determine the sensitivity and detection limit of our thermodynamic sensor and the results shown in Figure 4.6(a) and 4.6(b). For comparison purposes between different species, the term "percentage response" was used, which is defined as the power differences at each temperature stage divided by power used to maintain temperature in presence of inert gas at such stage. The concentration tests were performed at 400°C and the response of the nanocomposite catalyst loaded with 12 wt.% Pd was linear with respect to TATP and H_2O_2 as shown in Figure 4.6(a) and 4.6(b). Both responses were repeatable when the vapor concentration was reduced to 0.045 μg/ml and 0.14 μg/ml, respectively. The sensor exhibited a response time of less than 5 seconds whereas recovery took significantly longer to reach baseline. The additional time required for recovery was caused by the slow depletion of residual target gas after the supply was cut off.

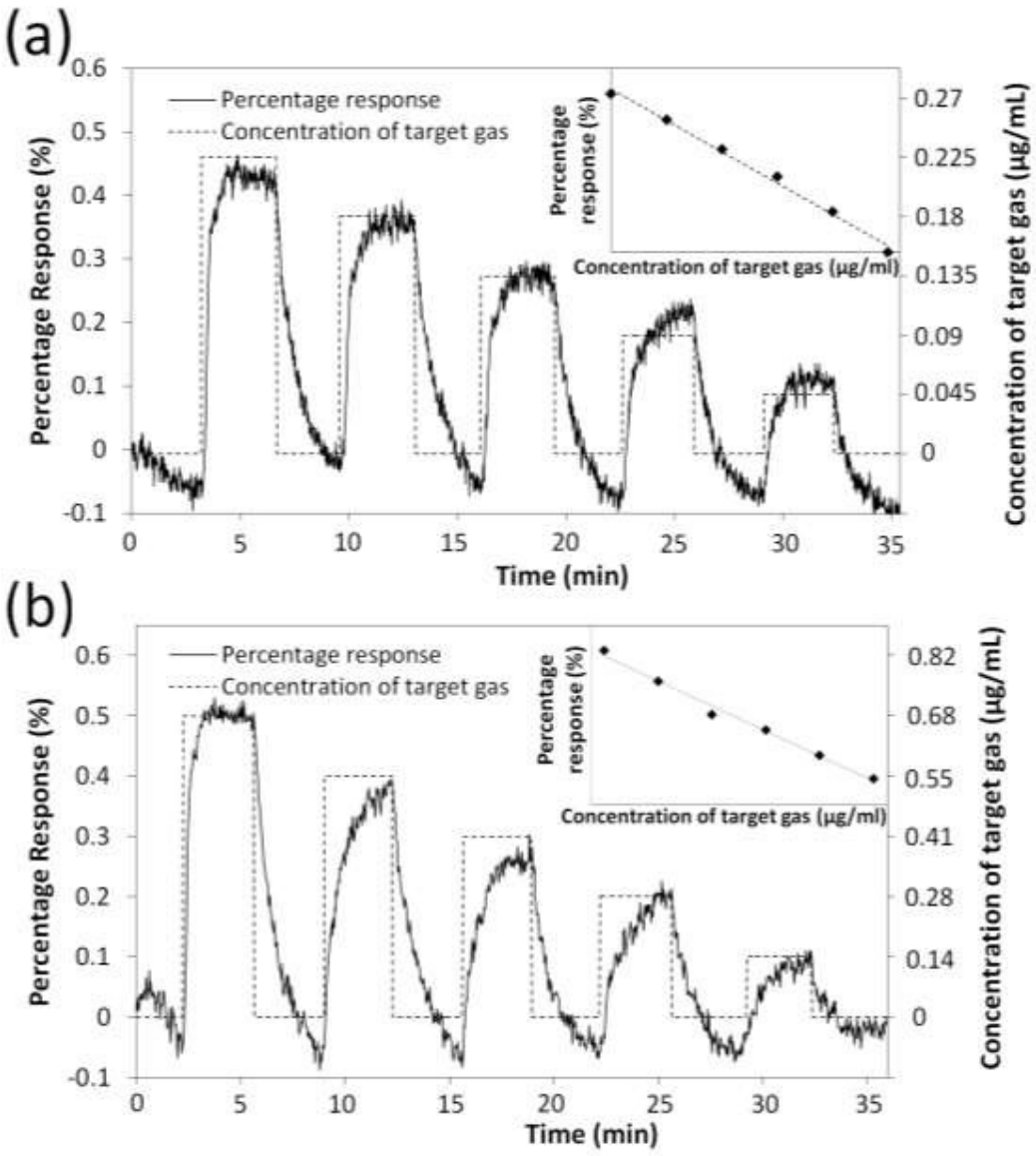

Figure 4.6 Response of a 12 wt.% Pd nanocomposite to (a) H_2O_2 and (b) TATP as a function of concentration in the vapor phase at 400°C.

Figure 4.7 shows the magnitude of the heat effect observed for a number of nanocomposite catalysts as a function of palladium loading in the presence of 0.68 µg/ml TATP and 0.225 µg/ml H_2O_2. At palladium loadings less than 8 wt.%, the sensors exhibit a relatively poor response compared to the un-doped SnO_2 catalysts.

However, at higher palladium loadings, there was a substantial increase in sensor response, which abruptly decreased when more than 12 wt.% Pd was incorporated into the catalyst. Higher palladium loadings in the catalyst showed almost no response to TATP and H_2O_2. While there was a substantial improvement in the maximum response to the two target molecules at a 12 wt.% palladium loading, the selectivity between these two target molecules was also significantly improved. A nanocomposite catalyst with a 8 wt.% palladium loading yielded the greatest selectivity (H_2O_2 relative to TATP) while a 12 wt.% palladium loading yielded the greatest sensitivity as shown in Figure 4.10.

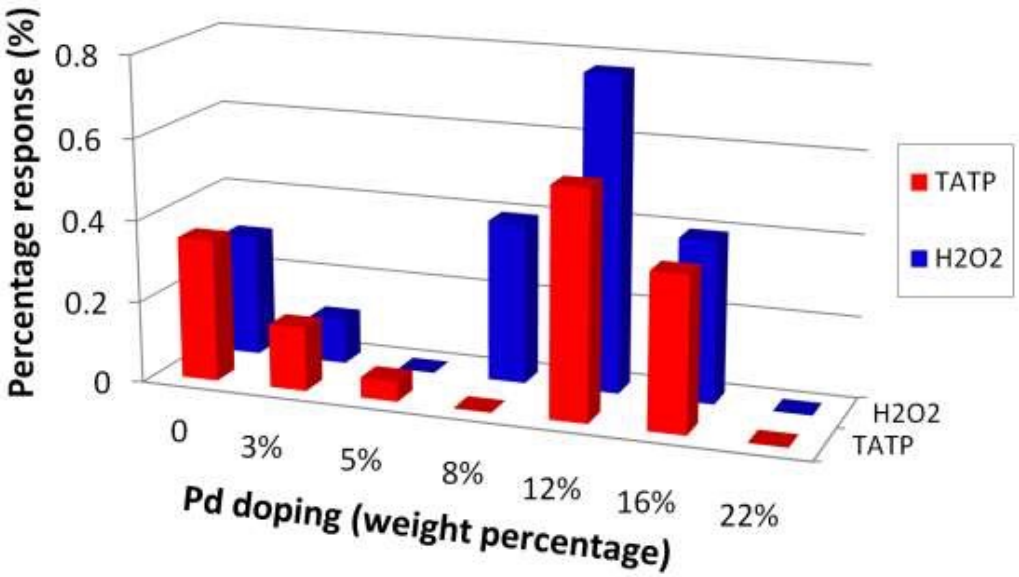

Figure 4.7 Summary of sensitivity and selectivity of Pd:SnO_2 nanocomposite catalyst with various Pd loadings to H_2O_2 and TATP at 400°C.

4.1.3 Effect of palladium doping amount

The role that palladium additions play when added to a metal oxide matrix such as SnO_2 has been addressed to some extent in the literature [8-17]. However, the

exact nature depended on variables including loading method [8-9], loading concentration [9-10], working temperature [11] and species of analytic gases [12-15], each of which played important roles in identifying the specific mechanism. In the current study, sensors using stoichiometric SnO_2 catalysts in the absence of Pd particles exhibited higher sensitivity to oxidizing vapors such as H_2O_2 and TATP compared to sensors using sub-stoichiometric SnO_{2-x}. At low Pd loadings, Pd atoms diffused uniformly into SnO_2 matrix and formed two possible bond types: (1) a strong Pd-Sn alloy metallic bond which was suggested by Tsud, et al [16] and (2) a Pd-O and O-Pd-O ionic bond which was confirmed in XPS. The first type of bond reduced the number of active SnO_2 molecules per unit surface area while the second type of bond essentially gettered oxygen atoms from the stoichiometric SnO_2 leaving a non-stoichiometric SnO_2. This can be a possible cause for the reduction in sensor response for palladium loadings in the range 0 - 8 wt.%. Meanwhile, both O-Pd-O bonds and Pd-O bonds were present in this loading range, as confirmed by XPS but the sensitivity of this catalyst decreased as shown in Figure 4.10. This suggests that neither O-Pd-O nor Pd-O independently functioned in a catalytic role.

As the Pd loading was increased, metastable oxygen molecules in the catalyst were released during annealing and diffused throughout the film. However, this oxygen was insufficient for Pd atoms to form O-Pd-O bonds, resulting in the disappearance of the PdO_2 peak as indicated by XPS and shown in Figure 4.3(b). Instead, relatively small Pd metallic clusters encapsulated in a PdO-SnO_2 matrix were formed, resulting in an increase in the Pd peak [16]. In addition, the Sn 3d peak intensity remained constant, whose presence corresponds to stoichiometric SnO_2. This

observation could occur by sharing oxygen atoms associated with PdO as indicated by the XPS spectra in Figure 4.3(a). Nanocomposite catalysts fabricated with 12 wt.% Pd and 88wt.% SnO_2 lead to a maximum in response, regardless of Pd loading in the Pd:SnO_2 nanocomposite. As the Pd loading was increased beyond this level, the size of Pd clusters increased, resulting in a relatively large Pd metallic XPS peak. As a result, the Pd clusters displaced the SnO_2 and caused an additional decrease in amount of SnO_2 and thus, a decrease in sensor response. Also, those sensors with palladium loadings greater than 22% showed no response to peroxides, indicating that neither the palladium nor the Pd^{2+} could function as catalysts.

The experiments suggest that the palladium itself, regardless of its oxidation state, did not affect the sensitivity of the Pd:SnO_2 catalyst but instead, appeared to amplify the signal by varying the oxidation state of SnO_2. Sensors with palladium loadings of 12 wt.% exhibited the maximum sensitivity (sensor response) to both TATP and H_2O_2.

4.1.4 Protocol of TATP identification

As indicated in Figure 4.7, a SnO_2 catalyst with a 12 wt.% palladium loading provided the greatest response to both TATP and H_2O_2at a temperature of 395°C. Thus, sensors with a 12 wt.% Pd loading were selected for long term exposure tests and were maintained at 400°C for prolonged periods as an early warning indicator; i.e. once a positive signal was received for an unknown vapor, measures could be taken to further identify the species of the suspect vapor. The sensor was then scanned at various temperature setpoints ranging from 150°C to 450°C to collect a characteristic signature as a function of temperature. H_2O_2 and TATP have significantly different

positive trigger points and their peak response temperatures can be used as a unique signature to distinguish TATP from H_2O_2. The Pd: SnO_2 nanocomposites with 5 wt.% and 8 wt.% palladium loadings were also employed. The 5 wt.% palladium catalysts only responded to TATP and showed no response to H_2O_2 while the 8 wt.% palladium catalysts gave opposite responses, as shown in Figure 4.7. These two sets of sensors provided a certain redundancy in response, which will help mitigate false positives.

4.2 Evaluation of the orthogonal sensor platform

4.2.1 Catalyst characterization

Oxidation states of metallic species in the SnO_2 and ZnO catalyst as a function of depth were characterized by XPS as shown in Figure 4.8. Position 1, 2 and 3 in both figures refer to the as-annealed surface 100Å and 600Å below the surface of the catalyst, respectively. Energy states associated with the Sn $3d_{5/2}$ and Sn $3d_{3/2}$ electrons show only slight changes as a function of depth with the exception that both 3d peaks taken at position 1 appear sharper, as shown in Figure 4.8(b). When sampled from position 1 to position 3, as shown in Figure 4.8(c), a phase transition was observed, during which the Sn 4d peak at 27.2 eV (+4 state) decreased and a shoulder associated with the Sn 4d peak at 26.6 eV (+2 state) increased and eventually formed a new peak. This indicated that a transition from stoichiometric SnO_2 at surface of catalyst to a nonstoichiometric SnO_{2-x} had occurred below the surface. From Figure 4.8(d), Zn 2p doublets can be observed, indicating that multiple oxidation states exist at the surface of ZnO catalyst most likely due to the oxygen introduced during annealing processes. Also the Zn $2p_{3/2}$ peaks at positions 2 and 3 shifted to lower binding energies and

appear sharper when compared to the peak at position 1, indicating that a uniformZnO_{1-Y} ayer had formed below the surface. This assumption was confirmed in Figure 4.8(e) by the disappearance of ZnO secondary peaks corresponding to the 3s and 3p states and an increase in intensity of the 3d peak as a function of position, which was verified as a transition in oxidation state.

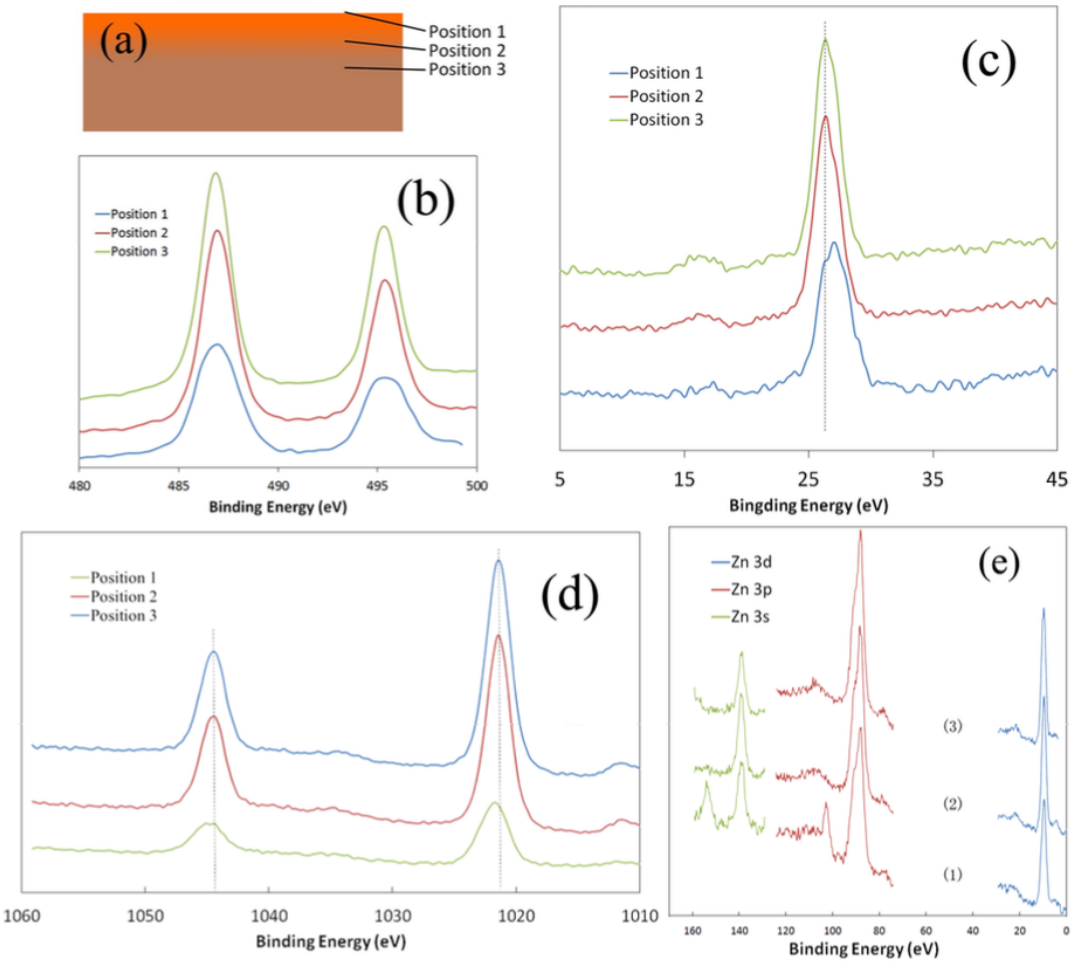

Figure 4.8 X-ray photoelectron spectra (XPS) results of SnO_2 catalyst. 3(a) indicates the sampling position in a cross-section diagram of catalyst; Sn $3d_{5/2}$ and Sn $3d_{3/2}$ states were shown in 3(b) and 4d states in 3(c). XPS results of ZnO catalyst. 3(d) indicates the Zn 2p states and 3s, 3p and 3d states in 3(e).

4.2.2 Sensor characteristics

Figure 4.9 shows a typical response from orthogonal sensors using SnO_2 and ZnO as catalysts in presence of 2,6-DNT. Responses using SnO_2 atalyst are presented in Figure 9(a), and responses using ZnO catalyst were initially collected from separate platforms, each individually tuned for optimal thermodynamic and conductometric response. Each sensor was pre-stabilized at 410°C for 15 minutes before recording data. DNT was then introduced into the test chamber after 1 minute for a period of 360 seconds as shown along the horizontal axis in Figure 4.9(a) and 4.9(b). The sensor employing SnO_2 catalyst exhibited the fastest thermodynamic response time (less than 5 seconds) whereas the conductometric response took significantly longer (60 - 80 seconds) to reach equilibrium and did not show a sharp transition after introduction of target gas. However, both thermodynamic and conductometric signals completely recovered to the baseline values within 5 minutes. Both the thermodynamic and conductometric signals using a ZnO catalyst demonstrated a rapid response time (less than 10 seconds). However, both responses took a longer time to reach equilibrium and recover, compared to those produced with a SnO_2 catalyst.

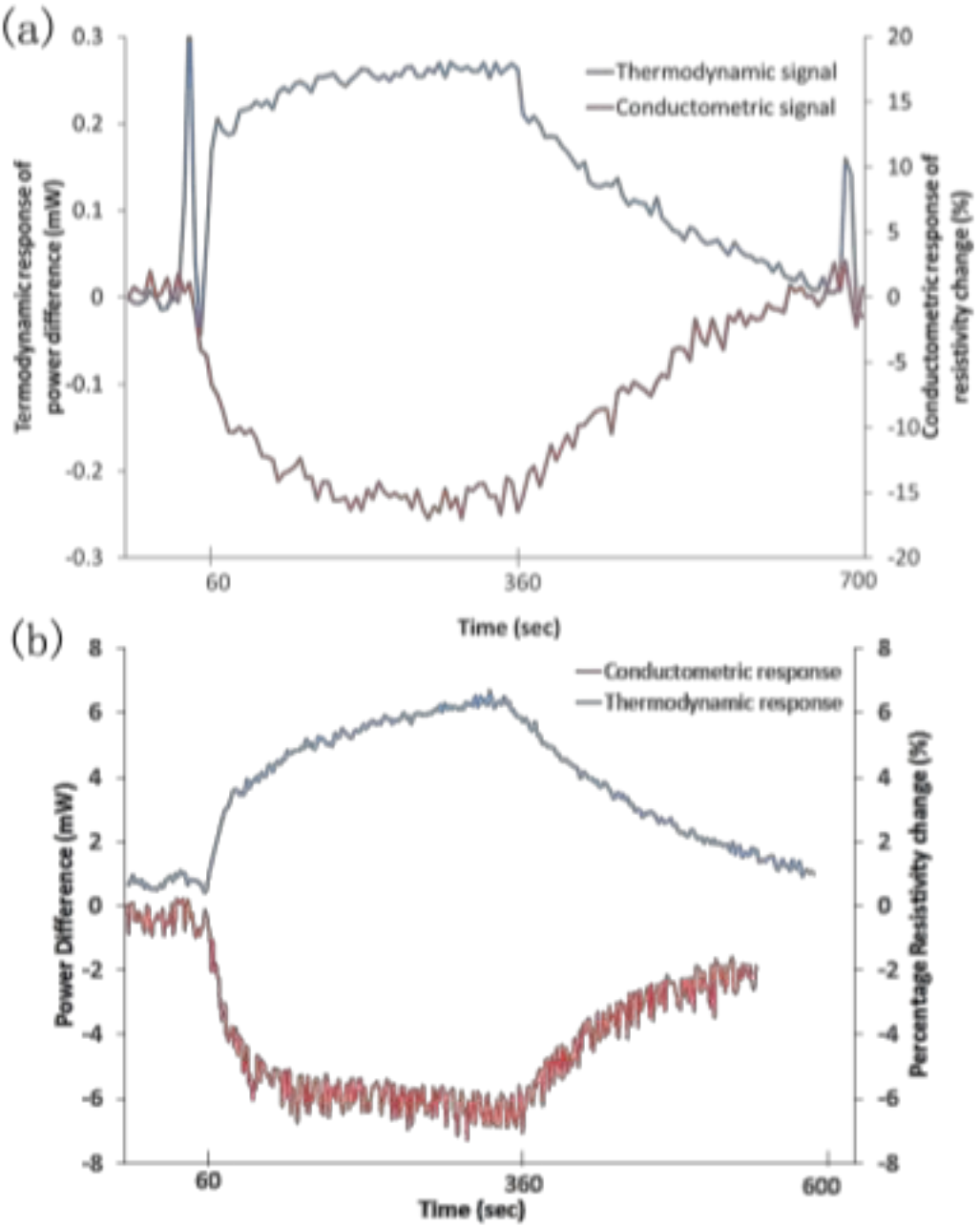

Figure 4.9 Thermodynamic response (blue) and conductometric response (red) to 2, 6-DNT at 410 °C taken simultaneously with SnO_2 (a) and ZnO (b) orthogonal sensor.

The difference in response times and recovery times between the two sensing platforms was attributed to their detection mechanisms. The thermodynamic platform measures the heat effect associated with the catalytic decomposition of the target gas, which was initiated instantly as the target gas molecules interact with the surface of

catalyst. When additional target gas molecules are introduced, same decomposition occurs immediately. This formed a dynamic equilibrium where decomposition rate was the rate-controlling step. The conductometric platform measures the charge carrier concentration which depended on donating or accepting extra charge carriers as the target gas molecule was adsorbed onto or desorbed from the surface of catalyst. This process also resulted in a dynamic equilibrium where the adsorption and desorption rate is the rate-controlling step. Since the chemical reaction rate is an order of magnitude faster than physical adsorption rate, the thermodynamic signal exhibits a much faster response time and recovery time compared to that of conductometric signal.

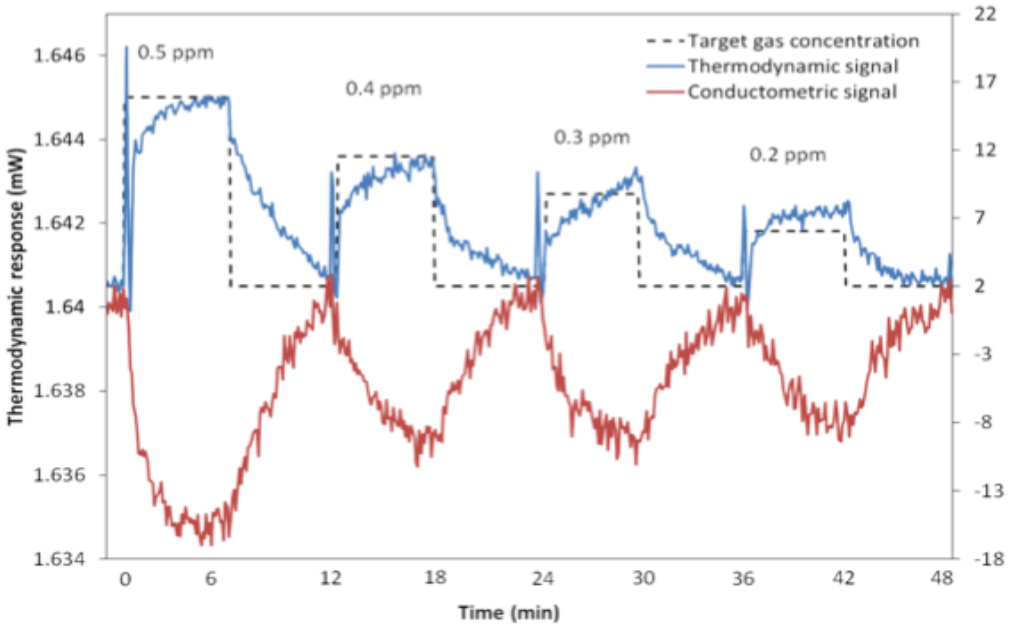

Figure 4.10 Orthogonal response of SnO_2 (where conductometric response is presented in red and thermodynamic response in blue) as a function of 2,6-DNT vapor concentration (black dashed line) at 410°C.

The orthogonal sensor response to 2,6-DNT as a function of DNT vapor concentration (at 410°C employing SnO_2) is shown in Figure 4.10. Here, the thermodynamic

response was linear with respect to DNT vapor concentration whereas the conductometric response remained the same as the DNT vapor concentration decreased. Both responses were repeatable when the vapor concentration was reduced from 0.5 ppm to 0.2 ppm.

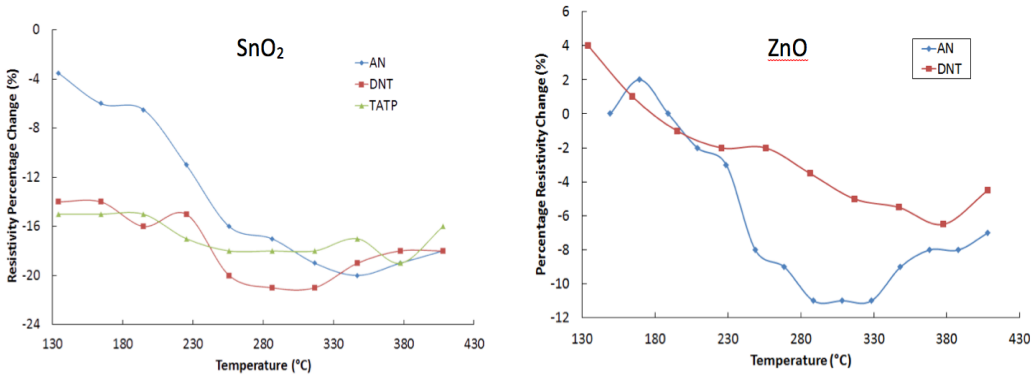

Figure 4.11 Conductometric response of SnO_2 (a) and ZnO (b) to ammonia nitrate (blue), 2,6- DNT (red) and TATP (green) as a function of temperature.

The conductometric response to ammonium nitrate, DNT and TATP vapor as a function of temperature employing SnO_2 and ZnO as catalysts are shown in Figure 4.11. The responses of both catalysts to ammonium nitrate was proportional to temperature at low temperature ranges (<250°C) and then decreased with temperature as it was raised over 350°C. 2, 6-DNT showed similar behavior relative to ammonium nitrate but only exhibited a shallow peak at 280°C with both catalysts. The TATP signal produced from the SnO_2 catalyst changed very little with the temperature, whereas these sensors employing ZnO catalyst did not show a conductometric response to TATP and therefore, were not included here. These differences in sensor response could be caused by the differences in vapor pressure of target molecules and differences in the functional groups and molecular structures between the target molecules. However, the exact mechanism remains unknown due to the complexity of

the processes. As a result, all three compounds (TATP, DNT and ammonium nitrate) exhibited unique signatures (orthogonal responses), which could be used to further characterize their presence and mitigate false positives and negatives.

4.3 Preconcentrator Evaluation

4.3.1 Effectiveness of using a dynamic control

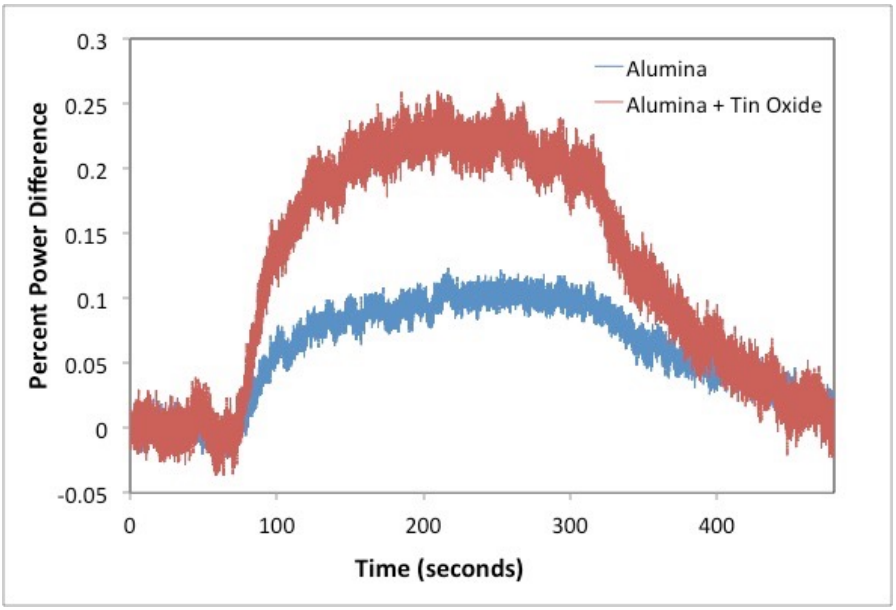

Figure 4.12 Thermodynamic response of SnO2 catalyst to 2,6- DNT (red) and the simultaneously responding dynamic control (blue).

Before the preconcentrator is discussed in detail, it is worth detailing the benefits of using a dynamic control sensor to eliminate extraneous heat signals. Take for instance Figure 4.12, depicting a single step test at 400ºC for 2,6-DNT using a stoichiometric SnO_2 catalyst. The step response from the catalyst microheater is plotted on the same axes as the response from the control, and it can be observed that the catalyst response is much larger. Both the dynamic control and the catalyst coated sensor responds to the adsorption and desorption of molecules on the alumina surface. Adsorption can either be chemiadsorption , the result of a covalent bond between the

adsorbent and the analyte causing a relatively large heat effect, or physiadsorption, the result of weak van der Waals attractions causing a relatively smaller heat effect. Alumina is mostly non-reactive thus will likely physiadsorb any analytes or vapors [18, 19]. Another contributing thermodynamic effect is the sensible heat effect change that occurs when the explosive vapors are introduced to the sensor. Though the explosive vapors are only present at trace levels, the heat capacity of many of these energetic materials are so large relative to that of air, that the change can be registered by our thermodynamic sensor. If the incoming gas to the sensor is considered as a "coolant," the air containing trace explosive molecules is a better coolant than pure air and thus the sensor requires slightly more power to maintain a constant temperature. A small contributing heat effect could also be the presence of nickel oxide on the surface of the microheater. Previous study has shown that NiO reacts with a few target explosives [20], and can form on the surface of the microheaters after sputtering before the it is coated with the dielectric. Although, any NiO present is embedded under alumina cement and is unlikely to be a major contributing thermodynamic factor.

That leaves the catalyst coated sensor only to catalytically react to the analyte, resulting in a larger thermodynamic signal than that of the dynamic control. Thus, when determining the power difference at this temperature set point, the crest of the dynamic control response is used as a baseline instead of the power requirements during the flow of pure air. Signatures that can be used to identify a particular explosive using a particular catalyst can now be obtained with more clarity because the pure catalytic heat effects can be isolated.

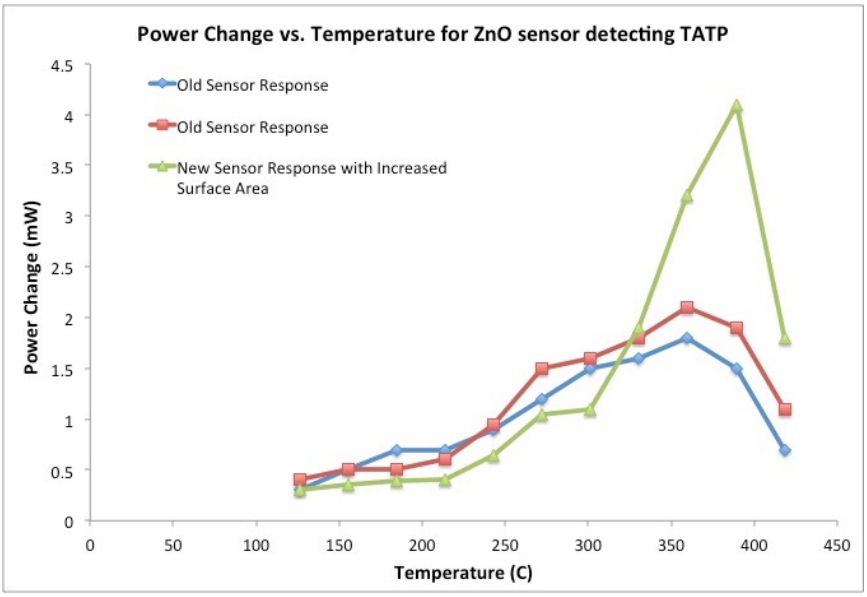

Figure 4.13 Thermodynamic signal of a ZnO catalyst detecting 7 ppm TATP.

Figure 4.13 shows one such signature obtained for TATP using a ZnO film. On the same axes are signatures from two different sensors that do not have the benefit of a thermodynamic control. Between 125ºC-300ºC the new signature falls below the previous signature, indicating that there are heat affects that the old signal is accounting for that are indeed filtered from the latest result. Also, there is a very pronounced peak at 375ºC, much larger in magnitude than before. The resolution of this peak is due to the use of a dynamic control to filter out the extraneous heat signals, but the magnitude change was due to another reason entirely.

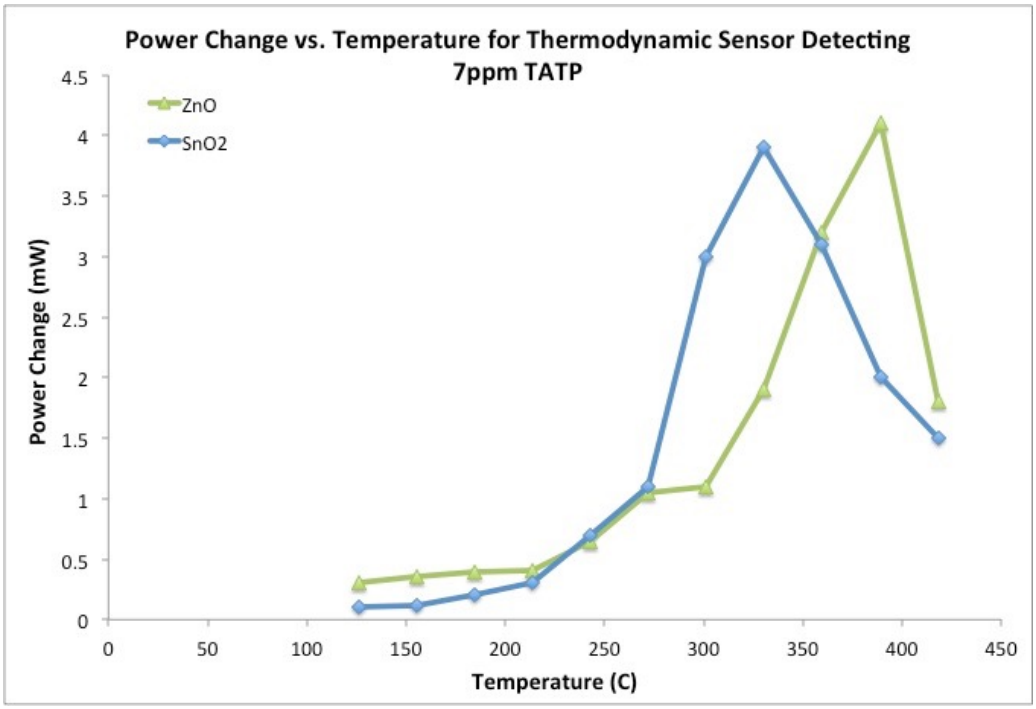

Figure 4.14 Thermodynamic signatures of SnO_2 (blue) and ZnO (green) to 7ppm TATP.

An added benefit of this approach is the enhancement in sensitivity due to the high surface area of the alumina cement. The primary purpose of the cement was as a dielectric to prevent electrical shorts between the Ni microheater and the semi-conductive catalyst film. In the orthogonal sensor, Ni electrodes were placed on top of the cement as well, making it necessary to polish the cement surface and bevel the edges to make the surface conducive to deposition by sputtering. In these thermodynamic sensors used for evaluation of the dynamic control, the cement films were left as is, remaining highly porous. It is also the nature of sputtered films that they coat the substrate surface, preserving any and all surface features. The result was a high-surface area catalyst surface with a much higher density of catalytic sites, directly improving sensitivity. Testing with these sensors yielded a large increase in magnitude of the thermodynamic signal for testing with ZnO and SnO_2, as seen in Figure 4.14. An interesting feature of this plot is the shift in peak placement in the

signature for each catalyst. The peak occurs at 375ºC with ZnO, but using SnO_2 the peak occurs at 325ºC. This peak corresponds to the largest catalytic heat effect, and because it occurs at different temperatures for different catalysts, it reinforces that these signals are unique and can be used to identify an unknown vapor as TATP. Finally, a concentration test was conducted using SnO_2 to determine if the detection limit for TATP had changed (Figure 4.15) . Without the alumina cement, the sensor was able to detect TATP at 537 parts per billion (ppb), but with the enhanced surface area, the detection limit was reduced to 134 ppb.

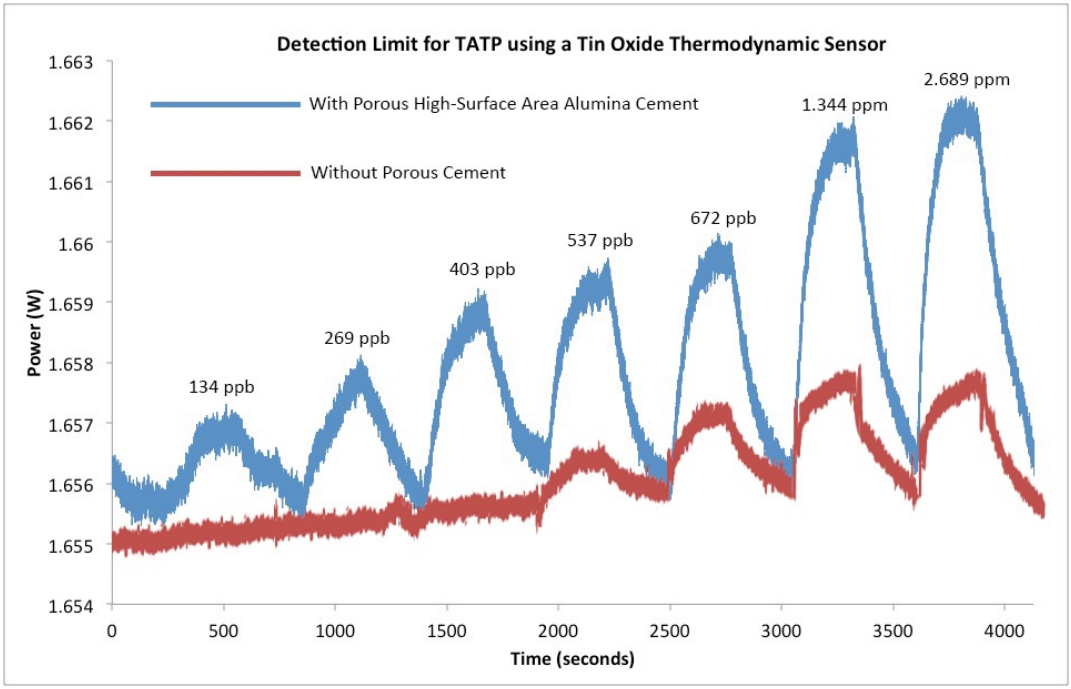

Figure 4.15 Concentration test illustrating the detection limit of TATP using a SnO_2 catalyst.

4.3.2 Preconcentrator results

The first polystyrene preconcentration test was conducted using a stoichiometric SnO_2 catalyst and 2,6-DNT, resulting in the step response in Figure 4.16. The polystyrene film used in this test was measured to be approximately 10 µm.

Partway through the step, a small peak is observed, corresponding to the start of the preconcentrator's desorption phase. The power change as a result of these preconcentrated molecules was small. However, the expected power change as a result of the added heat from the preconcentrator was expected to be negative. The fact that the direction of the response is positive led to the determination that a method to filter out the thermal desorption heat effects was necessary to resolve any increase in sensitivity.

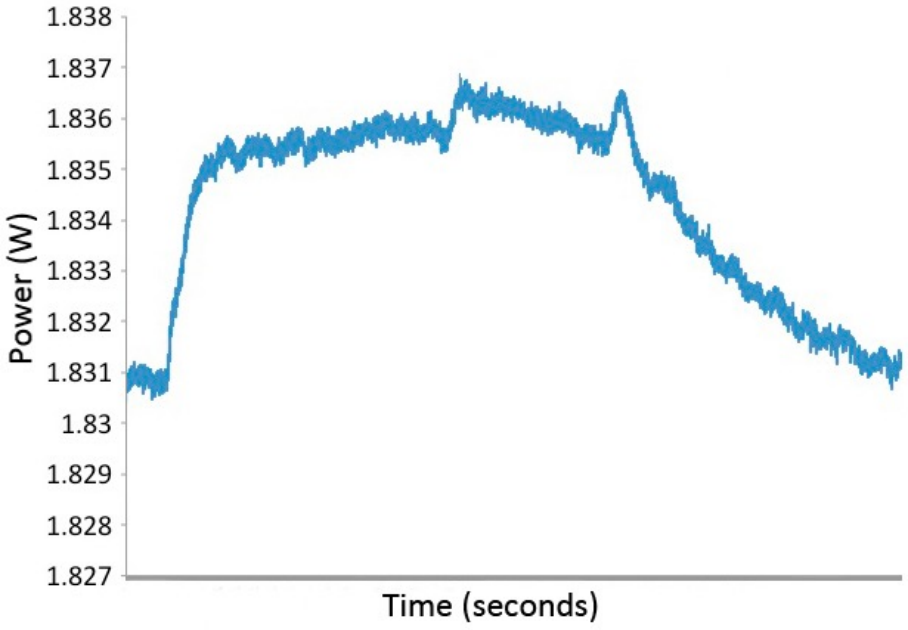

Figure 4.16 Preconcentration test conducted using a stoichiometric SnO_2 catalyst and 2,6-DNT

Implementing a dynamic control sensor along with the SnO2 sensor, and conducting the same experiment with DNT, yielded the signal seen in Figure 4.17. The signal on top is from the catalyst coated sensor and closely resembled the sensor response in Figure 4.16. However, the figure on the bottom from the dynamic control sensor shows the negative change in power associated with the thermal desorption phase of the preconcentrator. There are three significant changes in the signal, as

indicated in Figure ## by the numbers (1) through (3). (1) marks the beginning of DNT delivery to both the preconcentrator and the sensors further downstream. During this time the preconcentrator was collecting DNT molecules and was thus maintained at room temperature. (2) indicates when the preconcentrator is heated from 20ºC to 97ºC to begin the thermal desorption of the trapped DNT molecules. At this point the dynamic control exhibits a downward power change, responding to the rise in the temperature of the incoming air, which is expected. The catalyst coated sensor exhibits a positive change, indicating that more DNT is reaching the catalyst surface, thereby increasing the magnitude of the response. Finally, (3) is the point at which the preconcentrator is turned off and reference gas is reintroduced to the chambers to observe the sensor's recovery.

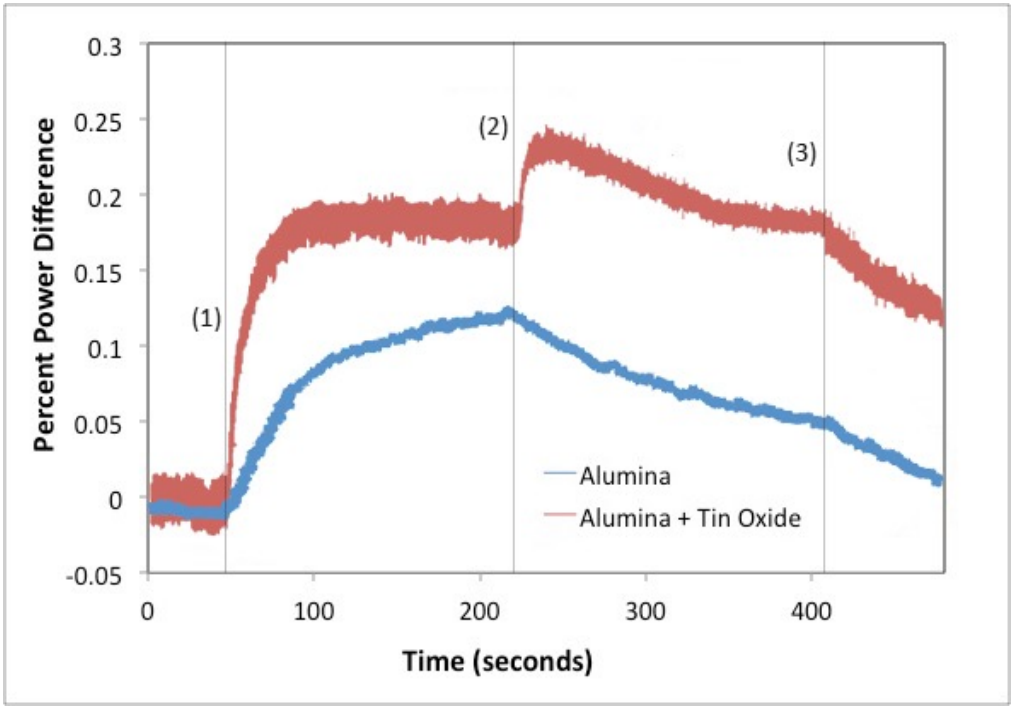

Figure 4.17 Preconcentration test conducted using a stoichiometric SnO_2 catalyst and 2,6-DNT using the dynamic control method: (1) beginning of DNT delivery to sensors (2) preconcentrator begins thermal desorption (3) preconcentrator is turned off and reference gas is reintroduced to the chambers

Using this dynamic control method, the extraneous heat activity, which now encompasses the thermal desorption of the preconcentrator, can be filtered from the catalyst signal. The new power change is determined by measuring the difference between the power of the catalyst sensor signal between points (2) and (3) and the power of the dynamic control in that same interval. It can be seen on this signal that using the preconcentrator increases the magnitude of this power difference, from 0.1% to 0.15%.

4.3.3 Factors affecting preconcentrator operation

Additional tests were then conducted, using the same testing protocol and sensor configuration while varying some key test parameters. A second preconcentrator, with a much thinner polystyrene film, was interchanged with the first. The thickness was measured to be less than 1 μm. It was expected that the decrease in thickness of the adsorbent film would lower the retention volume, thus resulting in a smaller thermodynamic signal during thermal adsorption. What was observed was no significant change in the magnitude of the thermodynamic signal, indicating that the retention volume of the sorbent was independent of the thickness of the film. The spin-coated polymer films are likely dense and nonporous, only allowing the adsorption of molecular species on the planar polymer surface.

It was then hypothesized that shortening or lengthening the collection time would decrease or increase the thermodynamic sensor response respectively. Figure 4.18 shows the effect of collection time on the magnitude of the change. At low collection times, the relationship is almost linear indicating that longer collection times result in proportionally larger responses. This was true until collection was

allowed to occur for 200 seconds or longer. Increasing the time any further yielded diminishing returns. It appears that after 200 seconds of collection, the adsorption sites on the polystyrene film are all occupied and the film becomes saturated. It is also worth noting that at time 0, there is a power difference between the two sensors. This is likely due to heat losses that occur in the distance between the preconcentrator and the sensor chambers.

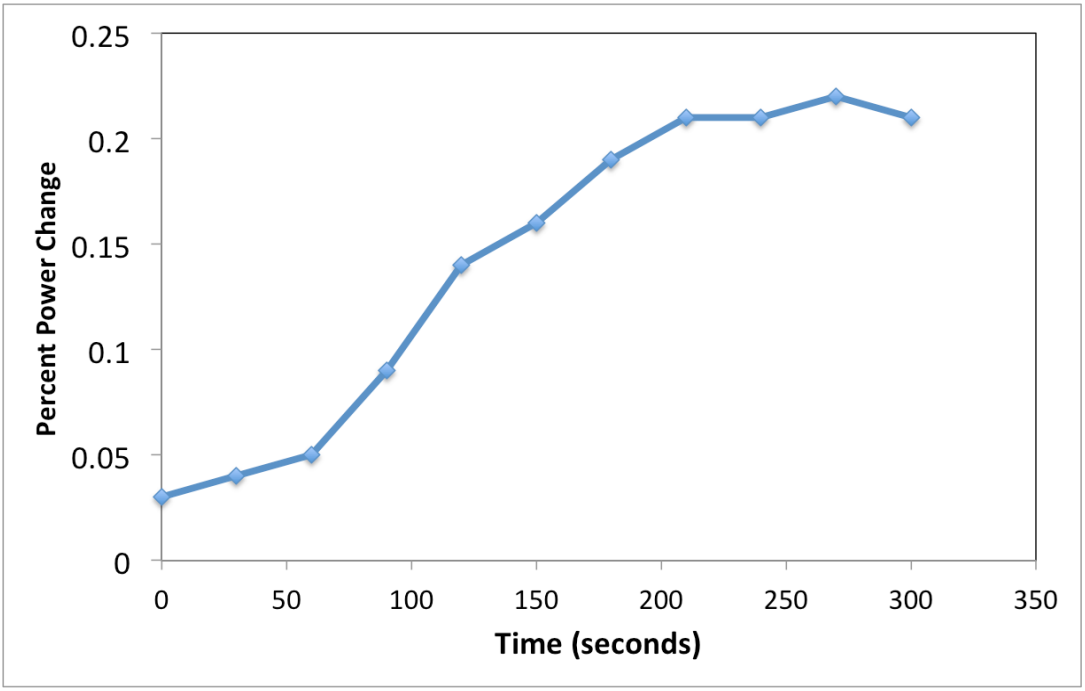

Figure 4.18 Effect of preconcentrator collection time on the magnitude of the thermodynamic sensor response.

Some sources also report that flow rate is an important factor in the adsorption process [18-19]. Figure 4.19 shows different power changes recorded at different flow rates. It was important for this test to vary the flow rate, but maintain the same volume of air that passes over the sensors. For instance, when the flow rate was at 100 sccm, the collection period lasted 2 minutes. When the flow rate was reduced to 50 sccm, the collection period was lengthened to 4 minutes, making the total volume (and

thus total amount of analyte) the same in both experiments. The result was a proportional relationship between the flow rate of the gas and the resulting thermodynamic signal. Several sources indicate that the increased pressure in the preconcentrator favors the adsorption process. This is a positive result for preconcentration because it indicates that in order to accelerate the adsorption process, the flow rate could be increased. The preconcentrator geometry in this case is also such that not every analyte molecule comes in contact with the adsorbent film and is captured. If an increased flow rate could be paired with a preconcentrator design that ensured contact with a greater percentage of the incoming air, a larger increase in response would be observed.

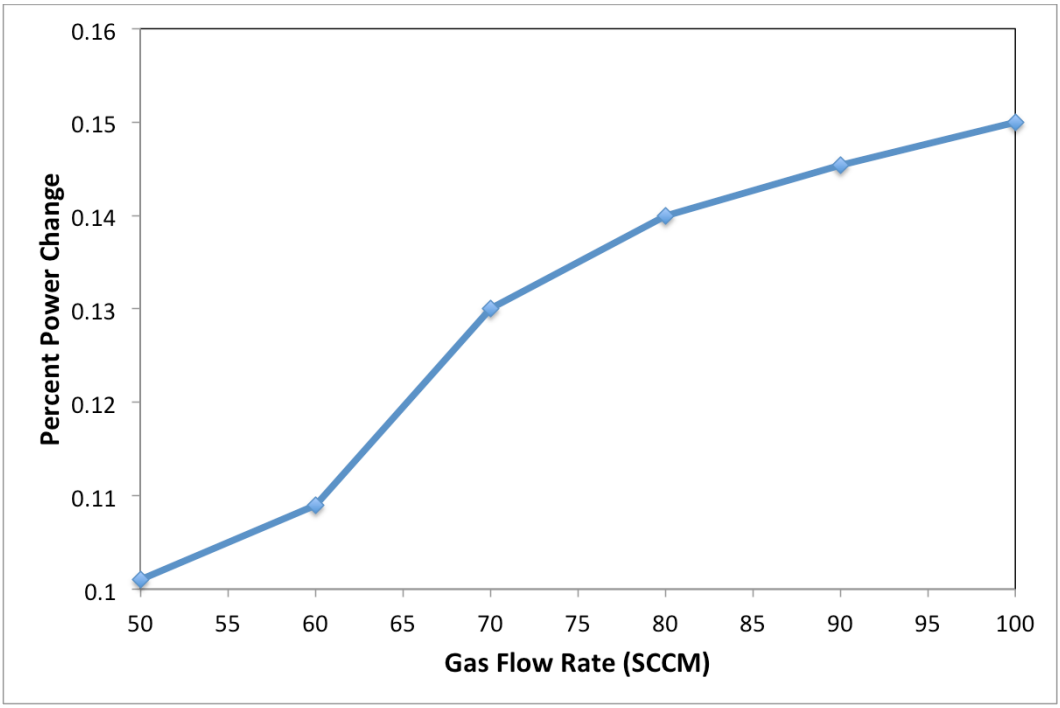

Figure 4.19 Effect of flow rate on the magnitude of the thermodynamic sensor response.

Other analytes were also tested to determine any and all changes in preconcentrator design. Out of all the analytes tested, 2,6-DNT had the most dramatic results, and this agrees with many sources that indicate polystyrene has a high affinity

for nitroaromatic compounds. Tests were conducted with both TATP and AN as the analyte. TATP did adsorb to the polymer surface, however the resulting increase in power difference during thermal desorption was less than 0.05%, suggesting either a low adsorption or desorption rate for TATP using polystyrene. AN did not show any measurable response, even at large collection times, confirming many sources that indicate ammonium nitrate adsorbs with great difficulty.

4.3.4 Implications

Overall, the preconcentrator was successful in increasing the sensitivity of the sensor. At the same target gas concentration, the magnitude of the sensor response increased from 0.1% to 0.15%. The dynamic control method is also successful on its own and will likely be a fixture in all of the experimentation moving forward. As it stands based on these experiments, the preconcentrator can be operated successfully in a semi-continuous process, albeit with a longer than desired time constant. When considering the practical application of this method, a timing scheme could be developed that cycles the preconcentrator between collection and desorption repeatedly. Figure 4.18 indicated that a maximum analyte retention occurred at collection times as low as 200 seconds, and 120 seconds would be a reasonable amount of time to desorb enough analyte to illicit a response. In addition, time must be allowed for the preconcentrator to cool back to its collection temperature, which it currently does passively in approximately 60 seconds. The attractiveness of this vapor sensor in general is the potential for instantaneous results, thus adding a waiting period totaling more than 4 minutes between results is undesirable. To implement this preconcentrator in real time, steps will have to be taken to reduce the collection time

and to boost the retention volume of the adsorbent. This could be done by increasing the size and changing the geometry

These experiments also reveal that the preconcentrator requires a specific adsorbent to attract a specific analyte. Polystyrene was only successful in adsorbing, 2,6-DNT, but a different sorbent could easily be implemented in its place. Polystyrene also has a thermal limitation. Its glass transition temperature at 100ºC places a restriction on thermal desorption, however, some sources indicate that higher temperatures are necessary for more complete desorption of collected DNT. Spin coating the polystyrene also resulted in a dense film that was evidently only capable of surface adsorption. Experimentation will have to be done into sorbents that vary according to specificity, thermal stability and deposition technique.

4.4 Thermodynamic analysis of the MEMS platform

4.4.1 Solid State Sensor

As a reference, the energy input required for the operation of the solid-state sensor will be calculated here. The energy, q, required to heat the sensor from room temperature to an elevated operating temperature is:

$$q = C_p(T - T_i)n$$

where C_p is the heat capacity of the substrate, n is the number of moles in the substrate, T_i is room temperature and T is the desired operating temperature, which on average is approximately 400°C. We will assume for simplicity that the contributions to thermal mass of the microheater and dielectric films are negligible with respect to the bulk alumina. Thus the total heat capacity can be taken as the specific heat

capacity of alumina (79.04 J/mol-K). The number of moles can substituted by density resulting in the following:

$$q = \frac{C_p \rho V}{M}(T - T_i)$$

where ρ is the density of alumina (3.9 g/cm^3), V is the volume (calculated to be 0.063 cm^3 based on the dimensions of the sensor) and M is the molecular mass of alumina (102 g/mol). Thus, substituting all of these values yields a total heat of 72.35 J. In order to determine the heat required to maintain the sensor at that elevated temperature, Fourier's Law will be applied. For simplicity, we will assume that the bulk of the heat lost by the sensor occurs in the direction normal to the plane of the microheater. If we consider only the active area of the microheater, this direction has the largest cross sectional area and will contribute the most to heat loss. The simplification will be made that the primary means of heat transfer are convection and conduction, ignoring radiation. The heat lost, using a modification of Fourier's Law of combined conduction and convection is:

$$q = UA\Delta T$$

Where A is the cross sectional area of the active area of the microheater (calculated to be 0.3338 cm^2 based on sensor dimensions), ΔT is 400°C - 20°C = 380°C, and U is the overall heat transfer coefficient, which in the +x direction is:

$$U = \left(\frac{1}{h} + \frac{\Delta x}{k}\right)^{-1}$$

where h is the convection heat transfer coefficient of air (approximately 55.6 W/m^2-K for the natural convection of air over a static plate of this size), k is the thermal

conductivity of alumina (30 W/m-K) and Δx is the thickness of the alumina substrate (0.5 mm). In the –x direction U = h. Thus:

$$q_{total} = q_{+x} + q_{-x} = \left(\frac{1}{h} + \frac{\Delta x}{k}\right)^{-1} A\Delta T + hA\Delta T$$

which when all of the appropriate values are substituted in corresponds to 1.410 W. This value is in agreement with typical power requirements for microheaters at 400°C, which can require anywhere from 1.5 W to 2.0 W to maintain constant elevated temperature. This theoretical value is an underestimation because it does not take into account conduction and convection heat losses in the y or z directions. It will be noted that contributions to heat loss are largely due to natural convection, conduction playing only a small role.

4.4.2 URI MEMS sensor

The same equation from the solid state calculations can be used to calculate the heat required to elevate the single sensor MEMS to 400°C from room temperature:

$$q = \frac{C_p \rho V}{M}(T - T_i)$$

however, this time there are two different substrate materials to consider: Si and Pyrex glass. There is also a cavity underneath the active microheater, so the equation must now account for the reduced mass, therefore:

$$q_{total} = q_{Si} + q_{glass} = \left(\frac{C_{p,Si}\rho_{Si}V_{Si}}{M_{Si}} + C_{p,glass}m_{glass}\right)(T - T_i)$$

The values of each of these parameters is summarized in Table 4.1. Substituting all of these values yields a total heat of 1.178 J.

	Silicon	Pyrex Glass
Thermal conductivity, k	149 W/m-K	1.005 W/m-K
Density, ρ	2.329 g/cm^3	2.23 g/cm^3
Volume, V	4.93 x 10^{-4} cm^3	1.24 x 10^{-3} cm^3
Molar mass, M	28.085 g/mol	-
Heat Capacity, C_p	19.789 J/mol-K	0.84J/g-K

Table 4.1. Summary of material properties in the URI MEMS sensor.

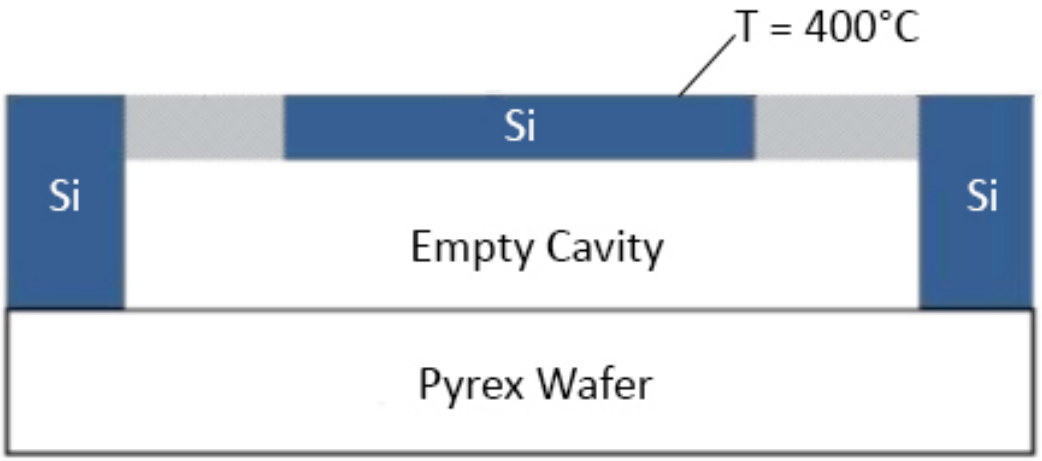

Figure 4.20. Cross sectional schematic of the URI MEMS sensor. The Si membrane is 0.5 um thick, the empty cavity is 0.195 mm thick, and the Pyrex wafer is 0.5 mm thick. The active microheater surface is 1 mm x 1 mm.

The heat required to maintain temperature will also be calculated using Fourier's Law. A cross-section is available in Figure 4.20 illustrating this configuration. Applying Fourier's law,

$$q = UA\Delta T$$

In the upward direction, heat loss is due to natural convection, thus:

$$q = hA\Delta T$$

The heat transfer coefficient for air, h, is recalculated to be 10.45 W/m^2-K because the geometry is much smaller. In the downward direction, heat loss is due to combined conduction and convection:

$$q = UA\Delta T$$

$$U = \left(\frac{1}{h} + \frac{\Delta x_{Si}}{k_{Si}} + \frac{\Delta x_{air}}{k_{air}} + \frac{\Delta x_{pyrex}}{k_{pyrex}} + \frac{1}{h}\right)^{-1}$$

The values for the parameters in this equation are available in Table 4.1. Substituting these values into the equation yields an operating power of 1.97 mW.

4.4.3 Latest MEMS design

Again, the same equation from the solid state calculations can be used to calculate the heat required to elevate the MEMS chip to 400°C from room temperature:

$$q = \frac{C_p \rho V}{M}(T - T_i)$$

The materials to consider are the substrate, which is silicon wafer with a cavity etched into it, and the suspended membrane, composed of stacked layers of silicon dioxide and silicon nitride. Thus,

$$q_{total} = q_{Si} + q_{SiO2} + q_{Si3N4}$$

$$q_{total} = \left(\frac{C_{p,Si}\rho_{Si}V_{Si}}{M_{Si}} + \frac{C_{p,SiO2}\rho_{SiO2}V_{SiO2}}{M_{SiO2}} + \frac{C_{p,Si3N4}\rho_{Si3N4}V_{Si3N4}}{M_{Si3N4}}\right)(T - T_i)$$

The values needed for this calculation are provided in Table 4.2 and substituting them into the previous equation yields a total heat of 0.3144 J (or 0.0789 J for each sensor on the chip).

	Silicon	Silicon Dioxide	Silicon Nitride
Thermal conductivity, k, W/m-K	149	1.4	26.5
Density, ρ, g/cm^3	2.329	2.648	3.44
Volume, V, cm^3	4.93 x 10^{-4}	6.25 x 10^{-6}	2.50 x 10^{-6}
Molar mass, M, g/mol	28.085	60.08	140.28
Heat Capacity, C_p, J/mol-K	19.789	43.98	99.68

Table 4.2. Summary of material properties for new MEMS sensor design.

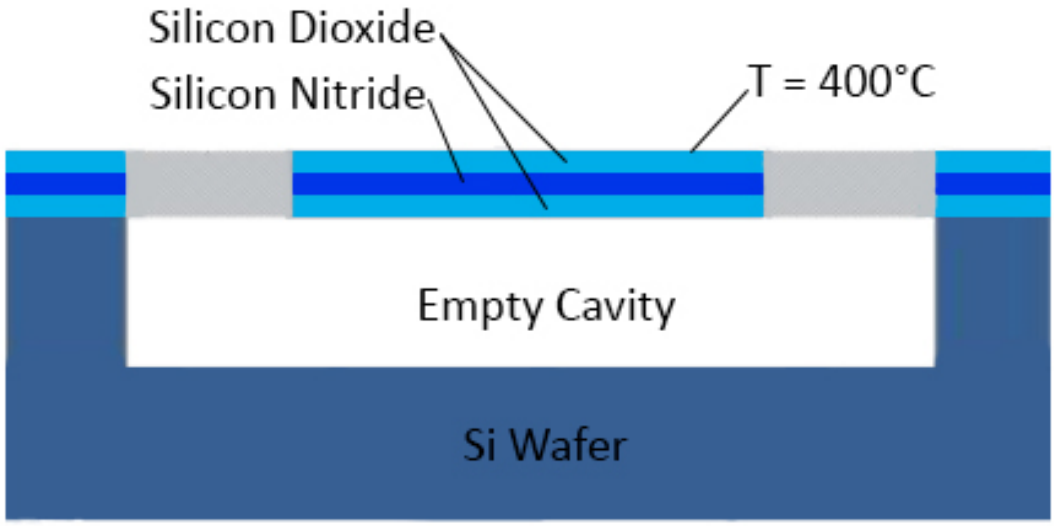

Figure 4.21. Cross sectional schematic of the new MEMS sensor. The membrane is composed of 150 nm SiO_2 / 100 nm Si_3N_4 / 100 nm SiO_2, the empty cavity is 0.19 mm thick, and the etched Si wafer is 10um thick. The active microheater surface is 0.25 mm x 0.25 mm.

The heat required to maintain temperature will also be calculated using Fourier's Law. A cross-section is available in Figure 4.21 illustrating this configuration. Applying Fourier's law,

$$q_{total} = UA\Delta T$$

In the upward direction, heat loss is due to natural convection, thus:

$$q_{up} = hA\Delta T$$

The heat transfer coefficient h is the same as in the URI MEMS, 10.45 W/m^2-K. In the downward direction, heat loss is due to combined conduction and convection:

$$q_{down} = UA\Delta T$$

$$U = \left(\frac{1}{h} + \frac{\Delta x_{SiO2}}{k_{SiO2}} + \frac{\Delta x_{Si3N4}}{k_{Si3N4}} + \frac{\Delta x_{SiO2}}{k_{SiO2}} + \frac{\Delta x_{air}}{k_{air}} + \frac{\Delta x_{Si}}{k_{Si}} + \frac{1}{h}\right)^{-1}$$

Substituting the values available in Table 4.2, the total power necessary to maintain one of the four sensors on the new MEMS chip design is 0.495 mW.

4.4.4 Overall Comparison

	Solid State	URI MEMS	New MEMS
Energy required to heat from 20°C to 400°C	72.35 J	1.178 J	0.079 J
Power required to maintain 400°C	1.410 W	1.97 mW	0.495 mW
Catalyst area	0.33 cm^2	0.01 cm^2	6.25 x 10^{-4} cm^2

Table 4.3 Comparing the heat requirements for all three sensor platforms.

Table 4.3 summarizes the estimations of the previous sections. These calculations exclude heat losses due to radiation and the conduction heat loss in the horizontal direction (across the suspended bridges in the MEMS), but it is a reasonable assumption that the largest heat loss is due to natural convection, and that is the means of comparison here. The results indicate that the MEMS sensors consume considerably less power than their solid-state counterpart. Furthermore, the newest iteration of the MEMS sensor consumes even less, due to thinner membranes, a

smaller active surface area and an overall smaller thermal mass. It will be noted, however, that the smaller active surface area of the microheater on the MEMS devices are orders of magnitude smaller than the solid state device. The catalyst film on the solid-state sensor also has the benefit of the porosity of the alumina film underneath it, increasing surface area further. The MEMS catalyst would be featureless and planar. Results from a previous section in this paper indicate that surface is a crucial feature of a catalyst film to ensure sensitivity. It is unclear whether the measured surface are listed in Table 4.3 would be substantial enough to illicit a sensor response, even considering the expected rise in sensitivity that comes with a drastically reduced thermal mass.

References

[1] M. Amani, O.J. Gregory. “Grain growth and morphology of In_2O_3:Pd nanocomposite films”, Thin Solid Films, 542(2013)180-185.

[2] T. Zhang, L. Liu, Q. Qi, S. Li and G. Lu, "Development of microstructure In/Pd-doped SnO_2 sensor for low level CO detection," Sensors and Actuators B, vol. 139, pp. 287-291, 2009.

[3] V. Jimenez, J. Espinos and A. Gonzalez-Elipe, "Effect of texture and annealing treatments in SnO_2 and Pd/SnO_2 gas sensor materials," Sensors and Actuators B, vol. 61, pp. 23-32, 1999.

[4] T. Skala, K. Veltruska, M. Moroseac, I. Matolinova, A. Cirera and V. Matolin, "Redox process of Pd-SnO_2 system," Surface Science 566-568(2004)1217-1221, Vols. 566-568, pp. 1217-1221, 2004.

[5] R. Tan, Y. Guo, J. Zhao, Y. Li, T. Xu and W. Song, "Synthesis, characterization and gas-sensing properties of Pd-doped SnO_2 nano particles," Transactions of Nonferrous Metals Society of China, vol. 21, pp. 1568-1573, 2011.

[6] Y. Shen, T. Yamazaki, Z. Liu, D. Meng, T. Kikuta, N. Nakatani, M. Saito and M. Mori, "Microstructure and H_2 gas sensing properties of undoped and Pd-doped SnO_2 nanowires," Sensors and Actuators B, vol. 135, pp. 524-529, 2009.

[7] K. Schierbaum, U. Weimar and W. Gopel, "Conductance, work function and catalytic activity of SnO_2-based gas sensors," Sensors and Actuators B, vol. 3, pp. 205-214, 1991.

[8] C. B. Lim and S. Oh, "Microstructure evolution and gas sensitivities of Pd- doped SnO_2-based sensor prepared by three different catalyst-addition process," Sensors and Actuators B, vol. 30, pp. 223-231, 1996.

[9] S. Matsushima, T. Maekawa, J. Tamaki, N. Miura and N. Yamazoe, "New methods for supporting palladium on a tin oxide gas sensor," Sensors and Actuators B, vol. 9, pp. 71-78, 1992.

[10] M. Yuasa, T. Masaki, T. Kida, K. Shimanoe and N. Yamazoe, "Nano-sized PdO loaded SnO_2 nanoparticles by reverse micelle method for highly sensitive CO gas sensor," Sensors and Actuators B, vol. 136, pp. 99-104, 2009.

[11] L. Liu, T. Zhang, S. Li, L. Wang and T. Tian, "Preparation, characterization, and gas-sensing properties of Pd-doped In_2O_3 nanofibers," Materials Letters, vol. 63, pp. 1975-1977, 2009.

[12] N. Yamazoe, K. Kurokawa and T. Seiyama, "Effects of additives on semiconductor gas sensor," Sensors and Actuators, vol. 4, pp. 283-289, 1983.

[13] G. Tournier, C. Pijolat, R. Lalauze and B. Patissier, "Selective detection of CO and CH_4 with gas sensors using SnO_2 doped with palladium," Sensors and Actuators B, Vols. 26-27, pp. 24-28, 1995.

[14] Y. C. Lee, H. Huang, O. K. Tan and M. S. Tse, "Semiconductor gas sensor based on Pd doped SnO_2 nanorod thin films," Sensors and Actuators B, vol. 132, pp. 239-242, 2008.

[15] Y. Zhang, Q. Xiang, J. Xu, P. Xu, Q. Pan and F. Li, "Self-assemblies of Pd nanoparticles on the surfaces of single crystal ZnO nanowires for chemical

sensors with enhanced performances," Journal of Material Chemistry, vol. 19, pp. 4701-4706, 2009.

[16] N. Tsud, V. Johanek, I. Stara, K. Veltruska and V. Matolin, "XPS, ISS and TPD of Pd-Sn interactions on Pd-SnO_X systems," Thin Solid Films, vol. 391, pp. 204-208, 2001.

[17] J. Choi, I. Hwang, S. Kim, J. Park, S. Park, U. Jeong, Y. Kang and J. Lee, "Design of selective gas sensor using electrospun Pd doped SnO_2 hollow nanofibers," Sensors and Actuators B, vol. 150, pp. 191-199, 2010.

[18] Ras, M. R., F. Borrull, and R. M. Marcé. "Sampling and Preconcentration Techniques for Determination of Volatile Organic Compounds in Air Samples." *TrAC Trends in Analytical Chemistry,* 28.3 (2009): 347-61.

[19] Camara, E.h.m., P. Breuil, D. Briand, L. Guillot, C. Pijolat, and N.f. De Rooij. "Micro Gas Preconcentrator in Porous Silicon Filled with a Carbon Absorbent." *Sensors and Actuators B: Chemical* 148.2 (2010): 610-19.

[20] Amani M., Chu Y., Waterman K.L., Hurley C.M., Platek J.M., Gregory O.J., “Detection of Triacetone Triperoxide (TATP) using a thermodynamic based gas sensor”, Sensors and Actuators B, 162(2012)7-13

[21] Geankoplis, Christie John. Transport Processes & Separation Process Principles (includes Unit Operations). Essex: Pearson Education, 2014.

[22] Smith, J. M., Van Ness H. C., and Michael M. Abbott. Introduction to Chemical Engineering Thermodynamics: J.M. Smith, H.C. Van Ness, M.M. Abbott. Boston: McGraw-Hill, 2005.

[23] Campbell, Stephen A. Fabrication Engineering at the Micro and Nanoscale. New York: Oxford UP, 2013.

CHAPTER 5

CONCLUSION

5.1 Conclusion

The specific objective of this work was to take a solid state sensor that was successful in detecting vapor phase explosive molecules and make several key improvements to enhance the selectivity and sensitivity so that the sensor can one day be implemented in a real, portable device. These improvements were to be made in four specific ways: (1) Increasing the selectivity for TATP of the metal oxide catalyst film using combinatorial chemistry techniques, (2) combining a second independent sensing mechanism with the original thermodynamic sensor onto one orthogonal sensor platform to mitigate the detection of false positives, (3) increasing sensitivity and lowering the detection limit by implementing a preconcentrating device without compromising continuous detection, and finally, (4) migrating the sensor design to a smaller, more thermally efficient MEMS platform.

It was demonstrated that a sensor can be engineered to detect TATP and ignore the effects of interferent H_2O_2 molecules by doping SnO_2 films with Pd nanoparticles. Compared with a pure SnO_2 catalyst, incremental Pd additions modified the catalytic decomposition of TATP, resulting in unique sensor responses. At 5 wt. % Pd in SnO_2, the sensor responded to TATP but did not respond at all to H_2O_2. Also, at 12 wt. % Pd, the response to TATP and H_2O_2 was enhanced, indicating that sensitivity, not only selectivity, can be increased by modifying the composition of the catalyst.

An orthogonal detection system was also introduced to sense various explosives at increasingly lower concentrations, and more importantly, to minimize the frequency of false positives. The orthogonal detection system was composed of two independent sensing platforms, a thermodynamic based sensor and a conductometric based sensor. Both sensors obtain measurements from the same catalyst simultaneously and provide a redundancy in response for explosive identification. TATP, 2,6-DNT and ammonium nitrate were reliably detected. Each analyte displayed a unique conductometric signature and the results indicated a detection limit at the ppb level.

A preconcentrator was designed to enhance the sensitivity of the sensor and was successfully demonstrated. The magnitude of the sensor response increased by 50% and the preconcentrator could be operated in a semi-continuously, maintaining one of the most attractive features of this sensor platform: the capability to operate in real time. The dynamic control method was also successfully demonstrated and will likely be a fixture in all sensor experimentation and design moving forward.

Finally, two MEMS based sensor platforms were designed and fabricated. It was theoretically demonstrated that the newest iteration of the MEMS sensor consumes considerably less power, due to thinner membranes, a smaller active surface area and an overall smaller thermal mass, allowing for the possibility of creating networks of sensor arrays, even in a portable device.

5.2 Future Work

The end goal of this project has always been the real-world implementation of this vapor detection system in a practical, usable device. Towards that end, several areas of interest warrant further investigation including continued MEMS and preconcentrator development, research into how humidity affects explosive vapor detection, and the study of a wider range of analytes.

5.2.1 Preconcentration

A preconcentrator was successfully demonstrated, but improvements need to be made in a few key areas before it can be fully implemented. Research must be done into other sorbent polymers. Polystyrene was successful in adsorbing DNT, but not TATP or AN. Some alternatives include Tenax, which is an excellent sorbent for a wide range of molecules, and polycarbonate, polyvinylpyrrolidone and polyaniline, which have selective affinity for certain chemical groups. It will also be important moving forward to get quantitative results on the surface structure of the polymer and to determine how well the sorbent adsorbs and desorbs a particular analyte, instead of qualitatively and indirectly measuring that using our sensor [1-3].

5.2.2 MEMS

A working, testable MEMS device has yet to be developed. The platform isn't practical for research purposes because solid state sensors can be made quickly and in smaller batches to accommodate frequent changes in sensor or catalyst design. However, MEMS sensors are the essential next step towards commercialization. The thermodynamic analysis presented earlier in this work demonstrates how much more efficient the smaller platform is, opening up the possibility of operating hundreds of

sensors in networks and arrays simultaneously, even in a handheld or portable device [4].

A critical factor moving forward with the MEMS platform will be investigation into surface area. Use of the high surface area alumina cement showed that magnitude of the sensor response had nearly doubled. A quick comparison of the platforms, however, reveals that the area dedicated to the catalyst in the MEMS platform is orders of magnitude smaller than the catalyst on a solid state sensor. In order to fit a large amount of surface area into a small amount of space, a high surface area film would have to be deposited underneath the catalyst. This cannot be done with a material like alumina cement because the features are too small and the thin membrane would not be able to support its weight. A solution could be to grow nanowires. Sputtered films characteristically coat its substrate surface and preserve any porosity, surface structures or features. ZnO is a common nanowire material, and it could be left as is to act as the catalyst itself, or another oxide could be sputtered on top to inherit the high surface nanowire structure [5-6].

5.2.3 Humidity

Humidity has been known to play an important role in sensing mechanisms of many gas detection techniques [7-9]. Currently, our sensor is tested using dry air as the carrier gas, but a more realistic scenario would involve our sensor sampling air with unpredictable humidity, varying with climate and location. The effect of humidity toward sensor response, or at least a precise measurement of humidity in the current vapor sample, would be valuable information. We had proposed augmenting our current orthogonal system with a humidity sensor, a proposed design is depicted in

Figure 5.1. The polymer acts as a sorbent that selectively attracts water molecules. This would cause the film to swell, changing the capacitance of polymer which can then be recorded by the electrodes. The ultimate goal would be to establish a protocol that allows us to eliminate the influence of humidity on our sensor response.

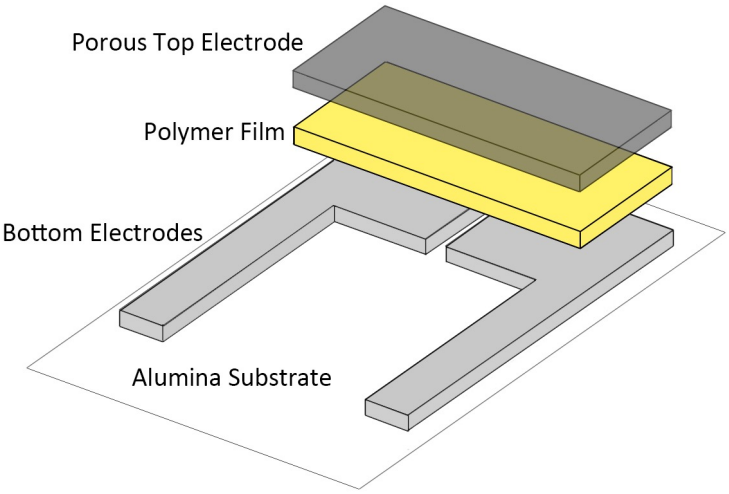

Figure 5.1 Proposed design of a humidity sensor.

5.2.4 Additional analytes

Finally, the only analytes that have been tested using this sensor have been TATP, 2,6-DNT and AN. It will be useful to demonstrate that the sensor has a wider range by testing other explosive compounds. It will also be necessary to demonstrate that the sensor can detect these specific analytes in the presence of a potential interferent. For instance, a field-test experiment can be conducted to test for TATP in the presence of water, hydrogen peroxide, acetone and DADP, or to test for TNT in the presence of 2,4-DNT, 2,6-DNT and other aromatic compounds like dinitrobenzene (DNB) [10].

References

[1] Ras, M. R., F. Borrull, and R. M. Marcé. "Sampling and Preconcentration Techniques for Determination of Volatile Organic Compounds in Air Samples." *TrAC Trends in Analytical Chemistry,* 28.3 (2009): 347-61.

[2] Camara, E.h.m., P. Breuil, D. Briand, L. Guillot, C. Pijolat, and N.f. De Rooij. "Micro Gas Preconcentrator in Porous Silicon Filled with a Carbon Absorbent." *Sensors and Actuators B: Chemical* 148.2 (2010): 610-19.

[3] Yabuki, T., and O. Nakabeppu. "Heat Transfer Mechanisms in Isolated Bubble Boiling of Water Observed with MEMS Sensor." International Journal of Heat and Mass Transfer 76 (2014): 286-97.

[4] Rafiee, P., and G. Khatibi. "A Fast Reliability Assessment Method for Si MEMS Based Microcantilevers." Microelectronics Reliability, 54 (2014):2180-2184.

[5] Hwang, In-Sung, Sun-Jung Kim, Joong-Ki Choi, Jaewan Choi, Hyunjin Ji, Gyu-Tae Kim, Guozhong Cao, and Jong-Heun Lee. "Synthesis and Gas Sensing Characteristics of Highly Crystalline ZnO–SnO2 Core–shell Nanowires." *Sensors and Actuators B: Chemical* 148.2 (2010): 595-600.

[6] Ji, Yajun. "One-step Method for Growing of Large Scale ZnO Nanowires on Zinc Foil." *Materials Letters* 138 (2015): 92-95. Web.

[7] M. Makinen, M. Silanpaa, A. K. Viitanen, A. Knap, J. M. Makela and J. Puton, "The effect of humidity on sensitivity of amine detection in ion mobility spectrometry," Talanta, vol. 84, pp. 116-121, 2011.

[8] H. E. Endress, R. Hartinger, M. Schwaiger, G. Gmelch and M. Roth, "A capacitive CO2 sensor system with suppression of the humidity interference," Sensors and Actuators B, vol. 57, pp. 83-87, 1999.

[9] A. Marsal, A. Cornet and J. R. Morante, "Study of the CO and humidity interference in La doped tin oxide CO2 gas sensor," Sensors and Actuators B, vol. 94, pp. 324-329, 2003.

[10] Ewing, Robert G., Melanie J. Waltman, David A. Atkinson, Jay W. Grate, and Peter J. Hotchkiss. "The Vapor Pressures of Explosives." *TrAC Trends in Analytical Chemistry* 42 (2013): 35-48. Web.

BIBLIOGRAPHY

Afzal A., Iqbal N., Mujahid A. and Schirhagl R., "Advanced vapor recognition materials for selective and fast responsive surface acoustic wave sensors: A review," *Analytica Chimica Acta*, vol. 787, pp. 36-49, 2013.

Agrawal J. P. and Hodgson R. D., Organic Chemistry of Explosives, Chichester, UK: John Wiley & Sons, Ltd, 2007.

Albert K. J. and Walt D. R., "High speed fluorescence detection of explosive like," *Analytical Chemistry*, vol. 72, p. 1947–1955, 2000.

Albert K. J., Lewis N. S., Schauer C. L., Sotzing G. A., Stitzel S. E., Vaid T. P. and Walt D. R., "Cross reactive chemical sensor arrays," *Chemical Reviews*, vol. 100, pp. 2595-2626, 2000.

Alfeeli, Bassam, Daniel Cho, Mehdi Ashraf-Khorassani, Larry T. Taylor, and Masoud Agah. "MEMS-based Multi-inlet/outlet Preconcentrator Coated by Inkjet Printing of Polymer Adsorbents." *Sensors and Actuators B: Chemical* 133.1 (2008): 24-32.

Amani M., Chu Y., Waterman K.L., Hurley C.M., Platek J.M., Gregory O.J., "Detection of Triacetone Triperoxide (TATP) using a thermodynamic based gas sensor", *Sensors and Actuators B*, 162(2012)7-13

Amani M., Gregory O.J., "Grain growth and morphology of In_2O_3:Pd nanocomposite films", *Thin Solid Films*, 542(2013)180-185

Ameel T.A., Warrington R.O., Wegeng R.S. and Drost M.K., "Miniaturization technologies applied to energy systems," *Energy Conversion and Management*, vol. 38, pp. 969-982, 1997

Aroon M. A., Ismail A. F., Matsuura T. and Montazer-Rahmati M. M., "Performance studies of mixed matrix membranes for gas separation: A review," *Separation and Purification Technology*, vol. 75, pp. 229-242, 2010.

Arshak K., Moore E., Lyons G. M., Harris J. and Clifford S., "A review of gas sensors employed in electronic nose applications," *Sensor Review*, vol. 24, pp. 181-198, 2004.

Asbury G. R., Klasmeier J. and Hill H. H., "Analysis of explosives using electrospray ionization/ion mobility spectrometry (ESI/IMS)," *Talanta*, vol. 50, pp. 1291-1298, 2000.

Banas A., Banas K., Bahou M., Moser H. O., Wen L., Yang P., Li Z. J., Li Z.J., Cholewa M., Lim S.K., Lim Ch.H., Cholewa M., Lim S. K. and Lim C. H., "Post-blast detection of traces of explosives by means of Fourier transform infrared spectroscopy," *Vibrational Spectroscopy*, vol. 51, pp. 168-176, 2009.

Barkauskas J., "Investigation of conductometric humidity sensors," *Talanta*, vol. 44, pp. 1107-1112, 1997.

Barsan N., Koziej D. and Weimar U., "Metal oxide-based gas sensor research: How to," *Sensors and Acutators B*, vol. 121, pp. 18-35, 2007.

Benson S., Lennard C., Maynard P. and Roux C., "Forensic applications of isotope ratio mass spectrometry—A review," *Forensic Science International*, vol. 157, pp. 1-22, 2006.

Berntsen T. G., "Global training centre of mine detection dogs in Bosnia: Breeding and training program," *Journal of Veterinary Behavior: Clinical Applications and Research*, vol. 4, p. 245–246, 2009.

Blue R., Vobeck Z., Skabara P. J. and Uttamchandani D., "The development of sensors for volatile nitro-containing compounds as models for explosives detection," *Sensors and Actuators B: Chemical*, vol. 176, pp. 534-542, 2013.

Brudzewski K., Osowski S. and Pawlowski W., "Metal oxide sensor arrays for detection of explosives at sub-parts-per million concentration levels by the differential electronic nose," *Sensors and Actuators B*, vol. 161, pp. 528- 533, 2012.

Bunyan P., Baker C. and Rurner N., "Application of heat conduction calorimetry to high explosives," *Thermochimica Acta*, vol. 401, pp. 9-16, 2003.

Burger A. and Wehrstedt K. D., "Azodicarboxylates: Explosive properties and DSC measurements," *Journal of Loss Prevention in the Process Industries*, vol. 23, p. 734–739, 2010.

Burns D. T. and Lewis R. J., "Analysis and characterisation of nitroglycerine based explosives by proton magnetic resonance spectrometry," *Analytica Chimica Acta*, vol. 300, pp. 221-225, 1995.

Buttigieg G. A., Knight A. K., Denson S., Pommier C. and Denton M. B., "Characterization of the explosive triacetone triperoxide and detection by ion mobility spectrometry," *Forensic Science International*, vol. 135, pp. 53-59, 2003.

Buxton T. L. and Harrington P. B., "Rapid multivariate curve resolution applied to identification of explosives by ion mobility spectrometry," *Analytica Chimica Acta*, vol. 434, pp. 269-282, 2001.

Cagan D. A., Munoz R. A., Tangkuaram T. and Wang J., "Highly sensitive electrochemical detection of trace liquid peroxide explosives at a Prussian-blue 'artificial-peroxidase' modified electrode," *Analyst*, vol. 131, pp. 1279-1281, 2006.

Camara, E.h.m., P. Breuil, and C. Pijolat. "Preconcentration Modeling for the Optimization of a Micro Gas Preconcentrator Applied to Environmental Monitoring." *Procedia Chemistry* 1.1 (2009): 662-65.

Camara, E.h.m., P. Breuil, D. Briand, L. Guillot, C. Pijolat, and N.f. De Rooij. "Micro Gas Preconcentrator in Porous Silicon Filled with a Carbon Absorbent." *Sensors and Actuators B: Chemical* 148.2 (2010): 610-19.

Camara, E.h.m., P. Breuil, D. Briand, N.f. De Rooij, and C. Pijolat. "A Micro Gas Preconcentrator with Improved Performance for Pollution Monitoring and Explosives Detection." *Analytica Chimica Acta* 688.2 (2011): 175-82.

Campbell, Stephen A. Fabrication Engineering at the Micro and Nanoscale. New York: Oxford UP, 2013. Print.

Capua E., Cao R., Sukenik C. N. and Naaman R., "Detection of triacetone triperoxide (TATP) with an array of sensors based on non-specific interactions," *Sensors and Actuators B*, vol. 140, p. 122–127, 2009.

Caron T., Cuillemot M., Montmeat P., Veignal F., Perraut F., Prene P. and Serein-Spirau F., "Ultra trace detection of explosives in air: Development of a portable fluorescent detector," *Talanta*, vol. 81, p. 543–548, 2010.

Carreto-Vazquez V. H., Wojcik A. K., Liu Y., Bukur D. B. and Mannan M. S., "Miniaturized calorimeter for thermal screening of energetic materials," *Microelectronics Journal*, vol. 41, pp. 874-881, 2010.

Carter J. C., Angel S. M., Lawrence-Snyder M., Scaffidi J., Whipple R. E. and Reynolds J. G., "Standoff Detection of High Explosive Materials at 50 Meters in Ambient Light Conditions Using a Small Raman Instrument," *Applied Spectroscopy*, vol. 59, pp. 120-138, 2005.

Casey V., Cleary J., D'Arcy G. and McMonagle J. B., "Calorimetric combustible gas sensor based on a planar thermopile array: fabrication, characterisation, and gas response," *Sensors and Actuators B*, vol. 96, p. 114–123, 2003.

Caygill J. S., Davis F. and Higson S. P., "Current trends in explosive detection techniques," *Talanta*, vol. 88, pp. 14-29, 2012.

Cerioni L. M. and Pusiol D. J., "A new method to obtain frequency offsets in NQR multi-pulse sequences," *Hyperfine Interactions*, vol. 159, pp. 389- 393, 2005.

Charles P. T. and Kusterbeck A. W., "Trace level detection of hexahydro-1,3,5-trinitro-1,3,5-triazine (RDX) by microimmunosensor," *Biosensors and Bioelectronics*, vol. 14, p. 387–396, 1999.

Charlesworth J. M., Partridge A. C. and Garrard N., "Mechanistic studies on the interactions between poly (pyrrole) and organic vapors," *Journal of Physical Chemistry*, vol. 97, pp. 5418-5423, 1993.

Chen W., Wang Y., Bruckner C., Li C. and Lei Y., "Poly[meso-tetrakis(2-thienyl)porphyrin] for the sensitive electrochemical detection of explosives," *Sensors and Actuators B*, vol. 147, p. 191–197, 2010.

Chen Y., Liu H., Fitch M. J., Osiander R., Spicer J. B., Shur M. and Zhang X. C., "THz diffuse reflectance spectra of selected explosives and related compounds," *Proceedings of SPIE*, vol. 5790, pp. 19-24, 2005.

Cho J., Anandakathir A., Kumar A., Kumar J. and Kurup P. U., "Sensitive and fast recognition of explosives using fluorescent polymer sensors and pattern recognition analysis," *Sensors and Actuators B*, vol. 160, p. 1237– 1243, 2011.

Choi J., Hwang I., Kim S., Park J., Park S., Jeong U., Kang Y. and Lee J., "Design of selective gas sensor using electrospun Pd doped SnO_2 hollow nanofibers," *Sensors and Actuators B*, vol. 150, pp. 191-199, 2010.

Choi W. K., Song S. K., Cho J. S., Yoon Y. S., Choi D., Jung H. J. and Koh S. K., "H_2 gas-sensing characteristics of SnO_x sensors fabricated by a reactive ion-assisted deposition with/without an activator layer," *Sensors and Actuators B*, vol. 40, pp. 21-27, 1997.

Chu F. and Yang J., "Study of nitro aromatic explosives sensor based on fluorescence quenching," *Optik - International Journal for Light and Electron Optics*, vol. 122, pp. 2246-2248, 2011.

Collin O. L., Zimmermann C. M. and Jackson G. P., "Fast gas chromatography negative chemical ionization tandem mass spectrometry of explosive compounds using dynamic collision-induced dissociation," *Mass Spectrometry*, vol. 279, pp. 93-99, 2009.

Cong H., Radosz M., Towler B. F. and Shen Y., "Polymer–inorganic nanocomposite membranes for gas separation," *Separation and Purification Technology*, vol. 55, pp. 281-291, 2007.

Cook D. J., Decker B. K., Maislin G. and Allen M. G., "Through container THz sensing: applications for explosives screening," *Proceedings of SPIE*, vol. 5354, pp. 55-62, 2004.

Cotte-Rodriguez I., Chen H. and Cooks R. G., "Rapid trace detection of triacetone triperoxide (TATP) of complexation detections of desorption electrospray ionization," *Chemical Communications*, vol. 5, pp. 953-955, 2006.

Datskos P. G., Lavrik N. V. and Sepaniak M. J., "Detection of explosive compounds with the use of microcantilevers with nanoporous coatings," *Sensor Letters*, vol. 1, pp. 25-32, 2003.

Demchenko A. P., Introduction to Fluorescence Sensing, Netherland: Springer Netherlands, 2009.

Diesel G., Brodbelt D. and Pfeiffer D. U., "Reliability of assessment of dogs' behavioural responses by staff working at a welfare charity in the UK," *Applied Animal Behaviour Science*, vol. 115, p. 171–181, 2008.

Dioone B. C., Roundbehler D. P., Achter E. K., Hobbs J. R. and Fine D. H., "Vapor Pressure of Explosives," *Journal of Energetic Materials*, vol. 4, p. 447, 1986.

Dubnikova F., Kosloff R., Zeiri Y. and Karpas Z., "Novel approach to the detection of triacetone triperoxide (TATP), its structure and its complexes with ions," *Journal of Physical Chemistry A*, vol. 106, p. 4951–4956, 2002.

Dutta A. and Basu S., "Modified metal-insulator-metal (M-I-M) hydrogen gas sensors based on zinc oxide," *Journal of Materials Science: Materials in Electronics*, vol. 6, pp. 415-418, 1995.

Eiceman G. A., Preston D., Tiano G., Rodriguez J. and Parmeter J. E., "Quantitative calibration of vapor levels of TNT, RDX, and PETN using a diffusion generator with gravimetry and ion mobility spectrometry," *Talata*, vol. 45, pp. 57-74, 1997.

Eisele I., Doll T. and Burgmair M., "Low Power gas detection with FET sensors," *Sensors and Actuators B*, vol. 78, pp. 19-25, 2001.

Eles P. T. and Michal C. A., "Two-photon excitation in nuclear quadrupole resonance," *Chemical Physics Letters*, vol. 376, pp. 268-273, 2003.

Eliasson C., Macleod N. A. and Matousek P., "Noninvasive detection of concealed liquid explosives using Raman spectroscopy," *Analytical Chemistry*, vol. 79, pp. 8185-8189, 2007.

Endress H. E., Hartinger R., Schwaiger M., Gmelch G. and Roth M., "A capacitive CO_2 sensor system with suppression of the humidity interference," *Sensors and Actuators B*, vol. 57, pp. 83-87, 1999.

Eranna G., Joshi B. C., Runthala D. P. and Gupta R. P., "Oxide materials for development of integrated gas sensors: A comprehensive review," *Critical Review of Solid State and Materials Sciences*, vol. 29, pp. 111-188, 2004.

Ewing R. G., Atkinson D. A., Eiceman G. A. and Ewing G. J., "A critical review of ion mobility spectrometry for the detection of explosives and explosive related compounds," *Talanta*, vol. 54, pp. 515-529, 2001.

Ewing, Robert G., Melanie J. Waltman, David A. Atkinson, Jay W. Grate, and Peter J. Hotchkiss. "The Vapor Pressures of Explosives." *TrAC Trends in Analytical Chemistry* 42 (2013): 35-48. Web.

Fan Y., Han P., Liang P., Xing Y., Ye Z.and Hu S., "Differences in etching characteristics of TMAH and KOH on preparing inverted pyramids for silicon solar cells," *Applied Surface Science*, vol. 264, pp. 761-766, 2013.

Federici J. F., Schulkin B., Huang F., Gary D., Barat R., Oliveira F. and Zimdars D., "THz imaging and sensing for security applications—explosives, weapons and drugs," *Semiconductor Science and Technology*, Vols. S266-S280, p. 20, 2005.

Foltynowicz R. J., Allman R. E. and Zuckerman E., "Terahertz absorption measurement for gas-phase 2,4-dinitrotoluene from 0.05 THz to 2.7 THz," *Chemical Physics Letters*, vol. 431, pp. 34-38, 2006.

Fordham S., High Explosives and Propellants, Fordham, Stanley, UK: Pergamon Press Ltd., 1980.

Furton K. G. and Myers L. J., "The scientific foundation and efficacy of the use of canines as chemical detectors for explosives," *Talanta*, vol. 54, pp. 487- 500, 2011.

Gaft M. and Nagli L., "UV gated Raman spectroscopy for standoff detection of explosives," *Optical Materials*, vol. 30, pp. 1739-1746, 2008.

Gaggiotti G., Galdikas A., Kaciulis S., Mattogno G. and Setkus A., "Temperature dependencies of sensitivity and surface chemical composition of SnO_X gas sensors," *Sensors and Actuators B*, vol. 25, p. 516–519, 1995.

Gardner J. W. and Bartlett P. N., Electronic Noses – Principles and Applications, Oxford, UK: Oxford University Press, 1999.

Garroway A. N., Buess M. L., Miller J. B., Suits B. H., Hibbs A. D., Barrall G. A., Matthews R.and Burnett L. J., "Remote sensing by nuclear quadrupole resonance," *IEEE Transactions, Geoscience and Remote Sensing*, vol. 39, pp. 1108-1118, 2001.

Garroway A. N., Buess M. L., Yesinowski J. P. and Miller J. B., "Narcotics and explosive detection by ^{14}N pure NQR," *Proceedings of SPIE*, vol. 2092, pp. 318-327, 1993.

Gazit I. and Terkel J., "Domination of olfaction over vision in explosives detection by dogs," *Applied Animal Behaviour Science*, vol. 82, pp. 65- 73, 2003.

Gazit I. and Terkel J., "Explosives detection by sniffer dogs following strenuous physical activity," *Applied Animal Behaviour Science*, vol. 81, pp. 149- 161, 2003.

Geankoplis, Christie John. Transport Processes & Separation Process Principles (includes Unit Operations). Essex: Pearson Education, 2014.

Goel M., "Recent developments in electroceramics: MEMS application for energy and environment," *Ceramics International*, vol.30, pp. 1147-1154, 2004.

Grechishkin V. S. and Sinyavskii N. Y., "New technologiesnuclear quadrupole resonance as an explosive and narcotic detection technique," *Physics Uspekhi*, vol. 40, pp. 393-406, 1997.

Green E. M., "Explosives Regulation in the USA," *Industrial Minerals*, vol. 465, p. 78, 2006.

Grevea J. O. A., Greve A., Olsen J., Privorotskaya N., Senesac L., Thundat T., King W. P. and Boisen A., "Micro-calorimetric sensor for vapor phase explosive detection with optimized heat profile," *Microelectronic Engineering*, vol. 87, p. 696–698, 2010.

Guerrero L. A., "Quick Learning Techniques: Dogs used to detect narcotics and explosives," *Journal of Veterinary Behavior: Clinical Applications and Research*, vol. 4, p. 253, 2009.

Gupta N. and Dahmani R., "AOTF Raman spectrometer for remote detection of explosives," *Spectrochimica Acta A*, vol. 56, pp. 1453-1456, 2000.

Habib M. K., "Controlled biological and biomimetic systems for landmine detection," *Biosensors and Bioelectronics*, vol. 23, pp. 1-18, 2007.

Hall N. J., Smith D. W. and Wynne D. L., "Training domestic dogs (Canis lupus familiaris) on a novel discrete trials odor-detection task," *Learning and Motivation*, p. In press, 2013.

Harper R. J., Almirall J. R. and Furto K. G., "Identification of dominant odor chemicals emanating from explosives for use in developing optimal training aid combinations and mimics for canine detection," *Talanta*, vol. 67, pp. 313-327, 2005.

Haverbeke A., Laporte B., Depiereux E., Giffroy J. M. and Diederich C., "Training methods of military dog handlers and their effects on the team's performances," *Applied Animal Behaviour Science*, vol. 113, pp. 110- 122, 2008.

Hayward I. E., Kirkbride T. E., Batchelder D. N. and Lacey R. J., "Use of a Fiber Optic Probe for the Detection and Identification of Explosive Materials by Raman Spectroscopy," *Journal of Forensic Sciences*, vol. 40, pp. 883-334, 1995.

Heeger A. J., "Semiconducting and metallic polymers: the fourth generation of polymeric materials," *Current Applied Physics*, vol. 1, pp. 247-267, 2001.

Holly R. and Hingerl K., "Fbrication of silicon vertical taper structures using KOH anisotropic etching," *Microelectronic Engineering*, vol. 83, pp. 1430-1433, 2006.

Holmgren E., Ek S. and Colmsjo A., "Extraction of explosives from soil followed by gas chromatography–mass spectrometry analysis with negative chemical ionization," *Journal of Chromatography A*, vol. 1222, pp. 109- 115, 2012.

Hu Y., Huang P., Guo L., Wang X. and Zhang C., "Terahertz spectroscopic investigations of explosives," *Physics Letters A*, vol. 359, pp. 728-732, 2006.

Hu Y., Tan O. K., Pan J. S., Huang H. and Cao W., "The effects of annealing temperature on the sensing properties of low temperature nano-sized $SrTiO_3$ oxygen gas sensor," *Sensors and Actuators B*, vol. 108, p. 244– 249, 2005.

Huang J., Kuo D. and Shew B., "The effects of heat treatment on the gas sensitivity of reactively sputtered SnO_2 films," *Surface and Coatings Technology*, vol. 79, pp. 263-267, 1996.

Huang S. D., Kolaitis L. and Lubman D. M., "Detection of explosives using laser desorption in ion mobility spectrometry/mass spectrometry," *Applied Spectroscopy*, vol. 41, pp. 1371-1376, 1987.

Hung N. L., Kim H., Hong S. K. and Kim D., "Enhancement of CO gas sensing properties of ZnO thin films deposited on self-assembled Au nanodots," *Sensors and Actuators B*, vol. 151, pp. 127-132, 2010.

Hwang S., Kim Y. Y., Lee J. H., Seo D. K., Lee J. Y. and Cho H. K., "Irregular electrical conduction types in tin oxide thin films induced by nanoscale phase separation," *Journal of the American Ceramic Society*, vol. 95, pp. 324-332, 2012.

Hwang, In-Sung, Sun-Jung Kim, Joong-Ki Choi, Jaewan Choi, Hyunjin Ji, Gyu-Tae Kim, Guozhong Cao, and Jong-Heun Lee. "Synthesis and Gas Sensing Characteristics of Highly Crystalline ZnO–SnO2 Core–shell Nanowires." *Sensors and Actuators B: Chemical* 148.2 (2010): 595-600.

Industry Report, Sensors Markets 2016, Freedonia, 2013.

Intelliegence Reform and Terrorism Prevention Act of 2004, Public Law, December 2004, 108-458.

Ippolito S. J., Kandasamy S., Kalantar-zadeh K. and Wlodarski W., "Hydrogen sensing characteristics of WO3 thin film conductometric sensors activated by Pt and Au catalysts," *Sensors and Actuators B*, vol. 108, pp. 154-158, 2005.

Izake E. L., "Forensic and homeland security applications of modern portable Raman spectroscopy," *Forensic Science International*, vol. 202, pp. 1-8, 2010.

Janata J., Josowicz M., Vanysek P. and Michael DeVaney D., "Chemical sensors," *Analytical Chemistry*, vol. 70, p. 179–208, 1998.

Janni J., Gilbert B. D., Field R. W. and Steinfeld J. I., "Infrared absorption of explosive molecule vapors," *Spectrochimica Acta Part A: Molecular and Biomolecular Spectroscopy*, vol. 53, pp. 1375-1381, 1997.

Janssen, S., T. Tessmann, and W. Lang. "High Sensitive and Selective Ethylene Measurement by Using a Large-capacity-on-chip Preconcentrator Device." *Sensors and Actuators B: Chemical* (2014)

Jezierski T., Adamkiewicz E., Walczak M., Porkopczyk M. and Wziatek M., "Factors affecting drugs and explosives detection by dogs in experimental tests," *Journal of Veterinary Behavior: Clinical Applications and Research*, vol. 8, p. e33, 2013.

Ji, Yajun. "One-step Method for Growing of Large Scale ZnO Nanowires on Zinc Foil." *Materials Letters* 138 (2015): 92-95. Web.

Jimenez V., Espinos J. and Gonzalez-Elipe A., "Effect of texture and annealing treatments in SnO2 and Pd/SnO2 gas sensor materials," *Sensors and Actuators B*, vol. 61, pp. 23-32, 1999.

Kannan G. K., Nimal A. T., Mittal U., Yadava R. D. and Kapoor J. C., "Adsorption studies of carbowax coated surface acoustic wave (SAW) sensor for 2,4-dinitro toluene (DNT) vapour detection," *Sensors and Actuators B*, vol. 101, pp. 328-334, 2004.

Kanu A. B., Wu C. and Hill H. H. Jr., "Rapid preseparation of interferences for ion mobility spectrometry," *Analytica Chimica Acta*, vol. 610, pp. 125- 134, 2008.

Karasek F. W. and Denney D. W., "Detection of 2,4,6-trinitrotoluene vapours in air by plasma chromatography," *Journal of Chromatography*, vol. 93, pp. 141- 147, 1974.

Kato K., Omoto H., Tomioka T. and Takamatsu A., "Optimum packing density and crystal structure of tin-doped indium oxide thin films for high- temperature annealing processes," *Applied Surface Science*, vol. 257, p. 9207–9212, 2011.

Kemp M. C., "Explosive Detection by Terahertz Spectroscopy- A Bridge Too Far?," Terahertz Science and Technology, IEEE, vol. 1, pp. 282-292, 2011.

Kemp M. C., Taday P. F., Cole B. E., Cluff J. A., Fitzgerald A. J. and Tribe W. R., "Security applications of terahertz technology," *Proceedings of SPIE*, vol. 5070, pp. 44-52, 2003.

Khayamian T., Tabrizchi M. and Jafari M. T., "Analysis of 2,4,6-trinitrotoluene, pentaerythritol tetranitrate and cyclo-1,3,5-trimethylene-2,4,6-trinitramine using negative corona discharge ion mobility spectrometry," *Talanta*, vol. 54, pp. 515-529, 2001.

Khlebarov Z. P., "Surface acoustic wave gas sensor," *Sensors and Actuators B*, vol. 8, pp. 33-40, 1992.

Kim S. S., Jayakody J. R. and Marino R. A., "Experimental investigations of the strong off resonant comb (SORC) pulse sequence in ^{14}N NQR," *Verlag der Zeitschrift für Naturforschung (A)*, vol. 47, pp. 415-420, 1993.

Korotcenkov G. and Cho B. K., "Engineering approaches for the improvement of conductometric gas sensor parameters: Part 1. Improvement of sensor

sensitivity and selectivity," *Sensors and Actuators B*, vol. 188, pp. 709- 728, 2013.

Korotcenkov G. and Cho B. K., "Instability of metal oxide based conductometric gas sensors and approaches to stability improvement (short survey)," *Sensors and Actuators B*, vol. 156, pp. 527-538, 2011.

Korotcenkov G. and Cho B. K., "Ozone measuring: what can limit application of SnO2-based conductometric gas sensor?," *Sensors and Actuators B*, vol. 161, pp. 28-44, 2012.

Korotcenkov G., Boris I., Brinzari V., Han S. H. and Cho B. K., "The role of doping effect on the response of SnO2-based thin film gas sensors: Analysis based on the results obtained for Co-doped SnO_2 films deposited by spray pyrolysis," *Sensors and Actuators B*, vol. 182, pp. 112-124, 2013.

Kriz D. and Ansell R. J., "Man Made Mimics of Antibodies and their Application in Analytical Chemistry," *Molecularly Imprinted Polymers*, vol. 23, p. 417–436, 2001.

Ladbeck R. S. and Karst U., "Determination of triacetone triperoxide in ambient air," *Analytical Chemistry*, vol. 482, pp. 183-188, 2003.

Latosinska J. N., "Nuclear Quadrupole Resonance spectroscopy in studies of biologically active molecular systems - a review," *Journal of Pharmaceutical and Biomedical Analysis*, vol. 38, pp. 577-587, 2005.

Leahy-Hoppa M. R., Fitch M. J. and Osiander R., "Terahertz spectroscopy techniques for explosives detection," *Analytical and Bioanalytical Chemistry*, vol. 395, pp. 247-257, 2009.

Lee K. B., Gu M. B. and Moon S. H., "Degradation of 2,4,6-trinitrotoluene by immobilized horseradish peroxidase and electrogenerated peroxide," *Water Research*, vol. 37, pp. 983-992, 2003.

Lee Y. C., Huang H., Tan O. K. and Tse M. S., "Semiconductor gas sensor based on Pd doped SnO_2 nanorod thin films," *Sensors and Actuators B*, vol. 132, pp. 239-242, 2008.

Lerchner J., Caspary D. and Wolf G., "Calorimetric detection of volatile organic compounds," *Sensors and Actuators B*, vol. 70, pp. 57-66, 2000.

Li X., Li Q., Zhou H., Hao H., Wang T., Zhao S., Lu Y.and Huang G., "Rapid, on-site identification of explosives in nanoliter droplets using a UV reflected fiber optic sensor," *Analytica Chimica Acta*, vol. 751, pp. 112- 118, 2012.

Li, J.-B., K. Jiang, and G. J. Davies. "Novel Die-sinking Micro-electro Discharge Machining Process Using Microelectromechanical Systems Technology." *Proceedings of the Institution of Mechanical Engineers, Part C: Journal of Mechanical Engineering Science* 220.9 (2006): 1481-487.

Lim C. B. and Oh S., "Microstructure evolution and gas sensitivities of Pd-doped SnO2-based sensor prepared by three different catalyst-addition process," *Sensors and Actuators B*, vol. 30, pp. 223-231, 1996.

Lima R. R., Carvalho R. A., Nascimento Fiho A. P., Silva M. L. and Demarquette N. R., "Production and deposition of adsorbent films by plasma polymerization on low cost micromachined non-planar microchannels for preconcentration of organic compound in air," *Sensors and Actuators B*, vol. 108, pp. 435-444, 2005.

Lin H. and Suslick K. S., "A colorimetric sensor array for detection of triacetone triperoxide vapor," *Journal of American Chemistry Society*, vol. 132, pp. 15519-15521, 2010.

Liu H., Chen Y., Bastiaans G. J. and Zhang X., "Detection and identification of explosive RDX by THz diffuse reflection spectroscopy," *Optics Express*, vol. 14, pp. 415-423, 2006.

Liu L., Zhang T., Li S., Wang L.and Tian T., "Preparation, characterization, and gas-sensing properties of Pd-doped In_2O_3 nanofibers," *Materials Letters*, vol. 63, pp. 1975-1977, 2009.

Liu Y., Ugaz V. M., North S. W., Rogers W. J. and Mannan S., "Development of a miniature calorimeter for identification and detection of explosives and other energetic compounds," *Journal of Hazardous Materials*, vol. 142, pp. 662-668, 2007.

Lopez-Avila V. and Hill H. H., "Field analytical chemistry," *Analytical Chemistry*, vol. 69, pp. 289-306, 1997.

Lubczyk D., Siering C., Lorgen J., Shifrina Z. B., Mullen K. and Waldvogel S. R., "Simple and sensitive online detection of triacetone triperoxide explosive," *Sensors and Actuators B*, vol. 143, pp. 561-566, 2010.

Ly S. Y., Kim D. H. and Kim M. H., "Square-wave cathodic stripping voltammetric analysis of RDX using mercury-film plated glassy carbon electrode," *Talanta*, Vols. 919-926, p. 58, 2002.

Makinen M., Silanpaa M., Viitanen A. K., Knap A., Makela J. M. and Puton J., "The effect of humidity on sensitivity of amine detection in ion mobility spectrometry," *Talanta*, vol. 84, pp. 116-121, 2011.

Marsal A., Cornet A. and Morante J. R., "Study of the CO and humidity interference in La doped tin oxide CO_2 gas sensor," *Sensors and Actuators B*, vol. 94, pp. 324-329, 2003.

Martin M., Crain M., Walsh K., McGill R. A., Houser E., Stepnowski J. and Stepnows S., "Microfabricated vapor preconcentrator for portable ion mobility spectroscopy," *Sensors and Actuators B*, vol. 126, pp. 447-454, 2007.

Martin, Michael, Mark Crain, Kevin Walsh, R. Andrew Mcgill, Eric Houser, Jennifer Stepnowski, Stanley Stepnowski, Huey-Daw Wu, and Stuart Ross. "Microfabricated Vapor Preconcentrator for Portable Ion Mobility Spectroscopy." *Sensors and Actuators B: Chemical* 126.2 (2007): 447-54.

Massok P., Loesch M. and Bertrand D., "Comparison for the between two Figaro sensors (TGS 813 and TGS 842) for the detection of methane, in terms of selectivity and long-term stability," *Sensors and Actuators B*, vol. 25, pp. 525-528, 1995.

Masunaga K., Hayama K., Onodera T., Hayashi K., Miura N., Matsumoto K. and Toko K., "Detection of aromatic nitro compounds with electrode polarization controlling sensor," *Sensors and Actuators B*, Vols. 427-434, p. 108, 2005.

Mathis J. A. and McCord B. R., "The analysis of high explosives by liquid chromatography/electrospray ionization mass spectrometry: multiplexed

detection of negative ion adducts," *Rapid Communications in Mass Spectrometry*, vol. 19, pp. 99-104, 2005.

Matin A., Yun C., Waterman K. L., Hurley C. M., Platek M. J. and Gregory O. J., "Detection of triacetone triperoxide (TATP) using a thermodynamic based gas sensor," *Sensors and Actuators B*, vol. 162, pp. 7-13, 2012.

Matsushima S., Maekawa T., Tamaki J., Miura N.and Yamazoe N., "New methods for supporting palladium on a tin oxide gas sensor," *Sensors and Actuators B*, vol. 9, pp. 71-78, 1992.

Matyas R., Selesovsky J. and Musil T., "Sensitivity to friction for primary explosives," *Journal of Hazardous Materials*, Vols. 213-214, pp. 236- 241, 2012.

Meaney M. S. and McGuffin V. L., "Luminescence-based methods for sensing and detection of explosives," *Analytical and Bioanalytical Chemistry*, vol. 391, pp. 2557-2576, 2008.

Michael Ben Alexandera T. F., Alexandera M. B., Friend T. and Haug L., "Obedience training effects on search dog performance," *Applied Animal Behaviour Science*, vol. 132, pp. 152-159, 2011.

Mikhaltsevitch V. T. and Rudakov T. N., "On the NQR detection of nitrogenated substances by multi-pulse sequences," *Physica Status Solidi (b)*, vol. 241, pp. 411-419, 2004.

Miller J. B., "Chapter 7 - Nuclear quadrupole resonance detection of explosives," in Counterterrorist Detection Techniques of Explosives, Oxford, UK, Elsevier, 2007, pp. 157-198.

Millot Y. and Man P. P., "Determination of quadrupole parameters with a composite pulse for spurious signal suppression," *Journal of Magnetic Resonance*, vol. 150, pp. 10-16, 2001.

Monterola M. P., Smith B. W., Omenetto N. and Winefordner J. D., "Photofragmentation of nitro-based explosives with chemiluminescence detection," *Analytical and Bioanalytical Chemistry*, vol. 391, pp. 2617- 2626, 2008.

Moore D. S. and Scharff R. J., "Portable Raman explosive detection," *Analytical and Bioanalytical Chemistry*, vol. 393, pp. 1571-1578, 2009.

Mullen C., Irwin A., Pond B. V., Huestis D. L., Coggiola M. J. and Oser H., "Detection of explosives and explosives-related compounds by single photon laser ionization time-of-flight mass spectrometry," *Analytical Chemistry*, vol. 78, p. 3807–3814, 2006.

Munoz B. C., Steinthal G. and Sunshine S., "Conductive polymer-carbon black composites-based sensor arrays for use in an electronic nose," *Sensor Review*, vol. 19, pp. 300-305, 1999.

Nakamoto, T., Y. Isaka, T. Ishige, and T. Moriizumi. "Odor-sensing System Using Preconcentrator with Variable Temperature." *Sensors and Actuators B: Chemical* 69.1-2 (2000): 58-62.

Neuhaus W., "Uber die Riechscharfe des Hundes fur Fettsauren," *Zeitschrift Fur Vergleichende Physiologie*, vol. 35, p. 527, 1953.

Nimal A. T., Mittal U., Singh M., Khaneja M., Kannan G. K., Kapoor J. C., Dubey V., Gutch P. K., Lal G., Vyas K. D. and Gupta D. C., "Development of handheld

SAW vapor sensors for explosives and CW agents," *Sensors and Actuators B*, vol. 135, pp. 399-410, 2009.

Osan T. M., Cerioni L. M., Forguez J. and Olle J. M., "NQR: From imaging to explosives and drugs detection," *Physica B: Condensed Matter*, vol. 389, pp. 45-50, 2007.

Oxley J. C., Smith J. L. and Chen H., "Decomposition of a multi-peroxidic compound: triacetone triperoxide (TATP)," *Propellants, Explosives, Pyrotechnics*, vol. 27, pp. 209-216, 2002.

Oxley J. C., Smith J. L., Shinde K. and Moran J., "Determination of the vapor density of triacetone triperoxide (TATP) using a gas chromatography headspace technique," *Propellants, Explosives, Pyrotechnics*, vol. 30, pp. 127-130, 2005.

Parajuli S. and Miao W., "Sensitive Determination of Hexamethylene Triperoxide Diamine Explosives, Using Electrogenerated Chemiluminescence Enhanced by Silver Nitrate," *Analytical Chemistry*, vol. 81, pp. 5267- 5272, 2009.

Park M., Cella L. N., Chen W., Myung N. V. and Mulchandani A., "Carbon nanotubes-based chemiresistive immunosensor for small molecules: Detection of nitroaromatic explosives," *Biosensors and Bioelectronics*, vol. 26, p. 1297–1301, 2010.

Pella P. A., "Measurement of the Vapor Pressure of TNT, 2,4-DNT, 2,6-DNT and EGDN," *Journal of Chemical Thermodynamics*, 1977, 9(4), 301, vol. 9, p. 301, 1977.

Perr J. M., Furton K. G. and Almirall J. R., "Gas chromatography positive chemical ionization and tandem mass spectrometry fot the analysis of organic high explosives," *Talanta*, vol. 67, pp. 430-436, 2005.

Pinnaduwage L. A., Boiadjiev V., Hawk J. E. and Thundat T., "Sensitive detection of plastic explosives with self-assembled monolayer-coated microcantilevers," *Applied Physics Letters*, vol. 83, pp. 1471-1473, 2003.

Primera-Pedrozo O. M., Soto-Feliciano Y. M. and Pacheco-Londo L. C., "Detection of high explosives using reflection absorption infrared spectroscopy with fiber coupled grazing angle probe/FTIR," *Sensing and Imaging*, vol. 10, pp. 1-13, 2009.

Rabenecker P. and Pinkwart K., "A Look Behind Electrochemical Detection of Explosives," *Propellants, Explosives, Pyrotechnics*, vol. 34, p. 274–279, 2009.

Rafiee, P., and G. Khatibi. "A Fast Reliability Assessment Method for Si MEMS Based Microcantilever Beams." *Microelectronics Reliability* Sep-Oct 2014 54.9-10 (2014): 2180-184.

Ras M. R., Borrull F. and Marce R. M., "Sampling and preconcentration techniques for determination of volatile organic compounds in air samples," *TrAC Trends in Analytical Chemistry*, vol. 28, pp. 347-361, 2009.

Rasanen R., Nousiainen M., Parakorpi K., Sillanripaa M., Polari L., Anttalainen O. and Utriainen M., "Determination of gas phase triacetone triperoxide with aspiration ion mobility spectrometry and gas chromatography–mass spectrometry," *Analytica Chimica Acta*, vol. 623, p. 59–65, 2008.

Ray M. D., Sedlacek A. J. and Wu M., "Ultraviolet mini-Raman lidar for stand- off, in situ identification of chemical surface contaminants," *Review of Scientific Instruments*, vol. 71, pp. 3485-3489, 2000.

Riva J., Marelli S. P., Redaelli V., Sforzini E., Luzi F. and Bondio G. P., "Effect of training on behavioral reactivity and neurotransmitter levels in drug detection dogs," *Journal of Veterinary Behavior: Clinical Applications and Research*, vol. 5, pp. 38-39, 2010.

Romain A. C. and Nicolas J., "Long term stability of metal oxide-based gas sensors for E-nose environmental applications: an overview," *Sensors and Actuators B*, vol. 146, pp. 502-506, 2010.

Rowell F., Seviour J., Lim A. Y., Elumbaring-Salazar C. G., Loke J. and Ma J., "Detection of nitro-organic and peroxide explosives in latent fingermarks by DART- and SALDI-TOF-mass spectrometry," *Forensic Science International*, vol. 221, pp. 84-91, 2012.

Sato K., Shikida M., Matsushima Y., Yamashiro T., Asaumi K., Iriye Y. and Yamamoto M., "Characterization of orientation-dependent etching properties of single-crystal silicon: effects of KOH concentration," *Sensors and Actuators A*, vol. 64, pp. 87-93, 1998.

Sauer K. L., Suits B. H., Garroway A. N. and Miller J. B., "Three-frequency nuclear quadrupole resonance of spin-1 nuclei," *Chemical physics Letters*, vol. 342, pp. 362-368, 2001.

Sayago I., Gutierrez J., Ares L., Robla J. I., Horrilo M. C., Getino J., Rino J. and Agapito J. A., "Long-term reliability of sensors for detection of nitrogen oxides," *Sensors and Actuators B*, vol. 26, pp. 56-58, 1995.

Schaller E., Bosset J. O. and Escher F., "Electronic noses and their application to food," *LebensmittelWissenschaft und-Jechnologie*, vol. 31, pp. 305-316, 1998.

Schierbaum K., Weimar U. and Gopel W., "Conductance, work function and catalytic activity of SnO2-based gas sensors," *Sensors and Actuators B*, vol. 3, pp. 205-214, 1991.

Seiyama T., Kato A., Fujishi K. and Nagatani M., "A New detector for gaseous components using semiconductive thin films," *Analytical Chemistry*, vol. 34, pp. 1502-1503, 1962.

Shankaran D. R., Gobi K. V., Sakai T., Matsumoto K., Toko K. and Miura N., "Surface plasmon resonance immunosensor for highly sensitive detection of 2,4,6-trinitrotoluene," *Biosensors and Bioelectronics*, vol. 20, p. 1750– 1756, 2005.

Sharma S. K., Misra A. K. and Sharma B., "Portable remote Raman system for monitoring hydrocarbon, gas hydrates and explosives in the environment," *Spectrochimica Acta A*, vol. 61, pp. 2404-2412, 2005.

Sharma S. K., Misra A. K., Lucey P. G., Angel S. M. and McKay C. P., "Remote Pulsed Raman Spectroscopy of Inorganic and Organic Materials to a Radial Distance of 100 Meters," *Applied Spectroscopy*, vol. 60, pp. 871- 876, 2006.

Shen C., Li J., Han H., Wang H., Jiang H. and Chu Y., "Triacetone triperoxide using low reduced-field proton transfer reaction mass spectrometer," *International Journal of Mass Spectrometry,* vol. 285, pp. 100-103, 2009.

Shen Y., Yamazaki T., Liu Z., Meng D., Kikuta T., Nakatani N., Saito M. and Mori M., "Microstructure and H2 gas sensing properties of undoped and Pd-doped SnO2 nanowires," *Sensors and Actuators B*, vol. 135, pp. 524- 529, 2009.

Shriver-Lake L. C., Patterson C. H. and Van Bergen S. K., "New Horizons: explosive detection in soil extracts with a fiber-optic biosensor," *Field Analytical Chemistry and Technology*, vol. 4, pp. 239-245, 2000.

Singh S., "Sensors-An effective approach for the detection of explosives," *Journal of Harzardous Materials*, vol. 144, pp. 15-28, 2007.

Skala T., Veltruska K., Moroseac M., Matolinova I., Cirera A. and Matolin V., "Redox process of Pd-SnO_2 system," *Surface Science*, Vols. 566-568, pp. 1217-1221, 2004.

Smith J. A., Blanz M., Rayner T. J., Rowe M. D., Bedford S. and Althoefer K., "^{14}N, quadrupole resonance and ^{1}H T1 dispersion in the explosive RDX," *Journal of Magnetic Resonance*, vol. 213, pp. 98-106, 2011.

Smith J. A., Rayner T. J., Rowe M. D., Barras J., Peirson N. F., Stevens A. D. and Althoefer K., "Magnetic field-cycling NMR and ^{14}N, ^{17}O quadrupole resonance in the explosive pentaerythritol tetranitrate (PETN)," *Journal of Megnetic Resonance*, vol. 204, pp. 139-144, 2010.

Smith, J. M., Van Ness H. C., and Michael M. Abbott. Introduction to Chemical Engineering Thermodynamics: J.M. Smith, H.C. Van Ness, M.M. Abbott. Boston: McGraw-Hill, 2005.

Spangler G. E. and Lawless P. A., "Ionization of nitrotoluene compounds in Negative ion plasma chromatography," *Analytical Chemistry*, vol. 50, pp. 884-892, 1978.

Spangler G. E., Carrico J. P. and Campbel D. N., "Recent advances in ion mobility spectrometry for explosives vapor detection," *Journal of Testing and Evaluation*, vol. 13, pp. 234-240, 1985.

Stambouli A., Bouri A. E., Bouayoun T. and Bellimam M. A., "Headspace GC/MS detection of TATP traces in post-explosion debris," *Forensic Science International* , vol. 146S, pp. 191-194, 2004.

Symanski S. S. and Bruckenstein S., "Conductometric sensor for parts per billion sulfur dioxide determination," *Analytical Chemistry*, vol. 58, pp. 1771- 1777, 1986.

Takats Z., Cotte-Rodriguez I., Talaty N., Chen H. and Cooks R. G., "Direct, trace level detection of explosives on ambient surfaces by desorption electrospray ionization mass spectrometry," *Chemical Communications*, vol. 41, pp. 1950-1952, 2005.

Tan R., Guo Y., Zhao J., Li Y., Xu T. and Song W., "Synthesis, characterization and gas-sensing properties of Pd-doped SnO_2 nano particles," *Transactions of Nonferrous Metals Society of China*, vol. 21, pp. 1568-1573, 2011.

Thammakhet C., Thavarungkul P., Brukh R., Mitra S. and Kanatharana P., "Microtrap modulated flame ionization detector for on-line monitoring of methane," *Journal of Chromatography A*, vol. 2005, pp. 243-248, 1072.

Todd M. W., Provencal R. A., Owano T. G., Paldus B. A., Kachanov A.,Vodopyanov K. L., Hunter M., Coy S. L., Steinfeld J. I. and Arnold J. T., "Application of mid-infrared cavity-ringdown spectroscopy to trace explosives vapor detection using a broadly tunable (6-8 μm) optical parametric oscillator," *Applied Physics B*, vol. 75, pp. 367-376, 2002.

Tournier G., Pijolat C., Lalauze R. and Patissier B., "Selective detection of CO and CH_4 with gas sensors using SnO_2 doped with palladium," *Sensors and Actuators B*, Vols. 26-27, pp. 24-28, 1995.

Tribe W. R., Newnham D. A., Taday P. F. and Kemp M. C., "Hidden object detection: security applications of terahertz technology," *Proceedings of SPIE*, vol. 5354, pp. 168-176, 2004.

Tsud N., Johanek V., Stara I., Veltruska K. and Matolin V., "XPS, ISS and TPD of Pd-Sn interactions on Pd-SnOx systems," *Thin Solid Films*, vol. 391, pp. 204-208, 2001.

Urbanski T., Chemistry and Technology of Explosives, London: Pergamon Press, 1964.

Uthanna S., Subramanyam T. K., Naidu B. S. and Rao G. M., "Structure–composition–property dependence of reactive magnetron sputtered ZnO thin films," *Optical Materials*, vol. 19, p. 461–469, 2002.

Vereshchaginam E., Wolters R. A. and Gardeniers J. G., "Measurement of reaction heats using a polysilicon based microcalorimetric sensor," *Sensors and Actuators A*, vol. 169, p. 308–316, 2001.

Waggoner L. P., "Chapter 3 – Detection of Explosives by Dogs," in Aspects of Explosives Detection, Oxford, UK, Elsevier, 2009, pp. 27-40.

Wakelin D., Isotopic ratio analysis of explosives traces – a new type of evidence, UK: United Kingdom Defence Evaluation and Research Agency report, 2000.

Wang B. and Lin Q., "Temperature-modulated differential scanning calorimetry in a MEMS device," *Sensors and Actuators B*, vol. 180, pp. 60-65, 2013.

Wang J., "Electrochemical Sensing of Explosives," Electroanalysis, vol. 19, p. 415–423, 2007.

Whelan D. J., Spear R. J. and Read R. W., "The thermal decomposition of some primary explosives as studied by differential scanning calorimetry," *Thermochimica Acta*, vol. 80, p. 149–163, 1984.

Wilkinson J., Konek C. T., Moran J. S., Witko E. M. and Korter T. M., "Terahertz absorp spectrum of triacetone triperoxide (TATP)," *Chemical Physics Letters*, vol. 478, pp. 172-174, 2009.

Williams D. E., "Semiconducting oxides as gas-sensitive resistors," *Sensors and Actuators B*, vol. 57, pp. 1-16, 1999.

Williams M. and Johnston J. M., "Training and maintaining the performance of dogs (Canis familiaris) on an increasing number of odor discriminations in a controlled setting," *Applied Animal Behaviour Science*, vol. 78, pp. 55- 65, 2002.

Wilson R., Clavering C. and Hutchinson A., "Paramagnetic bead based enzyme electrochemiluminescence immunoassay for TNT," *Journal of Electroanalytical Chemistry*, vol. 557, pp. 109-118, 2003.

Wong, Ming-Yee, Wei-Rui Cheng, Mao-Huang Liu, Wei-Cheng Tian, and Chia-Jung Lu. "A Preconcentrator Chip Employing μ-SPME Array Coated with In-situ-synthesized Carbon Adsorbent Film for VOCs Analysis." *Talanta* 101 (2012): 307-13.

Wu M., Ray M., Fung K. H., Ruckman M. W., Harder D. and Sedlacek A. J., "Stand-off Detection of Chemicals by UV Raman Spectroscopy," *Applied Spectroscopy*, vol. 54, pp. 196-220, 2000.

Xu J., Liu H., Yuan T., Kersting R. and Zhang X. C., "Advanced terahertz time-domain spectroscopy for remote detection and tracing," *Proceedings of SPIE*, vol. 5070, pp. 17-27, 2003.

Yabuki, T., and O. Nakabeppu. "Heat Transfer Mechanisms in Isolated Bubble Boiling of Water Observed with MEMS Sensor." *International Journal of Heat and Mass Transfer* 76 (2014): 286-97.

Yamazoe N., Kurokawa K. and Seiyama T., "Effects of additives on semiconductor gas sensor," *Sensors and Actuators*, vol. 4, pp. 283-289, 1983.

Yang W. Y., Kim W. G. and Rhee S. W., "Radio frequency sputter deposition of single phase cuprous oxide using Cu_2O as a target material and its resistive switching properties," *Thin Solid Films*, vol. 517, pp. 967-971, 2008.

Yinon J., "Analysis and detection of explosives by mass spectrometry," in Aspects of Explosives Detection, Oxford, UK, Elsevier, 2009, pp. 147- 169.

Yinon J., "Detection of explosives by electronic noses," *Analytical Chemistry*, vol. 75, pp. 99-105, 2003.

Yuan T., Liu H., Xu J., Al-Douseri F., Hu Y. and Zhang X. C., "Terahertz time-domain spectroscopy of atmosphere with different humidity," *Proceedings of SPIE*, vol. 5070, pp. 28-37, 2003.

Yuasa M., Masaki T., Kida T., Shimanoe K. and Yamazoe N., "Nano-sized PdO loaded SnO_2 nanoparticles by reverse micelle method for highly sensitive CO gas sensor," *Sensors and Actuators B*, vol. 136, pp. 99-104, 2009.

Zalewska A., Pawlowski W.and Tomaszewski W., "Limits of detection of explosives as determined with IMS and field asymmetric IMS vapour detectors," *Forensic Science International*, vol. 226, pp. 168-172, 2013.

Zang J., Guo C., Hu F., Yu L. and Li C., "Electrochemical detection of ultratrace nitroaromatic explosives using ordered mesoporous carbon," *Analytica Chimica Acta*, vol. 683, p. 187–191, 2011.

Zark A., Kaplan D. and Kendler S., "A MEMS-based microthermal analysis of explosive materials," *Sensors and Actuators A*, vol. 199, pp. 129-135, 2013.

Zhang T., Liu L., Qi Q., Li S. and Lu G., "Development of microstructure In/Pd-doped SnO_2 sensor for low level CO detection," *Sensors and Actuators B*, vol. 139, pp. 287-291, 2009.

Zhang W. H., Zhang W. D. and Chen L. Y., "Highly sensitive detection of explosive triacetone triperoxide by an In_2O_3 sensor," *Nanotechnology*, vol. 21, p. 315502, 2010.

Zhang Y., Ma X., Zhang S., Yang C., Zheng O. and Zhang X., "Direct detection of explosives on solid surfaces by low temperature plasma desorption mass spectrometry," *Analyst*, vol. 134, pp. 176-181, 2009.

Zhang Y., Xiang Q., Xu J., Xu P., Pan Q.and Li F., "Self-assemblies of Pd nanoparticles on the surfaces of single crystal ZnO nanowires for chemical sensors with enhanced performances," *Journal of Material Chemistry*, vol. 19, pp. 4701-4706, 2009.

Zimmermann S., Abel N., Baether W. and Barth S., "An ion-focusing aspiration condenser as an ion mobility spectrometer," *Sensors and Actuators B*, vol. 125, pp. 428-434, 2007.

Zubel I., Barycka I., Kotowska K. and Kramkowska M., "Silicon anisotropic etching in alkaline solutions IV: The effect of organic and inorganic agents on silicon anisotropic etching process," *Sensors and Actuators A*, vol. 87, pp. 163-171, 2001.